Republic of Iraq
Ministry of Higher Education and Scientific Research
University of Babylon / College of Science
Department of Physics

Analysis of Spectroscopic Properties for New Nanocomposites

A Thesis
Submitted to the Council of the College of Science, University of Babylon in Partial Fulfillment of the Requirements of the Degree of Doctor of Philosophy in Science /Physics

By

Fatema Sattar Jaber Mohamed

B.Sc. in physics / 2010

M.Sc. in physics / 2015

Supervised by

Prof. Dr.

Hayder Mohammed Abduljalil Abood

2022 A.D. *1444 A.H.*

Summary

In this study, the casting method was adopted to prepare new nanocomposites (PVA-TiO_2-Ag) and (PVA-SnO_2-Ag) using pure polyvinyl alcohol (PVA) polymer with a weight of (0.485 g) and the weight (0.0075 g) once for tin oxide SnO_2 and again for titanium oxide TiO_2, and finally adding different weight percentages (0. 0075, 0.015, 0.025, 0.03) g of silver nanoparticles (AgNPs). At the same time, a theoretical study was conducted on these prepared compounds using Gaussian 09 program and based on the theory of Density function by using the hybrid functional three effects Lee-Yang-Parr B3LYP level together with the Stuttgart Dresden triple zeta (SDD) basis sets. The best geometric optimization of the models was obtained by calculating the values of bonds and angles theoretically, and comparing them with previous studies, a good convergence was found between the two values. Also, using the time-dependent Schrödinger equation. The spectral properties were calculated, which included the infrared spectrum and the visible-ultraviolet spectra. It was found that the PVA polymer is absorbed in the ultraviolet region of electromagnetic radiation, and that the doping of the pure polymer by SnO_2, TiO_2 and AgNPs was one of the important methods for modulating the optical absorption of PVA.

The electronic properties were also calculated, which included calculating the value of the total energy (E_T), which started to decrease more when adding (AgNPs) to the nanocomposite (PVA-TiO_2) and (PVA-SnO_2), and this indicates that all samples prepared from nanocomposites have a good relaxation. The energy gap value of the pure polymer (PVA) was also calculated and the effect of adding nanomaterials was studied. It was found that the increase in the concentrations of nanomaterials added to the nanocomposite leads to a decrease in the energy gap value from (6.101) eV for the PVA polymer to (3.283) eV for the nanocomposites (PVA -SnO_2-Ag) and (1.336) eV for the nanocomposites (PVA-TiO_2-Ag).

Practically, the samples were subjected to an optical properties examination, where it was observing that the absorbance, absorption coefficient, extinction coefficient, refractive index, real and imaginary dielectric constants, and optical conductivity of the nanocomposites (PVA-TiO_2-Ag) and (PVA-SnO_2-Ag) increased with increasing concentration of (AgNPs), on the other hand there is a decrease. The value of the permeability and energy gap of the nanocomposites is clear with increasing concentration of (AgNPs).

The antibacterial activity of the nanocomposites (PVA-TiO_2-Ag) and (PVA-SnO_2-Ag) against Salmonella, E. Coli and Stenotrophomonas maltophilia as a model for Gram-negative bacteria and Bacillus cereus as a model for Gram-positive bacteria was studied. It was found that this antibacterial activity is caused by silver nanoparticles, the higher the concentration of (AgNPs), the greater area of inhibition, because (AgNPs) has a physical mechanism that works to damage the walls of bacteria cells. It was found that the nanocomposites (PVA-SnO_2-Ag) gave a higher activity than the nanocomposites (PVA-TiO_2-Ag) in inhibiting bacteria.

جمهورية العراق

وزارة التعليم العالي والبحث العلمي

جامعة بابل/ كلية العلوم

قسم الفيزياء

تحليل الخصائص الطيفية لمتراكبات نانوية جديدة

اطروحة

مقدمة إلى مجلس كلية العلوم- جامعة بابل

وهي جزء من متطلبات نيل درجة الدكتوراه فلسفة في العلوم /الفيزياء

من قبل

فاطمة ستار جابر محمد

بكالوريوس علوم فيزياء / ٢٠١٠

ماجستير علوم فيزياء / ٢٠١٥

بأشراف

أ. د.حيدر محمد عبد الجليل عبود

١٤٤٤هـ ٢٠٢٢ م

بِسْمِ اللَّـهِ الرَّحْمَـٰنِ الرَّحِيم

﴿إِنَّ وَلِيِّيَ ٱللَّهُ ٱلَّذِى نَزَّلَ ٱلْكِتَٰبَ ۖ وَهُوَ يَتَوَلَّى ٱلصَّٰلِحِينَ﴾

صِدَّقْ ٱللهُ العلي ٱلعِظَيِم

سورة الاعراف آية (١٩٦)

Dedicate

I dedicate this thesis to your pure soul

My dear father

The affectionate angel... the soul in which my soul lived

My dear mother

My Brother and Sisters with great love

To my beautiful baby

amna

Acknowledgements

Thanks and appreciation

Praise be to God, Lord of the Worlds, for his countless blessings, and the best prayers and peace be upon the best of the Messenger of God, Muhammad, his pure offspring, and his honorable companions.

I would like to express my thanks to the Dean of the College of Science and the Head of the Physics Department for their support.

I would also like to express my deepest gratitude and appreciation to my supervisor, Professor Dr. Haider Mohammed Abdel Jalil for his guidance, suggestions, support and encouragement to me through research work.

Finally, my most sincere gratitude to my dear mother and father, who taught me tenderness and lavished me with their generosity and tenderness so much. I also thank everyone who helped me conduct this thesis. I wish success to everyone.

Fatema

الخلاصة

في هذه الدراسة، تم اعتماد طريقة صب المحلول لتحضير مـــتراكبات نانوية جـــــديدة (PVA-TiO_2-Ag) و(PVA-SnO_2-Ag) وذلك باستخدام بوليمر بولي فينيل الكحول النقي (PVA) بوزن (0.485 غم) ووزن (0075 .0 غم) مرة لاوكسيد القصدير SnO_2 ومرة اخرى لاوكسيد التيتانيو واخيرا اضافة نسب وزنية مختلفة (0. 0075, 0.015, 0.025, 0.03) غم من جسيمات الفضة النانوية (AgNPs).
في نفس الوقت، تم اجراء دراسة نظرية على هذه المتراكبات المحضرة بأستخدام برنامج Gaussian 09 وبالاعتماد على نظرية دالية الكثافة من خلال استخدام المعاملات الوظيفية الهجينة الثلاثة وبتطبيق مستوى الدالة الهجينة لي –يانغ- بار جنبًا إلى جنب مع مجموعات الاساس شتوتغارت درسدن الثلاثية زيتا.
تم حساب الامثلية الهندسية للنماذج من خلال حساب قيم الاواصر والزوايا نظريا, ومقارنتها مع دراسات سابقة وقد وجد تقارب جيد بينهما. وكذلك تم استخدام معادلة شرودنجر المعتمدة على الزمن لحساب طيف الاشعة المرئية- فوق البنفسجية. ايضا تم حساب طيف الاشعة تحت الحمراء. وقد وجد أن بوليمر PVA يمتص في منطقة الأشعة فوق البنفسجية من الإشعاع الكهرومغناطيسي، وان تشويب البوليمر النقي بواسطة SnO_2 و TiO_2 مع AgNPs كانت إحدى الطرق المهمة لتعديل الامتصاص البصري للبوليمر PVA.
وكذلك تم حساب الخواص الالكترونية والتي تضمنت حساب قيمة الطاقة الكلية (E_T) والتي بدأت بالانخفاض اكثر عند اضافة (AgNPs) الى المتراكب النانوي (PVA-TiO_2) و (PVA-SnO_2) وهذا يشير الى ان جميع العينات المحضرة من المركبات النانوية لها استرخاء جيد. كذلك تم حساب قيمة فجوة الطاقة للبوليمر النقي (PVA) ودراسة تأثير إضافة المواد النانوية، حيث وجد أن الزيادة في تركيزات المواد النانوية المضافة إلى المتراكب النانوي تؤدي إلى تقليل قيمة فجوة الطاقة من (6.101 eV) للبوليمر PVA إلى (3.283 eV) للمتراكب (PVA-SnO_2-Ag) و (1.336) eV للمتراكب (PVA-TiO_2-Ag).
عمليا فقد خضعت العينات لفحص الخواص البصرية حيث تم ملاحظة زيادة الامتصاصية ومعامل الامتصاص ومعامل الخمود ومعامل الانكسار وثوابت العزل الحقيقي والخيالي والتوصيلية البصرية للمتراكبات النانوية (PVA-TiO_2-Ag) و (PVA-SnO_2-Ag) بزيادة تركيز (AgNPs), بالمقابل هناك نقصان واضح بقيمة النفاذية وفجوة الطاقة للمتراكبات النانوية مع زيادة تركيز (AgNPs).
تمت دراسة الفعالية المضادة للبكتيريا للمركبات النانوية (PVA-TiO_2-Ag) و (PVA- SnO_2-Ag) ضد بكتيريا السالمونيلا والإشريكية القولونية (E. Coli) و Stenotrophomonas maltophilia كنموذج للبكتيريا سالبة الجرام و Bacillus cereus تم اختياره كنموذج للبكتيريا موجبة الجرام، وقد وجد ان هذا

النشاط المضاد للبكتيريا ناتج عن جسيمات الفضة النانوية, فكلما زاد تركيز (AgNPs)، زادت مساحة التثبيط ، وذلك لأن (AgNPs) له آلية فيزيائية تعمل على إتلاف جدران خلايا البكتيريا. وقد وجد بأن المركبات النانوية ($PVA-SnO_2-Ag$) أعطى نشاطًا أعلى من المركبات النانوية ($PVA-TiO_2-Ag$) في تثبيط البكتيريا.

Contents

List of Symbols

Symbol	Meaning
Ψ	Wave function
$\hat{H}$	Hamiltonian operator
E	Energy of the system
$\hat{T}_e$	Electronic kinetic energy operator
$\hat{T}_n$	Nuclear kinetic energy operator
$\hat{V}_{ne}$	The attractive interactions operator between nuclei and electrons
$\hat{V}_{ee}$	The repulsive electron-electron interactions
$\hat{V}_{nn}$	The repulsive interactions operator between the nuclei
$Z_{A,B}$	The nuclei charge of atoms A and B
E_{XC}^{B3LYP}	The hybrid exchange-correlation functionals
E_{XC}^{LDA}	local spin density approximation to the correlation functional
E_X^{HF}	The Hartree–Fock exact exchange functional
E_c^{GGA}	The generalized gradient approximation formulated
E_X^{GGA}	The generalized gradient approximation formulated
X^{STO}	Slater wave function
N	Normalization factor
Y_{im}	Angular function
ξ	Orbital exponent
X^{GTO}	Gaussian wave function
M	Number of Gaussian primitives

Symbol	Meaning
E_{HOMO}	Energy of the Highest Occupied Molecular Orbital
E_{LUMO}	Energy of the Lowest Unoccupied Molecular Orbital
E_g	Energy gap
I_E	Ionization energy
E_A	Electron Affinity
E_T	Total Energy
η	Chemical Hardness
S	Chemical Softness
ω	Electrophilicity index
χ	Electronegativity
DFT	Density Functional Theory
UV-Vis	Ultraviolet-Visible
SCF	Self-Consistent Field
LDA	Local Density Approximation
LSDA	Local Spin Density Approximation
G09	Gaussian 09
$\rho(\vec{r})$	Electron Density
A	Absorbance
T	Transmittance
R	Reflectance
k	Extinction Coefficient
υ	Frequency
ε_1	Real Dielectric Constant
ε_2	Imaginary Dielectric Constant
σ	Optical conductivity
FT-IR	Fourier Transform Infrared Radiation
SEM	Scanning Electron Microscope

List of Figures

List of Tables

Examination Committee Certification

We certify that we have read this thesis entitled " **Analysis of Spectroscopic Properties for New Nanocomposites** " and as the examining committee, examined the student " **Fatema Sattar Jaber Mohamed** " in its contents and that, in our opinion meets of doctor of philosophy in physics in theoretical physics.

Signature
Name: **Dr.Nahida Bukeet Hasan**
Title: **Professor**
Address : **College of Science / University of Babylon**
Data : / /2022
(Chairman)

Signature
Name: **Dr.Jabbar Mansoor Khalaf**
Title: **Professor**
Address: **College of Education for Pure Sciences / University of Basra**
Data: / /2022
(Member)

Signature
Name: **Dr.Qusiy H. Al-Galiby**
Title: **Ass.Professor**
Address: **College of Education University of Al-Qadisiyah**
Data: / /2022
(Member)

Signature
Name: **Dr.Musa Kadhim Mohsen**
Title: **Ass.Professor**
Address: **College of Science / University of Babylon**
Data: / /2022
(Member)

Signature
Name: **Dr.Nidhal Mohammed O. Al-Shareefi**
Title: **Ass.Professor**
Address: **College of Science / University of Babylon**
Data: / /2022
(Member)

Signature
Name: **Dr.Hayder Mohammed AbdulJalil Abood**
Title: **Professor**
Address: **College of Science / University of Babylon**
Data: / /2022
(Member and Supervisor)

Approved by the University of Babylon a committee on graduate studies

Signature
Name: **Dr.Faez Ali Rashid Almaamori**
Title: **Professor**
Address: **Dean of College of Science / University of Babylon**
Data: / /2022

Supervisor Certification

I certify that this thesis entitled **(Analysis of Spectroscopic Properties for New Nanocomposites)** was prepared by (**Fatema Sattar Jaber Mohamad**) under my supervision at department of physics, college of science, University of Babylon, as a partial fulfillment of the requirements of Ph.D. degree in the theoretical Physics.

Signature:

Supervisor: Dr. Hayder Mohammed Abduljalil Abood

Title: Professor

Address: Department of Physics – College of Science - University of Babylon

Date: / /

Certification of the Head of the department

In view of the available recommendation, I forward this thesis for debate by the examining committee.

Signature:

Name: Dr. Samira Adnan Mahdi

Title: Ass. Professor

Address: Head of Department of Physics, College of Science, University of Babylon**.**

Date: / /

1.1 General Introduction

Materials in the nanoscale are dealt with nanotechnology, which is considered a field of applied science [1], which is used to treat matter in the atomic and molecular scale because it is one of the applications of science and technology, which has the ability to form micro and large materials with high atomic accuracy [2]. In the field of food, medicine and agriculture, nanoparticles have drawn the attention of researchers and scientists [3]. As for the science of polymers, previous studies showed the interest of nanotechnology in this science, as previous studies included in their research on nanoscale dimensions, but it was not known as nanotechnology until recently [4]. Nanoscience and nanotechnology have drawn great attention to nanomaterials. Nanostructure science and technology is a broad and interdisciplinary field of research and development that has grown exponentially worldwide in the past few years [5].

Based on the origin of Nanoparticles (NPs) and nanostructures, they can be classified into two categories, natural and synthetic, Natural nanomaterials are produced in nature by biological species. While Synthetic (engineered) nanomaterials as shown in Figure (1.1) are produced by mechanical, physical, chemical, biological or hybrid methods [6]. Has the potential to revolutionize the ways in which materials and products are created and the scope and nature of accessible jobs. It already has a large commercial uptake, which will definitely increase in the future [7]. Carbon-based nanoparticles are those that are entirely composed of carbon, they are divided as shown in Figure (1.2), and occasionally activated carbon in nano size [8].

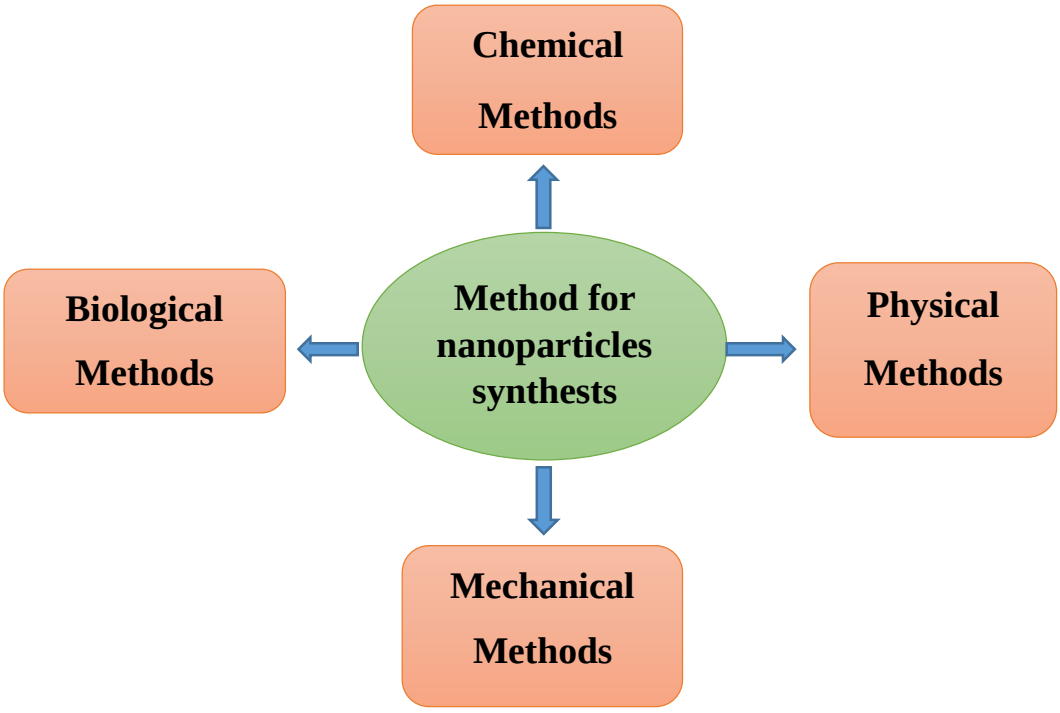

Figure 1.1. Variance process for the preparing of Synthetic nanoparticles [5].

Nanomaterials can be distinguished by having dimensions ranging from 1-100 nm, as an example of 1D film covers, 2D such as threads, and 3D dimensions are represented by particles [10]. For example, nano-carbon, silica, nano-silver, and carbon nanotubes), where it can be used in many applications, including biomedicine, electrochemistry and photochemistry. Figure (1.3) shows a group of nanomaterials (alloys, metals, metal dioxide, gold and carbon) with a variety of morphologies (shapes) [11].

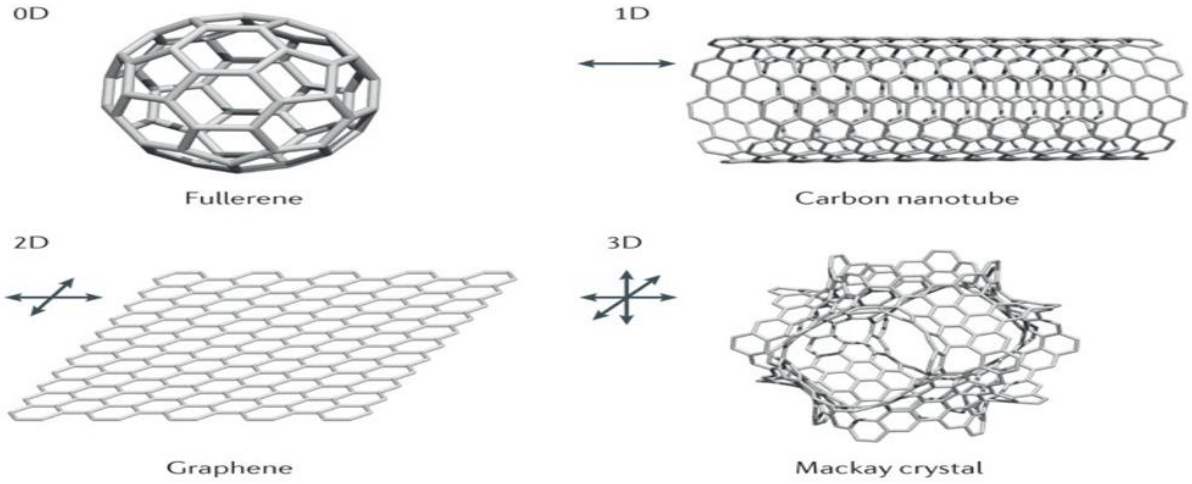

Figure 1.2. Carbon based nanoparticles [9].

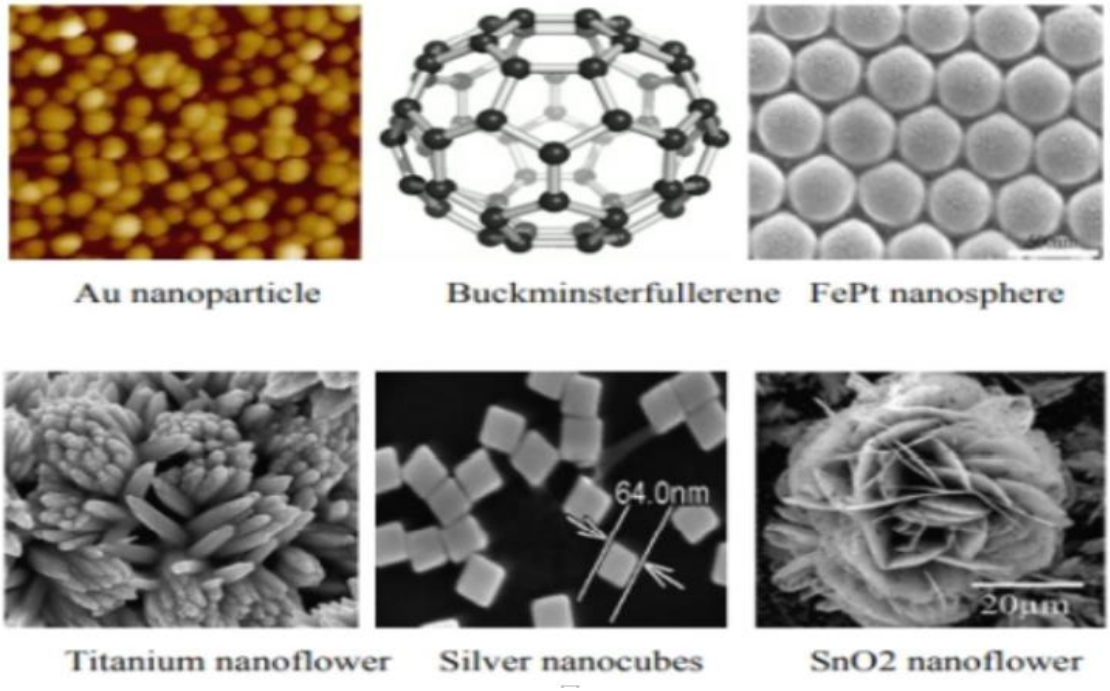

Figure 1.3. Nanomaterials with a variety of the morphologies [12]

1.2 Polymer Blend

A polymer blend is a combination of two or more polymers that have been combined to form a new material with distinct physical properties. In general, five types of polymer blends have been extensively studied: thermoplastic–thermoplastic blends, thermoplastic–rubber blends, thermoplastic–thermosetting blends, rubber–thermosetting blends, and polymer–filler blends.

Polymer blending has received a lot of attention as a simple and cost-effective method of creating polymeric materials with versatility for commercial applications. In other words, by carefully selecting the component polymers, the properties of the blends can be tailored to their intended use [13]. Today's market pressure is so intense that plastics manufacturers must provide better and more cost-effective materials with superior property combinations as a replacement for traditional metals and polymers. Although plastic raw materials are more expensive in terms of weight than metals, they are less expensive in terms of product cost. Furthermore, polymers are corrosion-resistant, have a light weight with good toughness (important for good fuel economy in automobiles and aerospace applications), and are used to make a variety of goods such as household plastic products, automotive interior and exterior components, biomedical devices, and aerospace applications. The development and commercialization of new polymers typically takes many years and is extremely expensive. However, by using a polymer blending process that is also very inexpensive to operate [14]. Polymer blends accounted for half of all plastics produced in 2010 as part of the replacement of traditional polymers. Today's polymer industry is becoming more sophisticated, with ultra-high-performance injection molding machines and extruders available to detect and manipulate phase separations and viscosity changes during the processing stages. While modern blending technology can greatly extend the performance capabilities of polymer

blends, increasing market pressure now dictates that polymer blends must perform under certain conditions for specific applications (e.g., mechanical, chemical, thermal, electrical). This is a significant challenge because the materials must frequently function at the limit of the properties that can be achieved; as a result, in-depth studies of the properties and performance of polymer blends are required [15].

1.3 Polymer Nanocomposites

Nanocomposites are multiphase solid materials with one, two or three dimensions of less than 100 nanometers (nm), or structures with nanoscale repeat distances between the different phases that comprise the material [16]. The concept behind nanocomposites is to use building blocks with nanometer dimensions to design and create new materials with unprecedented flexibility and physical property improvement. The matrix materials of nanocomposites are classified as polymer matrix nanocomposites (PMNC), metal matrix nanocomposites (MMNC), and ceramic matrix nanocomposites (CMNC) [17].

Polymeric nanocomposites made up of inorganic nanoparticles and organic polymers are a material class that has sparked a lot of interest in recent years [18]. Applications for nanocomposites include microelectronic packaging, medicine, automobiles, optical integrated circuits, drug delivery, injection molded products, sensors, membranes, aerospace, packaging materials, coatings, fire retardants, adhesives, and consumer goods, and many other uses. These advanced nanocomposites have numerous advantages, including low production costs and the ability to fabricate devices on a large scale and on flexible substrates [19]. Creating nanocomposites could be a solution for appropriately adjusting the properties of individual nanomaterials such as optical, electrical, thermal, and mechanical properties. Nanoparticles, in particular, are advanced technological materials due to their appealing electrical / electronic properties and high refractive index.

Nanocomposites of organic and inorganic materials can benefit from the properties of both organic polymers (dielectric, ductility and flexibility) and inorganic materials (high thermal stability, rigidity, strength, high refractive index and hardness), and thus have a wide range of applications [20].

1.4 Poly (Vinyl Alcohol) (PVA)

Polyvinyl alcohol (PVA) is a critical polymer because of its unique physical and chemical properties, and it has attracted numerous specialists over the years [21]. This polymer is available in powder, film, and fiber forms. It is a semi-crystalline polymer formed by the gathering of OH and hydrogen bonds [22- 24].

It is also regarded as one of the few vinyl polymers solvent in water with high straightforwardness and adaptability. It is now used in biomedical materials as a medication conveyance framework and layers for emulsification, estimating, and glues [25]. PVA can also be used in therapeutic applications, such as fake veins, manufactured digestion systems and contact lenses. Because of its resemblance to the living body, it has been identified as a therapeutic material [26]. Electrical properties of materials have long been of practical importance and theoretical interest. It is well understood that electric property estimations are powerful tools for depicting inorganic semiconductor doped on polymer nanocomposites, which provide information about electronic properties and demonstrate the relationships between structure and electrical properties of nanocomposites [27]. The polyvinyl liquor polymer was chosen as a host lattice in this concern due to the advantages of its high mechanical quality, water dissolvability, great natural solidity, and do pant subordinate electrical conductivity [28]. Polyvinyl liquor is a decent shielding material with low conductivity and dielectric loss, and thus important in the microelectronics industry; however, its electrical conductivity and charge

stockpiling ability can be significantly affected by doping. Where can adjust the electrical and optical properties of polymers depending on their reactivity with the host network [29]. As shown in Figure (1.4), PVA has a carbon chain backbone with hydroxyl groups that communicate with methane carbon.

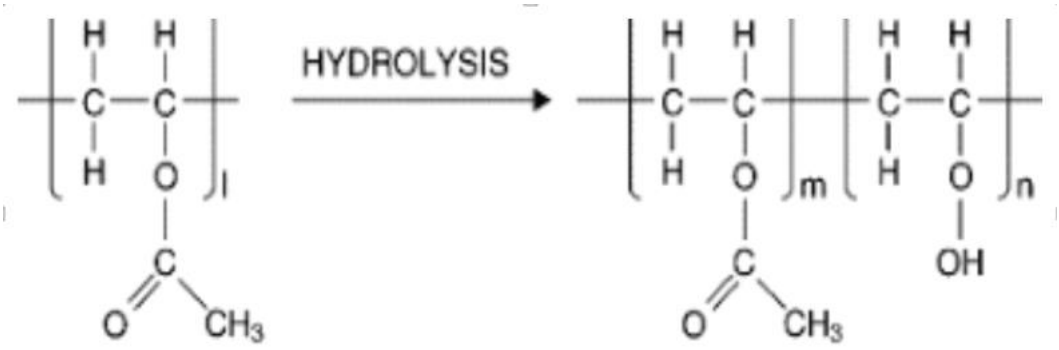

Figure 1.4. Preparation and molecular structure of polyvinyl alcohol [30].

1.5 Properties of Poly (vinyl alcohol) (PVA)

Poly (vinyl alcohol) (PVA) is a thermoplastic polymer derived from the hydrolysis of poly (vinyl acetate) (PVAc), rather than polymerization processes as with some other synthetic polymers. PVA still contains 1–2 mol percent acetyl groups after hydrolysis. Its degree of polymerization (DP) is primarily determined by the length of the PVAc macromolecular chain. PVAc is converted to PVA via base catalyzed alcoholysis or acid initiated hydrolysis. PVA is the most polar synthetic polymer; it has no odor, is nontoxic, is biocompatible, and is soluble in water, acids, and high polar solvents. Its molecular weight (MW) is determined by the (MW) of PVAc and the degree of hydrolysis PVA is well known for its use in the production of fibers, including its use in surgeries, artificial leather, tubing, gaskets with good stability to oil derivatives, rubber-like items, transportation belts, emulsifiers, paper and paperboard adhesives, and general purpose adhesives for

bonding paper, textiles, leather, and porous ceramic surfaces [31]. It should be made water insoluble when processed for textile fibers and other applications. This is done with an aqueous solution of sodium sulfate containing sulfuric acid and formaldehyde for PVA fiber.

Because PVA is a water-soluble synthetic polymer, if no precautions are taken against high temperatures, light exposure, microorganisms, and other environmental factors, it may degrade in the environment through photo degradation, biodegradation, and chemical degradation, which includes hydrolytic and oxidative processes. A group of researchers investigated the rheological behavior of an aqueous solution of PVA with varying MW and concentration that was subjected to freeze–thaw cycles. The results of the experiments indicate that the number of PVA segments participating in the crystalline junction points increases exponentially during freezing and decreases exponentially during thawing in the vicinity of the critical point [32].

1.6 Titanium Dioxide (TiO_2)

Titanium dioxide (TiO_2) has received a great deal of attention due to its unique properties and numerous applications [33], including photovoltaic devices, photo catalysis, environmental purification, optical coating and solar energy conversion. TiO_2 crystallization occurs in three forms: anatase, rutile and brookite, as showed in Figure (1.5). The anatase phase is of great interest in photocatalytic reactions and a photocell electrochemical that can be used to degrade several environmental pollutants (gaseous and liquid phases) under ultraviolet (UV) radiation due to its strong oxidative strength, non-toxicity, and long photostability [34]. TiO_2 powders have a wide range of industrial applications due to their unique optical, electrical, and catalytic properties [35]. TiO_2 has received a lot of attention because it is used

as an absorbent for ultraviolet radiation. When TiO_2 is exposed to UV light (> 385 nm), an electron/hole pair is formed [36].

Photocatalytic reactions take place primarily on the surface of titanium dioxide, where electrons are generated and holes are trapped. PVA film is combined with inorganic nanoparticles TiO_2 to improve new nano devices by improving optical, structural, electrical, and chemical properties. TiO_2 is used in tissue engineering and implantation applications due to its elegant biocompatibility and biomechanical properties (such as the easy formation of hydroxyapatite via the Ti–OH site, corrosion resistance, high stability, and increased bone growth rate) [37].

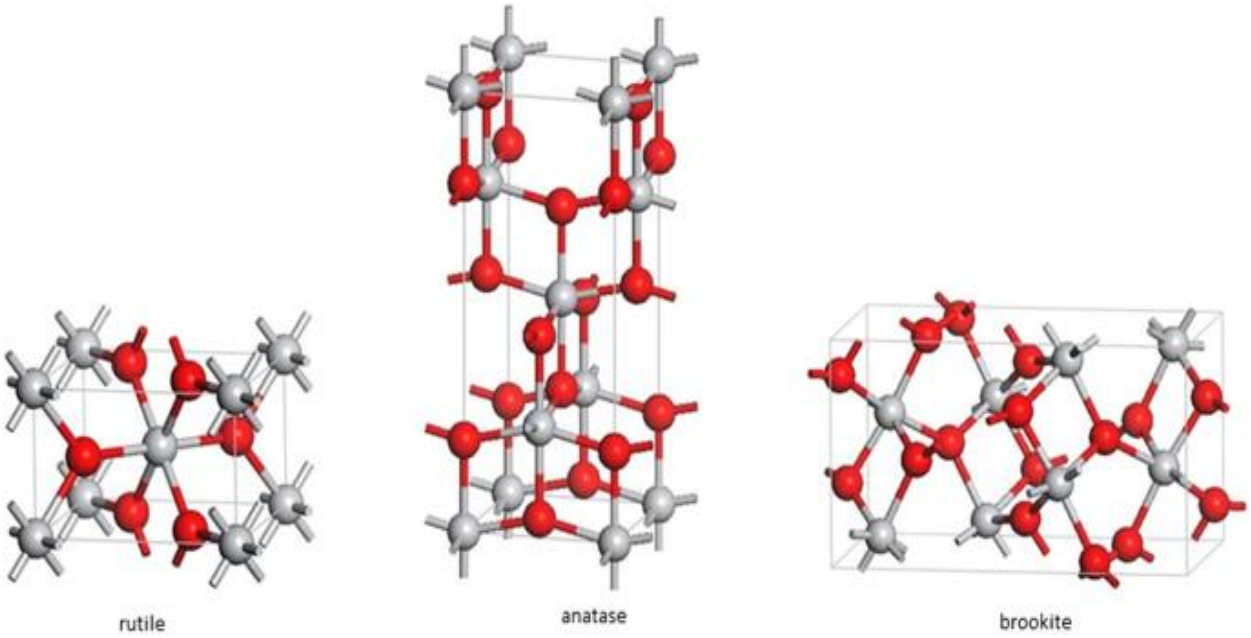

Figure 1.5. Tetragonal structures of crystalline forms of rutile, anatase and brookite TiO_2 NPs [38].

1.7 Tin Dioxide (SnO_2)

The study of semiconductor materials has made a significant contribution to technological advancement. Semiconductor materials are used extensively in electronic devices. Tin dioxide is one of the semiconductor materials. The semiconductor SnO_2 is an N-type semiconductor [39].

SnO_2 is a nanosized material that includes semiconductor materials. SnO_2 is commonly used as a foundation for solar cells, transparent conductive dioxide and gas sensors [40]. SnO_2 has several advantages, including high transparency, sensitivity to gas presence and a band gap of around ($E_g \cong 3.7$) eV [41, 42].

Several previous researchers used sol-gel spin coating, spray pyrolysis, and sol-gel dip-coating to prepare and grow SnO_2 layers, both pure and with doping additives [43]. The sol-gel dip coating method is the simplest, but the resulting layer is less homogeneous. The spray pyrolysis method has several advantages, including uniform and homogeneous size, but the hollow and uneven layer morphology. When compared to the other two techniques, the sol-gel spin coating has the most advantages, namely effective and evenly formed layers that are not hollow [44]. Figure (1.6) show the unit cell of SnO_2 nanoparticles contains two tin and four oxygen atoms, each tin atom is bound to six oxygen atoms at the corners of a regular octahedron, and every oxygen atom is surrounded by three tin atoms the corners of an equilateral triangle [45].

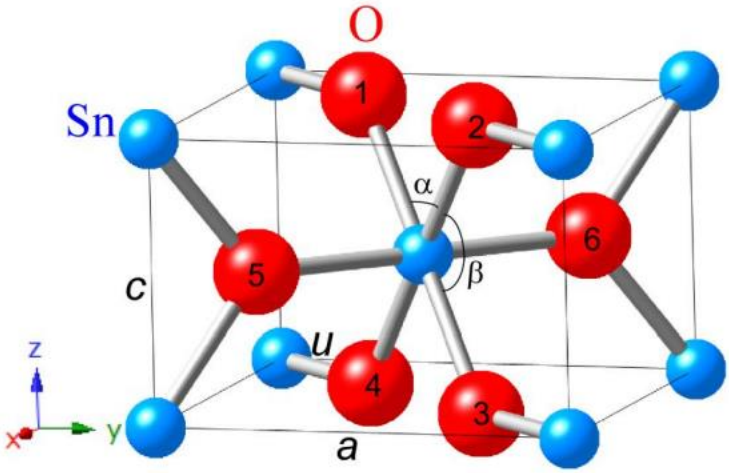

Figure 1.6. Crystal structure of the tetragonal SnO_2 with the cassiterite structure [45].

1.8 Silver Nanoparticles (AgNPs)

Because of their unique physical and chemical properties, silver nanoparticles AgNPs are increasingly being used in a variety of fields, including medicine, food, health care, consumer goods and industry, which among them optical, electrical and thermal properties, as well as high electrical conductivity and biological properties [46]. They have been used as antibacterial agents, in industrial, household and healthcare-related products, in consumer products, medical device coatings, optical sensors, and cosmetics, in the pharmaceutical industry, the food industry, in diagnostics, orthopedics, drug delivery, as anticancer agents, and have ultimately enhanced the tumor-killing effects of anticancer drugs [47]. AgNPs have recently been widely used in a variety of keyboards, wound dressings and biomedical devices. To meet the demand for AgNPs, a variety of synthesis methods have been used. In general, conventional physical and chemical methods appear to be prohibitively expensive and dangerous. Biologically prepared AgNPs, on the other hand, have a high yield, solubility and stability [48].

1.9 Literature Survey

Shaymaa, H. et al., [49], in (2011), have prepared PVA-LiF composites by casting technique , where the optical properties of (PVA-LiF) composite has been investigated with different percentages (0,3,6 and 6) wt.% . Results showed that the absorbance decreases with increase the weight percentage of lithium fluoride, absorption coefficient, extinction coefficient, refractive index and real and imaginary parts of dielectric constants are increasing with increase the lithium fluoride content.

Mustafa, A. et al., [50], in (2013), have been investigated the change in the optical band gap and activation energy for pure and doped Poly (vinyl alcohol) films with different cupper chloride concentrations. The optical properties were measured in the wavelength range from (200-800) nm at room temperature. The optical band gap (E_g) for allowed direct transition decrease with increase the concentration of cupper chloride. The activation energy for allowed direct transition band gap was evaluated using Urbach- edges method.

Vishwas M., et al., [51], in (2014), have used the TiO_2 (5, 10 and 15 mg) nano-particles to study the effect of it on optical, electrical and mechanical properties of poly (vinyl alcohol) (PVA) films were reported. The un-doped PVA films showed high transmittance in the visible region, however with the increase of TiO_2 doping the transmittance has decreased. Also found that the Raman spectrum shows characteristic scattering peaks of the PVA films at 1432, 1145, 920 and 852 cm^{-1} and the peak observed at 637 cm^{-1} is attributed to TiO_2 .

Sabah A., et al., [52], in (2014), have prepared pure polymer (polyvinyl alcohol (PVA)) films were prepared by using casting technique. The films were doped with Ni $(CH_3COO)_2$ salt at different concentrations (2, 4, 6, 8 and 10) wt% to investigate the effect of doping on some optical properties of the prepared films. The absorption and transmission spectra have been recorded in the wavelength range (190-1100) nm. The experimental results for (PVA-Ni $(CH3COO)_2$) films show that the electronic transition is allowed indirect transition, and the energy gap decreases within increasing the filler content. The absorption coefficient, refractive index, extinction coefficient and real and imaginary parts of dielectric constant are calculated and it is found that all these optical parameters are increased with increasing the filler content.

Shehap A., and Dana, [53], in (2016), have used Polymeric films based on polyvinyl alcohol (PVA) doped with titanium dioxide nanoparticles at different weight percentage (1.25, 2.5, 5, 7.5, 10 TiO_2/PVA) were prepared using the sonification and casting techniques. The structural properties of those samples were examined by XRD, FT-IR and UV-Visible .The XRD pattern revealed that the amorphous domain in PVA polymer matrix increased with raising the TiO2 content. The complexation of the dopant with the polymer was examined by FT-IR studies. The absorption spectra of UV-Visible light showed irregular changes of the absorption for high doping samples in UV range (7.5, 10 TiO_2 /PVA). Absorbance, transmittance and reflectance spectra were used for the determination of the optical constants. The results indicated that the optical band gap decreases with increasing TiO_2 content, while the refractive index increased to high value for the composites of high dopant.

Itab F. [54], in (2017), have studied the change in the optical properties for samples of pure PVA and PVA/K_2CrO_4 composite have been studied. The samples

were prepared with different percentage (1, 3, 5 and 7) %wt of K_2CrO_4 by casting method technique. And study the absorption, reflectance spectra, absorption coefficient, energy gap, extinction coefficient and transmittance spectra as a function of wavelength range (200-800) nm, also real and imaginary part of dielectric constant have been studied in the range of wave length. The results exhibit the optical properties change by the increase of K_2CrO_4 concentration, and the values of energy gap for indirect transitions decrease by the increase of the concentration of K_2CrO_4.

Khawla J., and Raja, [55], in (2018), have investigates a detailed study on the optical properties of PVA/Ag nanocomposite films. In this interest, PVA/Ag nanocomposites with different ways of study, the first prepared film by reduction 0.2M of Ag+ ions in 2 gm of PVA and study the transmission absorption coefficient, refractive index, extinction coefficient, reflection, real & imaginary part of the dielectric constant and the energy gap. The results proved that the best values of the absorbency was within the range (350-500) nm, as well as for both they noticed an increase of the refractive index, the extinction coefficient and reflectivity with increasing energy, the second step of research was by using Density Functional Theory (DFT), it was calculate spectrum absorption, intensity and energy gap for the same compound PVA/Ag, the cooperation of polyvinyl alcohol (PVA) nanofibers with silver (Ag) nanoparticles (mean width 8nm) has been displayed utilizing thickness useful hypothesis (DFT) computations. The physical adsorption of PVA through the hydroxyl gathering, to the Ag, were calculated by using DFT theory.

Vanathi V., et al., [56], in (2020), have studied details the impact of stabilizing agents on the structural, optical properties of $AgSnO_2$ core shell nanoparticles and its biological applications. The results were compared to study their effect on the structural and optical properties of the synthesized samples. The optical properties of the samples were investigated using UV–Vis spectra and the

band gap energy were calculated using Tauc plot. The antibacterial and antifungal activities of the chalcone dendrimer stabilized $AgSnO_2$ core – shell nanoparticles were tested against the pathogens Bacillus subtilis, Proteus mirabilis, Candida albicans and Aspergillus niger.

Aseel H., et al., [57], in (2020), have studied structural, optical and electrical properties of PVA/PEO/SnO_2 new nanocomposites for flexible devices, where fabrication of polyvinyl alcohol (PVA)–polyethylene oxide (PEO) blend doped with tin dioxide (SnO_2) nanocomposites has been investigated for flexible electrical and optical applications. The experimental results of optical properties for (PVA–PEO–SnO_2) nanocomposites showed that the nanocomposites have higher absorbance in UV region at wavelength range (200–280) nm. This behavior makes the nanocomposites may be used for optoelectronics applications.

Zeena M. [58], in (2021), have studied influence of nano silicon carbide (SiC) embedded in poly (Vinyl Alcohol) (PVA) lattice on the optical properties, and they notice that the optical parameters increased with increasing the concentration of SiC nanoparticles and also the energy gap for direct transition has decreased from 5.2 eV to 5.0 eV, while the indirect transition reduced from 4.3 eV to 4.0 eV. The results stated that increases in nano SiC in the structure of PVA lattice is accompanied with decreasing the energy gap value.

Alaa M. [59], in (2021), have used in the present work, gallium oxide nanoparticles (nGa_2O_3) are synthesized via the thermal microwave combustion method, while nanocomposites of polyvinyl alcohol (PVA) polymer with various concentrations of nGa_2O_3 (0, 1, 2, 3, 4, and 5 wt. %) are prepared by the casting technique. The structural characterization of nGa_2O_3, PVA, and films of PVA-Ga_2O_3 nanocomposites are studied using X-ray diffraction (XRD), High-resolution transmission electron microscopy (HRTEM), and Fourier-transform infrared spectroscopy. The HRTEM and XRD examinations showed that the prepared

nGa_2O_3 has an average crystallite size of ~5.6 nm and particle size of ~0.9 μm. On another side, the optical transmission spectra were performed in the spectral range 250 to 2500 nm at room temperature.

Soliman T. [60], in (2021), have prepared synthesize barium titanate ($BaTiO_3$) nanocrystalline particles and to fabricate polyvinyl alcohol (PVA) films hosting BaTiO3 in order to enhance structural and optical properties. By means of cast solution, the PVA - $BaTiO_3$ nanocomposite films are prepared. The polymer films are described by X-ray diffractometer (XRD), Fourier-Transform Infrared (FT-IR), UV-Vis spectroscopy and photoluminescence spectroscopy (PL). It is noticed that as the $BaTiO_3$ nanoparticles concentration increases in the PVA matrix, the optical band gap decreases. The extinction coefficient, refractive index, optical conductivity and dielectric constants of the polymer films are also improved.

Morsi, M. [61], in (2022), have prepared synthesize high dielectric constant nanocomposite polymer films based polyvinyl alcohol (PVA) with different weight ratios of nanoparticles TiO_2 (1.0, 2.5, 5.0, and 10 wt %) were prepared by the casting method. The structure of TiO_2 nanoparticles is studied, where the FT-IR spectra show a strong interaction between PVA and TiO_2 nanoparticles. The addition of TiO_2 nanoparticles to the composites improved their mechanical properties. PVA composite films filled with (5.0 wt %) TiO_2 nanoparticles exhibited the highest dielectric constant (ε') reached up to 26 at 25 ◦C and 100 Hz.

1.10 Aim of the study

The principle aims of this study are:

1. Fabrication of new types of (PVA-TiO_2-Ag) and (PVA-SnO_2-Ag) nanocomposites that it used in a wide variety of biomedical applications.
2. To clarify the effect of (AgNPs) concentrations added to the nanocomposites (PVA-TiO_2) and (PVA-SnO_2).
3. To use the prepare nanocomposites in biomedical applications for antibacterial activity of (PVA-TiO_2-Ag) and (PVA-SnO_2-Ag) nanocomposites.

2.1 Introduction

Molecular modeling is a set of techniques for investigating physical and chemical problems on a computer [62]. Computational physician and chemists can employ four main methods, they are molecular mechanics (MM) methods, semi empirical (SE) methods, ab initio methods and density functional theory (DFT) methods.

Schrödinger equation is the fundamental equation to describe the motions of atomic and subatomic system, electrons and nucleus. The time dependent Schrödinger equation is [63]:

$$i\hbar\frac{\partial}{\partial t}\Psi(\vec{r},t) = -\frac{\hbar^2}{2m}\nabla^2\Psi(\vec{r},t) + V(\vec{r},t)\Psi(\vec{r},t) \qquad (2.1)$$

As:

$$\hat{H}\Psi(\vec{r},t) = E\Psi(\vec{r},t) \qquad (2.2)$$

Where $\hat{H}$ is the energy operator or the Hamiltonian, acting on the wave function, and ∇^2 is the second derivative of the Laplacian, one will get the product of the eigenvalue E with the wave function Ψ(r, R). When the operator Hˆ is dependent of time, the Schrödinger equation then become well-known time-independent equation written for a molecular system as [64]

$$\hat{H}\Psi(\vec{r},R) = E\Psi(\vec{r},R) \qquad (2.3)$$

Where Ψ $(\vec{r},R)$ is the total wave function of the molecular system, r and R are the electron and the nuclei spatial coordinates, respectively, E is the total energy of the system and H the total Hamiltonian of the molecular system containing M nuclei and N electrons [65]:

$$\hat{H} = -\frac{1}{2}\sum_{i=1}^{N}\nabla_i^2 - \sum_{A=1}^{M}\frac{1}{2m_A}\nabla_A^2 - \sum_{i=1}^{N}\sum_{A=1}^{M}\frac{Z_A}{r_{iA}} + \sum_{i=1}^{N}\sum_{j>i}^{N}\frac{1}{r_{ij}} + \sum_{A=1}^{M}\sum_{B>A}^{M}\frac{Z_A Z_B}{r_{AB}} \quad (2.4)$$

Or

$$\hat{\mathrm{H}}_e = \hat{T}_e + \hat{T}_n + \hat{V}_{ne} + \hat{V}_{ee} + \hat{V}_{nn} \quad (2.5)$$

Where ($\hat{T}_e$) and ($\hat{T}_n$) are the electronic and nuclear kinetic energies, respectively, ($\hat{V}_{ne}$) is the attractive interactions between nuclei and electrons, ($\hat{V}_{nn}$) is repulsive interactions between the nuclei and ($\hat{V}_{ee}$) is repulsive electron-electron interactions. The system can actually be described as all electrons moving in a potential field of nuclei with fixed positions [66].

In Born-Oppenheimer Approximation, the electronic motion and the nuclear motion in molecules can be separated and the total wave function of a molecule takes the form [67]:

$$\Psi_{total} = \Psi_{electronic} \times \Psi_{nuclear} \quad (2.6)$$

The nuclear motion is much slower than the electronic motion because the nucleus is much heavier than the electrons. It could be considered as constant. The kinetic energy of nuclei is eliminated and the potential energy of nuclei-nuclei could be considered as fixed [68]. In terms of this, the kinetic energy of nuclei and the potential energy of nuclei-nuclei can be eliminated from the Hamiltonian operator, and the Hamiltonian operator $\hat{H}_e$ is simplified as following [69]:

$$\hat{H}_e = \hat{\mathrm{T}}_e + \hat{V}_{ne} + \hat{V}_{ee} \quad (2.7)$$

2.2 Density Functional Theory (DFT)

DFT has proven hugely successful in the calculation of structural properties of condensed matter systems and the electronic properties of simple metals. Its advantages include less demanding computational effort, less computer time, and in some cases better agreement with experimental values than is obtained from other procedures. The premise behind DFT is that the energy of a molecule can be determined from the electron density instead of a wave function [70, 71].

The original theorem applied only to finding the ground-state electronic energy of a molecule [72]. DFT focuses on the much simpler electron density $\rho(r)$. In general, the electron density is the number of electrons N per unit volume for a given state. It is dependent only on three coordinates independently of the number of electrons of the system, thus [73, 74]:

$$N = \int \rho(\vec{r}) d\vec{r} \qquad (2.8)$$

The difference between the methods of density function theory is the method of choosing the shape of function to calculate the energy of bonding and exchange.

2.3 The Hybrid Functional

Another set of functionals that are widely used are the hybrid exchange-correlation functionals. These combine the density function theory (DFT) with Hartree- Fock theory (HF). The most popular hybrid functional B3LYP (Becke's3 parameter exchange correlation functional which uses 3 parameters) and LYP (The Lee, Yang and Parr correlation functional) [75, 76].

$$E_{XC}^{B3LYP} = E_{XC}^{LDA} + a_0 (E_X^{HF} - E_X^{LDA}) + a_X (E_X^{GGA} - E_X^{LDA}) + a_c (E_c^{GGA} - E_c^{LDA}) \qquad (2.9)$$

Where a_0 = 0.20, a_X =0.72 and a_c= 0.81 are the three empirical parameters, E_X^{GGA} and E_c^{GGA} are the generalized gradient approximation formulated and E_X^{LDA} is the local density approximation of the exchange energy [77].

2.4 Basis Sets

A basis set is a set of functions used to describe the shape of the orbitals in an atom. Molecular orbitals and wave functions are created by taking linear combinations of basis functions. Most semi empirical methods use a predefined basis set. When Ab initio or (DFT) calculations are done, a basis set must be specified. Although it is possible to create a basis set from scratch, most calculations are done using existing basis sets. The type of calculation performed and basis set chosen are the two biggest factors in determining the accuracy of results. The basis set functions must be chosen to have a form that is useful in a physical sense [78-80]. That is, the functions should have large amplitude in regions of space where the electron probability density (the wave function) is also large, and small amplitudes where the probability density is small [81].

We can find electron distribution around the nucleus using several methods such as the use of hydrogen similarity functions, which are based on the Schrödinger equation for the hydrogen atom, or by the polynomial functions with adjustable coefficients. In addition, we also have the functions of Slater and Gauss functions (or Gaussian functions) [82].

2.4.1 Slater Type Orbitals (STOs)

Slater-type orbitals (STOs) are functions used as atomic orbitals in the linear combination of atomic orbitals molecular orbital method. They are named after the physicist John C. Slater, who introduced them in 1930. A typical (STO) is expressed as [83, 84]:

$$\chi^{STO} = Nr^{n-1}e^{-\xi r}Y_{lm}(\theta,\varphi) \quad (2.10)$$

Here *N* is the normalization constant, *r* is the distance of the electron from the atomic nucleus, n is a principal quantum number, ξ is a constant related to the effective charge of the nucleus, i.e. the nuclear charge being partly shielded by electrons. Y_{lm} is a spherical harmonic which describes the angular part of the wave function [85,86].

2.4.2 Gaussian Type Orbitals (GTOs)

GTOs can be written in terms of Cartesian coordinates as [87]:

$$X^{GTO} = Nx^{l_x}y^{l_y}z^{l_z}e^{-\xi r^2} \quad (2.11)$$

The sum of $l_x, l_y \; and \; l_Z$ determines the type of orbitals, ξ represents the orbital exponent. The r^2 dependence in the exponential is a deficiency of the (GTO) with respect to the Slater-Type Orbitals (STO). GTOs have two main problems. First an improper behavior nears the nuclei at $r \rightarrow 0$, second problem is that GTO falls off too rapidly far from the nuclei compared with the STO.

A rough estimate that three times as many GTOs as STOs are required in order to reach the same level of accuracy [88-90]. One of the disadvantages of STOs is that many-center integrals such as Coulomb and HF-exchange terms are difficult to compute with STOs. Therefore, it does not play a role in modern wave function based quantum chemistry codes. One of the advantages of the Gaussian basis set is that the product of two Gaussian functions is another Gaussian function. As a result, for the calculations of Coulomb and HF-exchange terms the analytical solution is available for the Gaussian functions. Therefore the GTO basis function in HF and related methods is popular because very efficient algorithms exist for analytically calculating the many-center integrals [91, 92].

In order to improve the GTO basis sets, one usually employs a contracted GTO basis set, in which several primitive Gaussian functions are mixed to give a contracted Gaussian function (CGF) as [93]:

$$\chi_j^{CGF} = \sum_i^M C_{ij}\chi_a^{GTO} \quad (2.12)$$

Here, M is the number of Gaussian primitives used in a linear combination and C_{ij} are the orbital expansion coefficients. The basis sets used in Gaussian are classified into minimal basis sets, split valence sets, polarization and diffuse functions and others [94].

2.4.2.1 Minimal Basis Sets

The minimal basis set is the minimum number of basis functions needed to describe the ground states of the component atoms in a molecule. A common name of minimal basis sets is STO-nG, the n (n=2 to 6) represents the number of Gaussian primitive functions that comprise a single basis function. In these basis sets, the same number of Gaussian primitives comprises core and valence orbitals. Minimal basis sets typically give rough results that are insufficient for research-quality publication, but are much cheaper than their larger counterparts. The following are examples of commonly used minimal basis sets: STO-2G, STO-3G, STO-6G [93, 94].

2.4.2.2 Split-Valence Basis Sets

The inner-shell atomic orbitals in terms of a split-valence basis set are represented by one basis function and the valence orbitals are represented by two or more basis functions. One easy method to extend a basis set is to increase the number of basis set functions used per orbital.

Split-valence basis sets employ more than one basis function of variable orbital exponents for each valence orbital and only one basis function for each core orbital. For instance, the valence double-zeta (VDZ) basis set uses two basis set functions per valence orbital while the valence triple-zeta (VTZ) uses three, and so on. While the split valence basis sets provide a better description of the molecular orbitals because they allow for variable atomic size, they still are not able to provide a balanced basis set on their own [95].

2.4.2.3 Polarization and Diffuse Functions

Polarization functions are functions of higher angular momentum such as d- type and f-type functions for heavy atoms and p-type and d-type functions for hydrogen and helium atoms [96]. This increases the flexibility of the basis set by allowing the shape of the orbital to change (i.e., become polarized in one direction). The inclusion of polarization functions can be important for systems in which hydrogen is involved such as hydrogen-bonding and proton transfers since these will allow the s-orbital to become distorted from its regular spherical shape. Polarization functions are used because they often result in more accurate computed geometries and vibrational frequencies [97].

The addition of polarization functions is indicated in brackets after the contraction scheme while diffuse functions denoted by '+'. For instance, the 6-31++G (d, p) basis set includes a set of d-type functions on all heavy atoms and p-type functions on hydrogen and helium. The first '+' indicates that diffuse s-type and p-type functions are included on heavy atoms, while the second '+' indicates that diffuse s-type functions have been included on hydrogen [98, 99].

2-5 Gaussian 09 (G09) Program

One of the famous programs in computational chemistry can work in the operating system windows and Linux and there are copies of capacities32 bit and 64 bit. All of the computational calculations were performed using the Gaussian 09 Revision- A.02 SMP suite of program with GUI (Graphical User Interface) called Gauss view, version 5.0.8 (GV5 for short) [95]. Gaussian 03 Revision B.01 with Gauss view 3.07(GV3for short) [100]. The '09' and '03' refer to the year 2009 and 2003, respectively, in which the software was published. G09 is the most recent version. G09 contains about 500,000 lines (very approximate) of FORTRAN and C++ code. Initiated by Sir John Pople (shared Nobel Prize with Walter Kohn in 1998) in the late 1960, the first distributed Gaussian package was labeled Gaussian 70 [101].

2.6 Structural Properties

The arrangement of atoms in the molecules and more specifically the electrons around the atom determine the energy level of that molecule. In fact, the energy of a molecular system varies even with small changes in its structure. This is why geometry is so important when performing calculations. The objective of a geometry optimization is to find the point at which the energy is at a minimum because this is where the molecule is most stable and most likely to be found in nature. All molecules possess geometry, characterized by [102]:

1. Number and types of atoms
2. Number and types of bonds
3. Relevant bond lengths r: $0 \leq r \leq \infty$(in units of angstroms (Å))

4. Relevant bond angles $\theta: 0 \leq \theta \leq 180°$ (in units of degrees)
5. Relevant dihedral angles: $-180° \leq \phi \leq 180°$ (an angle between four atoms, which signifies the 3-dimensional shape of the molecule).

Geometry optimization is a standard physical-chemistry calculation to find the lowest energy or largest relaxed conformation for a molecule. The approach is involving an iterative process, at each step, the molecular geometry is modified slightly and the energy of the molecule is compared with the last cycle. The computer moves the molecule a little, calculates the energy, moves it a little more, and keeps going until it finds the lowest energy. This is the minimum energy of the molecule and obtained at the optimized geometry [103,104].

2.7 Electronic Properties

2.7.1 HOMO, LUMO and Band Gap

The two most important molecular orbitals MOs are called the frontier orbitals in which they lie at the outmost boundaries of the electrons of the molecules, these MOs are the highest occupied molecular orbital HOMO and the lowest unoccupied molecular orbital LUMO. The HOMO, which is the highest energy orbital containing electrons, is the orbital acting as an electron donor. Inversely, the LUMO, is the lowest energy orbital having space to accept electrons. The energy gap is the difference of the energies between the two orbitals HOMO and LUMO [105]:

$$E_g = E_{LUMO} - E_{HOMO} \qquad (2.13)$$

HOMO and LUMO and their resulting energy gap not only determine the way of the molecule interacts with other species, but their energy gap (frontier orbital gap) helps characterize the chemical reactivity and kinetic stability of the molecule.

2.7.2 Total Energy, Ionization Energy and Electron Affinity

Total energy for a system is the sum of total kinetic and potential energy, at the optimized structure that the total energy of the molecule must be at the lowest value because the molecule is at the equilibrium point this means that the resultant of the effective forces is zero [106].

The ionization Energy (I_E) for a molecule is the amount of energy required to remove an electron from an isolated atom or molecule and expressed as the energy difference between the positive charged energy $E_{(+)}$ and the neutral $E_{(n)}$ according to the following relation:

$$I_E = E_{(+)} - E_{(n)} \quad (2.14)$$

The electron affinity (E_A) of a molecule or atom is the energy change when an electron added to the neutral atom to form a negative ion and expressed as the energy difference between the neutral energy $E_{(n)}$ and the negative charged energy $E_{(-)}$ according to the following relation:

$$E_A = E_{(n)} - E_{(-)} \quad (2.15)$$

In molecular orbital (MO) theory within the limitation of Koopmans´ theorem [107], the orbital energies of the frontier orbitals are given by:

$$I_E = -E_{HOMO} \quad (2.16)$$

$$E_A = -E_{LUMO} \quad (2.17)$$

Where E_{HOMO} is the energy of highest occupied molecular orbital, and E_{LUMO} is the energy of lowest unoccupied molecular orbital.

2.7.3 Electrophilicity (ω) and Electronegativity (χ)

The Electrophilicity is definition as an index measures the stabilization in energy when the system acquires an additional electronic charge from the environment [105]. On the other word, it can be defined as a measure of energy lowering due to maximal electron flow between donor and acceptor [108].

$$\omega = \frac{\kappa^2}{2\eta} \qquad (2.18)$$

Where κ chemical potential is associated with the negative of the electronegativity, η is the chemical hardness. We might define the electronegativity (it is defined as the power of an atom in a molecule to attract electrons to itself) as the negative of the electronic chemical potential [109]:

$$\chi = -\kappa = -\left[\frac{\partial E}{\partial N}\right]_V \qquad (2.19)$$

R. Mulliken defined electronegativity as the average of the ionization energy and electron affinity as follows [110]:

$$\chi = \frac{(IE+EA)}{2} \qquad (2.20)$$

And according to Koopmans' theorem, it can be defined as the negative value for average of the energy levels of the HOMO and LUMO [111,112]:

$$\chi = -\frac{(E_{HOMO}+E_{LUMO})}{2} \qquad (2.21)$$

Where χ is electronegativity.

So electronegativity is a measure of the tendency to attract electrons by an atom in a chemical bond and defined as the negative of the chemical potential in DFT [81,112].

2.7.4 Chemical Hardness (η) and Chemical Softness (S)

The chemical hardness (η) is a measure of the resistance to charge transfer. The theoretical definition of chemical hardness has been provided by the (DFT) as the second derivative of electronic energy with respect to the number of electrons N, for a constant external potential V(r) [108]:

$$\eta = \frac{1}{2}\left[\frac{\partial^2 E}{\partial N^2}\right]_V = \frac{1}{2}\left[\frac{\partial K}{\partial N}\right]_V = -\frac{1}{2}\left[\frac{\partial \chi}{\partial N}\right]_V \quad (2.22)$$

Finite difference approximation to chemical hardness gives,

$$\eta = \frac{IE-EA}{2} \quad (2.23)$$

The hard molecule has a large energy gap and the soft molecule has a small energy gap. In quantum theory, changes in the electron density of system result from the mixing of suitable excited state wave functions with the ground state wave function. A small energy gap means small excitation energies to the manifold of excited states. Therefore, soft molecules have small energy gaps. Their electron density change more easily than a hard molecule, and due to that, soft molecules will be more reactive than hard molecules [107].

The chemical softness S, is a property of molecules that measures the extent of chemical reactivity. It is the inverse of the chemical hardness (η)[113]:

$$S = \frac{1}{2\eta} = \left[\frac{\partial^2 N}{\partial E^2}\right]_V = \left[\frac{\partial N}{\partial K}\right]_V \quad (2.24)$$

2.8 Optical Properties

The search of optical properties has increased because of their applications in integrated optics like optical information, optical modulation and optical data storage. The study of optical absorption is useful for elucidation of the electronic

structure and determine the direct and indirect transitions [114]. The addition of nanoparticles in polymer improves the electrical, optical and mechanical properties of the materials. The developments of polymer nanocomposite structures are because of their ease of processing and production, good adhesion with reinforcing elements, light weight, resistance to corrosive environment and in some cases ductile mechanical performance [115,116].

2.8.1 Absorbance (A) and Transmittance (T)

Optical properties of materials are very important due to it can obtain information about the internal structure, the nature of the bonds and their employment by knowing the amount of absorbance, reflectance and transmittance of these materials [117]. The optical properties for polymers has wide applications in optical devices and electronic devices like fuel cells, solar cells, solid state batteries and medical technological applications [118].

The absorption coefficient α can be calculated from the optical spectrum by the following equation [119,120]:

$$\alpha = 2.303(A/t) \quad (2.25)$$

Where, t is the sample thickness and A is defined by log (I_0/I) where I_0 and I are the incident intensity and transmitted intensity beams, respectively. The direct and indirect transitions, the simplified general equation is [121]:

$$\alpha h \upsilon = B(h \upsilon - E_g)^m \quad (2.26)$$

Where, υ is the frequency, B is a constant, h is Planck's constant E_g is the energy band gap between the valence band and the conduction band, and m can take the values 2, 3, 1/2 or 3/2 for transitions designated as indirect allowed, indirect forbidden, direct allowed and direct forbidden, respectively, as shown in

Figure (2.1). The calculation of values of optical energy band gap includes the plotting of $(\alpha h \upsilon)^{1/m}$ against $h \upsilon$ [122-126].

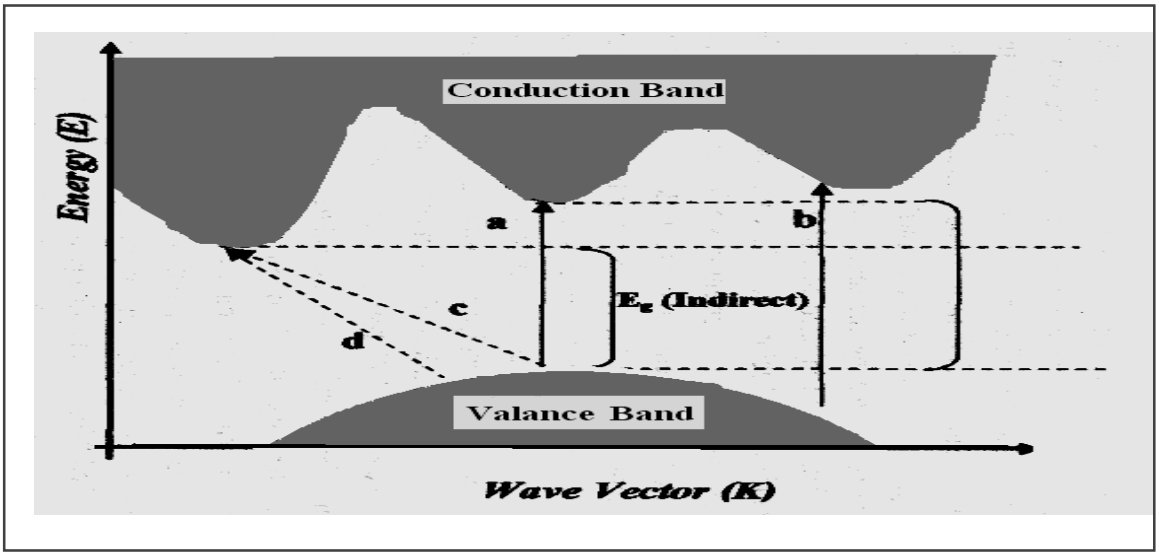

Figure 2.1. The transition process [124].

(a) Allowed direct transition. **(c) Allowed indirect transition.**

(b) Forbidden direct transition. **(d) Forbidden indirect transition.**

The transmission (T) has been determined from values of reflectance (R), and absorbance (A), using the relation [127]:

$$A + R + T = 1 \qquad (2.27)$$

2.8.2 Absorption Regions

Absorption regions can be classified to three regions [128]:

A) High absorption region: the magnitude of absorption coefficient (α) is larger or equal to (10^4 cm^{-1}).

B) Exponential region: the value of absorption coefficient (α) is equal to ($1\ cm^{-1} < \alpha < 10^4\ cm^{-1}$).

C) Low absorption region: the absorption coefficient (α) is very small, it is about ($\alpha < 10^4 cm^{-1}$), as shown in Figure (2.2) which shows the absorption regions.

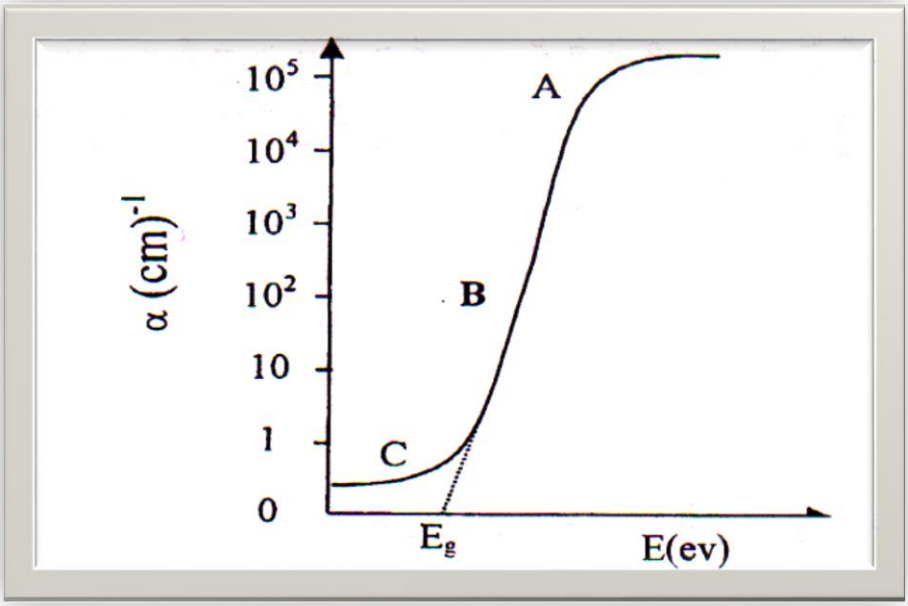

Figure 2.2. Absorption regions [128].

2.8.3 Refractive Index and Extinction Coefficient

The index of refraction of a material is the ratio of the velocity of the light in vacuum to that of the specimen [129]:

$$n = \frac{c}{V} \quad (2.28)$$

Where (c) is the velocity of the light in vacuum and (v) is the velocity of the light in sample.

$$n^* = n - i\,k \quad (2.29)$$

Where: n^* is complex refractive index, n is real part of refractive index and k is imaginary part of refractive index (extinction coefficient).

The relation between absorption coefficient and the extinction coefficient (k) is

$$k = \frac{\alpha\,\lambda}{4\,\pi} \quad (2.30)$$

Here λ is the wavelength.

The real part of refractive index (n) can be determined by [130]:

$$n = \frac{1+\sqrt{R}}{1-\sqrt{R}} \quad (2.31)$$

Where R is the reflectance to estimate the nature of absorption.

2.8.4 Dielectric Constant and Optical Conductivity

The complex permittivity represents the relationship between the electric and magnetic fields in a material. The imaginary part is directly related to the resistivity, while the real part means the material has a capacitive or inductive optical response. The real part and the imaginary part of the dielectric constant was obtained using relations [131].

$$\varepsilon = (\varepsilon_1 - i\,\varepsilon_2) \quad (2.32)$$

$$\varepsilon_1 = (n^2 - k^2) \quad (2.33)$$

$$\varepsilon_2 = (2nk) \quad (2.34)$$

The optical conductivity (σ) has been determined by [132]:

$$\sigma = \frac{\alpha\, nc}{4\pi} \quad (2.35)$$

2.9 Fourier Transform Infrared Radiation (FT-IR)

Fourier Transform Infrared Radiation (FT-IR) is a technique used to obtain an infrared spectrum of absorption or emission of a solid, liquid or gas. FT-IR spectrometer simultaneously collects high-spectral-resolution data over a wide spectral range. This confers a significant advantage over a dispersive spectrometer, which measures intensity over a narrow range of wavelengths at a time. The term Fourier-transform infrared radiation originates from the fact that a Fourier transform (a mathematical process) is required to convert the raw data into the actual spectrum [133].

2.10 Scanning Electron Microscope (SEM)

A scanning electron microscope (SEM) is a type of electron microscope that produces images of a sample by scanning the surface with a focused beam of electrons. The electrons interact with atoms in the sample that contain information about the samples surface topography. The most common SEM mode is detection of secondary electrons emitted by atoms excited by the electron beam. The number of secondary electrons can be detected depending on specimen topography [134].

3.1 Introduction

In this chapter, we will be explain how to prepare samples of (PVA-SnO_2-Ag) and (PVA-TiO_2-Ag) nanocomposites. The measurements that were tested for the samples, it's included optical measurements, Fourier Transform Infrared Radiation FT-IR, and scanning electron microscope (SEM). Also the application of antibacterial activity was measured.

3.2 The Materials were Used in This Work

For the purpose of obtaining the nanocomposite, several materials were used with specific weight ratios. These materials include:

3.2.1 Polymer: The polymer is used in this work:

Poly (Vinyl Alcohol) (PVA): This type of polymer is found in powder from US Research Nanomaterials, Inc, USA with very high purity (99.8%).

3.2.2 Metals dioxide Nanoparticles

1. **Tin dioxide nanoparticles (SnO_2):** used as powder with particle diameter (50-70) nm from EPRUI Company and high purity (99.9%).
2. **Titanium dioxide nanoparticles (TiO_2):** used as powder from Nano Shell USA company with size (30-50) nm and high purity (99.9%).
3. **Silver nanoparticles (Ag):** used as powder with particle diameter (20) nm from EPRUI Company and high purity (99.9%).

3.3 Preparation of Nanocomposites (PVA-SnO_2-Ag) and (PVA-TiO_2-Ag)

Initially, powdered polyvinyl alcohol (PVA) was dissolved at a concentration of (0.5) gm in (50) ml of distilled water, using a magnetic

stirrer which is a device widely used in laboratories and consists of a rotating magnet or a stationary electromagnet that creates a rotating magnetic field.

Then the solution was poured into the mold (petri dish with10 diameter). after that nanocomposites of (PVA-SnO_2-Ag) and (PVA-TiO_2-Ag) were prepared by dissolving (0.485) gm of PVA with (0.0075) gm of SnO_2 of the nanocomposites (PVA-SnO_2) and (0.0075) gm of TiO_2 for (PVA-TiO_2) nanocomposites in 50 ml of distilled water, using a magnetic stirrer to mix the polymer and nanoparticles for 30 min to obtain a more homogeneous solution at room temperature. Then AgNPs was added to (PVA-SnO_2) and (PVA-TiO_2) at different concentrations which are (0.0075, 0.015, 0.025 and 0.03) gm. The casting method is used to prepare samples of (PVA-SnO_2-Ag) and (PVA-TiO_2-Ag) in a mold (petri dish with10 diameter). The thickness of the prepared samples was measured using a digital micrometer, the thickness range was (0.01-0.009) cm. Table (3.1) Weight percentages for nanocomposites, and Figure (3.1) show the diagram of Schematic of work.

Table 3.1. Weight percentages for nanocomposites (PVA-SnO_2-Ag) and (PVA-TiO_2-Ag)

PVA gm	SnO_2 gm	TiO_2 gm	Ag gm	Weight of Sample
0.5	0	0	0	0.5 gm
0.485	0.0075	0.0075	0. 0075	
0.47	0.015	0.015	0.015	
0.45	0.025	0.025	0.025	
0.44	0.03	0.03	0.03	

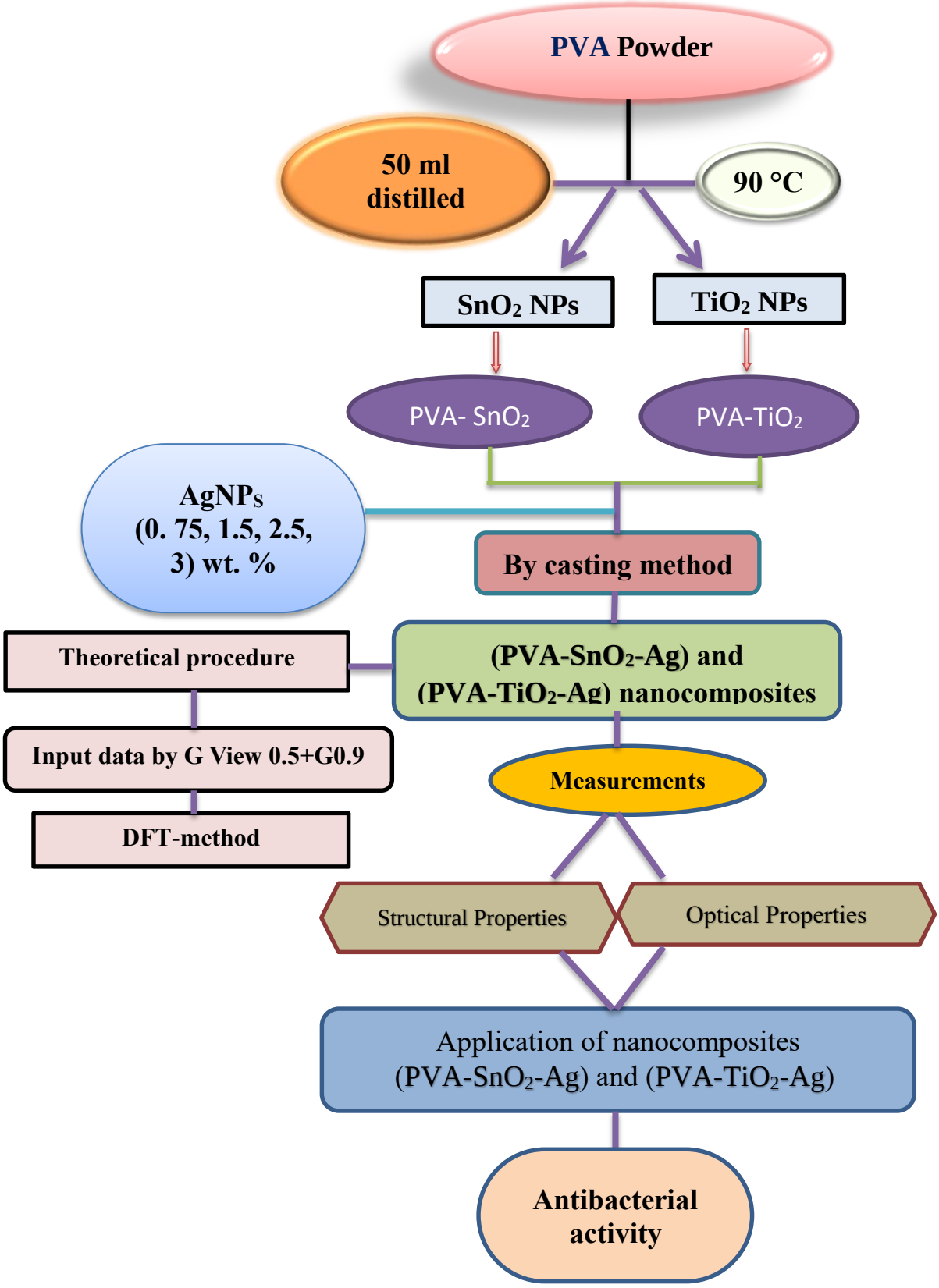

Figure 3.1. Schematic of work.

3.4 Measurements of Structural Properties for (PVA-SnO_2-Ag) and (PVA-TiO_2-Ag) Nanocomposites

3.4.1 FT-IR Spectrometer

FT-IR spectra for of (PVA-SnO_2-Ag) and (PVA-TiO_2-Ag) nocomposites were recorded by FT-IR (Bruker Company, German origin, type vertex-70). In University of Babylon, College of Education for Pure Sciences. Fourier transform infrared spectrometer in wavenumber range (1000-4000) cm^{-1}.

3.4.2 Optical Microscopic

The (PVA-SnO_2-Ag) and (PVA-TiO_2-Ag) nanocomposites samples are examined by using the optical microscope (supplied from Olympus name (Toup View) type (Nikon-73346) in University of Babylon, College of Education for Pure Sciences.

3.4.3 Scanning Electron Microscope

The surface morphology of (PVA-SnO_2-Ag) and (PVA-TiO_2-Ag) nanocomposites for concentration (0. 75wt. %), (1.5wt. %), (2.5wt. %) and (3 wt. %),were tested by using scanning electron microscope (ARYA Electron Company) in Tehran University, Iran.

3.5 Optical Properties Measurements for (PVA-SnO_2-Ag) and (PVA-TiO_2-Ag) Nanocomposites

The optical properties of (PVA-SnO_2-Ag) and (PVA-TiO_2-Ag) nanocomposites are measured by using the double beam spectrophotometer (Shimadzu, UV-1800Å) in wavelength (220-820) nm.

3.6 Antibacterial Activity Application Measurements of for (PVA-SnO_2-Ag) and (PVA-TiO_2-Ag) Nanocomposites

Certain types of bacteria were used to determine their sensitivity to nanocomposites (PVA-SnO_2-Ag) and (PVA-TiO_2-Ag), as the sensitivity of four types of bacteria was studied, namely: Bacillus cereus, Stenotrophomonas maltophilia, Escherichia coli, Salmonella.

Salmonella is a genus of Gram-negative bacteria that are pathogenic to the gastrointestinal tract or may cause typhoid fever. While Escherichia coli is also a Gram-negative, rod-shaped coliform bacterium of the genus Escherichia commonly found in the lower intestine of warm-blooded organisms. Stenotrophomonas maltophilia is an aerobic, nonfermentative, Gram-negative bacterium. It is an uncommon bacterium and human infection is difficult to treat [135]. While Bacillus cereus is a Gram-positive, rod-shaped, facultative anaerobic, motile, spore-forming bacterium commonly found in soil, food and marine sponges [136].

4.1 Introduction

The results of the structural, optical and electronic properties of the pure PVA polymer as well as the nanocomposites (PVA-SnO_2-Ag) and (PVA-TiO_2-Ag) were discussed in this current work. Also studying effect of nanomaterials like Titanium dioxide (TiO_2), Tin dioxide (SnO_2) and Silver nanoparticles (AgNPs) on properties belong to polymer composite. Ground-state calculations are theoretically performed using density function theory (DFT) and the Gauss View program at the B3LYP level with Basis set (SDD). Time-dependent self-consistent field DFT (TD-SCF) methods with base function (B3LYP) and (SDD) basis set are used to calculate excited states.

While experimental results includes structural and optical measurements of the proposed pure PVA and its nanocomposites. The current work presents the results and discussion of the structural, electronic, and optical properties of pure materials (PVA), (PVA-SnO_2), (PVA-TiO_2), (PVA-SnO_2-Ag) and (PVA-TiO_2-Ag) nanocomposites. Following the discovery of theoretical and practical calculations for these characteristics, a comparison was made between the theoretical and experimental results.

The polymer's and its nanocomposites' antibacterial activity was also discussed in terms of applications.

4.2 The Structural Properties of Pure PVA and its Nanocomposites

4.2.1 Optical, Scanning Electron Microscope and Molecular Geometry

Figures (4.1, 4.2) show the optical microstructure, so they express the morphology of the prepared samples. Figure (4.1-A) show the diffusion of pure PVA with a perfect homogeneity. Sample (4.1-B) is represented of mixing pure PVA with (SnO_2-Ag). From this sample assembly there is a homogeneous distribution between the polymer and (SnO_2-Ag), Figure (4.1- C, D, E) characterize the mixture (PVA-SnO_2) with a different percentage of AgNPs where we note that the nanoparticles are uniformly distributed within the mixture (PVA-SnO_2). Figure (4.2-A) shows the pure polymer (PVA) which is uniformly distributed upon the surface morphology of the samples (PVA-TiO_2), Figure (4.2-B-D) indicates the uniform distribution of AgNPs. The nanoparticles form a paths network inside the (PVA-TiO_2-Ag) and (PVA-SnO_2-Ag) nanocomposites [137, 138]. In contrast, the geometrical optimization of nanocomposites was theoretical calculated. The (PVA-SnO_2-Ag) and (PVA-TiO_2-Ag) structures were designed using Gauss View 5.0.8 and relaxed using the Gaussian 09 package of programs by employing the DFT with the B3LYP/SDD level. The optimized relax structure of polymer pure (PVA) (75 Atoms), (PVA-SnO_2) (74 Atoms), (PVA-TiO_2) (74 Atoms), (PVA-SnO_2-Ag) (74 Atoms) and (PVA-TiO_2-Ag) (74 Atoms) is shown in Figures (4.3). Table (4.1) shows the optimized parameters for (PVA-SnO_2-Ag) and (PVA-TiO_2-Ag) involving the bond length in Angstrom ($^{\circ}$A) and bond angle in degree. The calculated bond values in this work agree well with previous studies which in the Table (4.1), indicating that a relax was obtained for polymer pure (PVA), (PVA-SnO_2), (PVA-TiO_2), (PVA-SnO_2-Ag) and (PVA-TiO_2-Ag) with appropriate SDD basis sets.

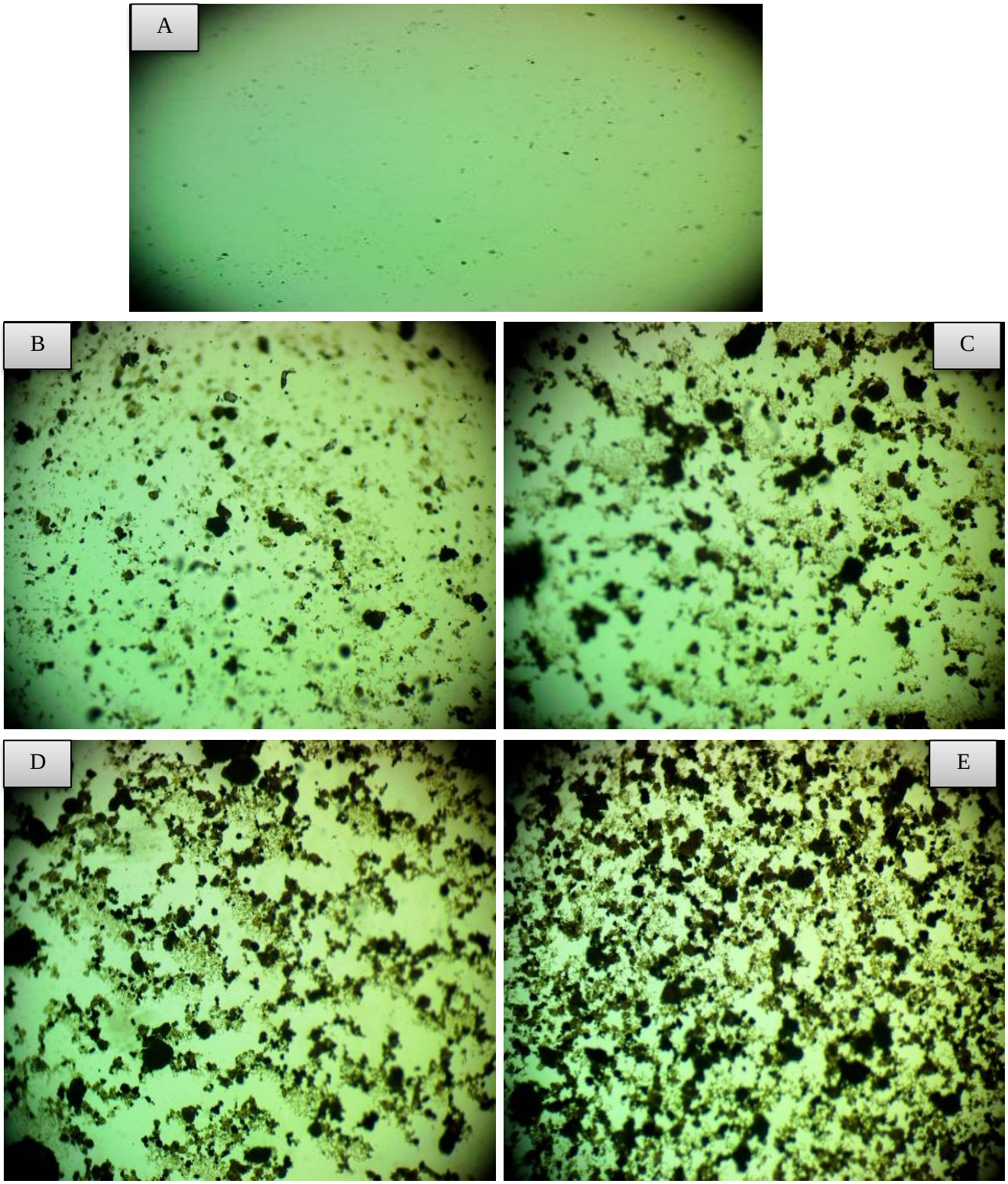

Figure 4.1. Photomicro graphs (× 10) for (PVA-SnO_2-Ag) nanocomposites. A- for pure PVA, B- for (PVA-SnO_2-Ag) nanocomposite for 0.75 wt.% Ag NPs, C-for 1.5 wt.% Ag NPs and D- for 2.5 wt.% Ag NPs, E- for 3 wt.% Ag NPs.

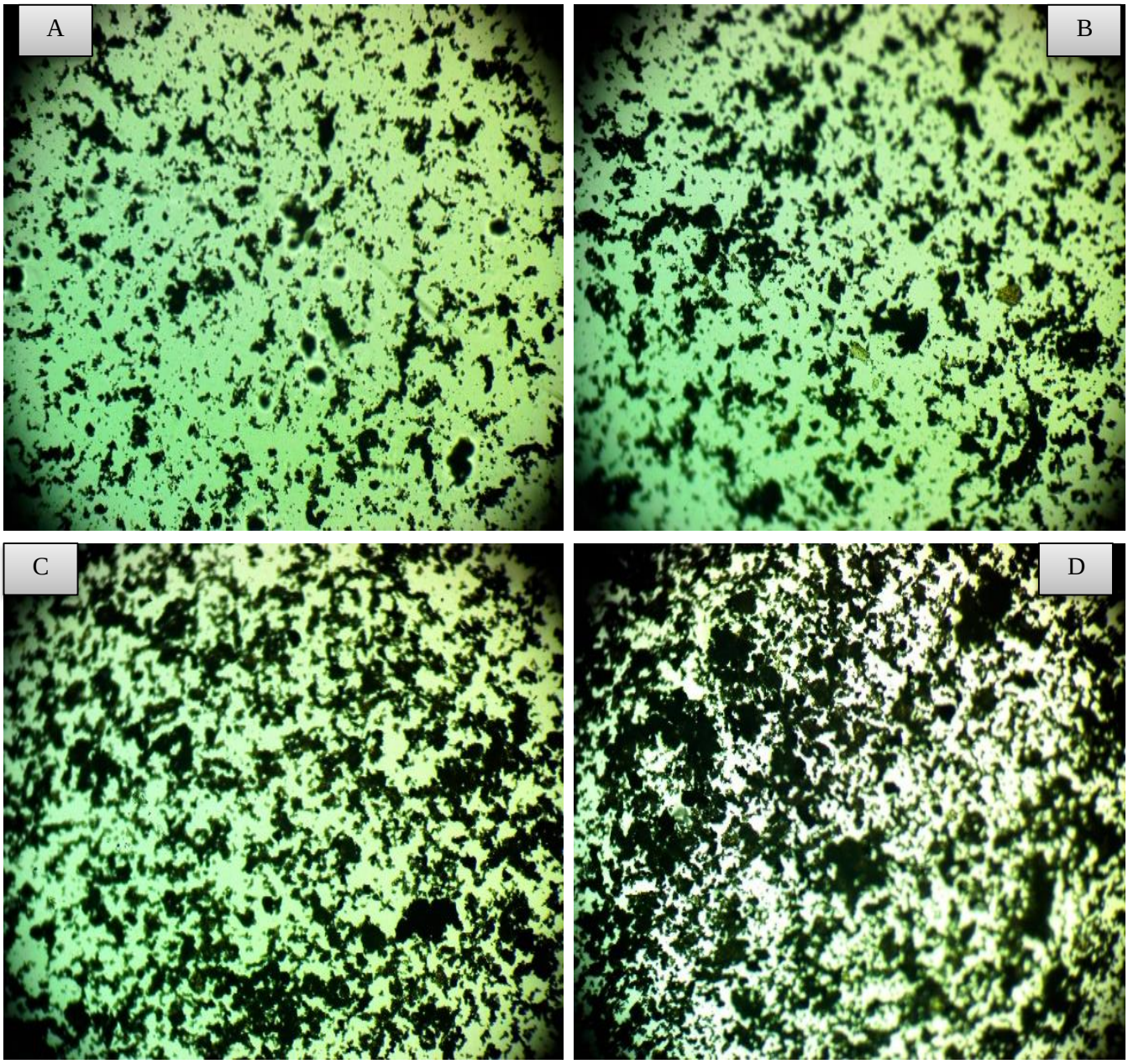

Figure 4.2. Photomicro graphs (× 10) for (PVA-TiO_2-Ag) nanocomposites. A- for (PVA-TiO_2-Ag) nanocomposite for 0.75 wt.% Ag NPs, B-(PVA-TiO_2-Ag) for 1.5 wt.% Ag NPs and C- for 2.5 wt.% Ag NPs, D-(PVA-TiO_2-Ag) for 3 wt.% Ag NPs.

The pure polymer (PVA)	
(PVA-SnO_2) nanocomposites	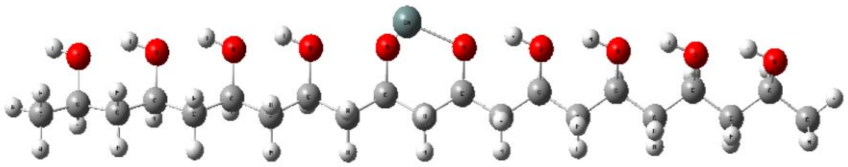
(PVA- TiO_2) nanocomposites	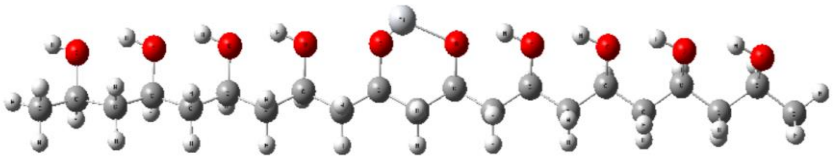
(PVA-SnO_2-Ag) nanocomposites	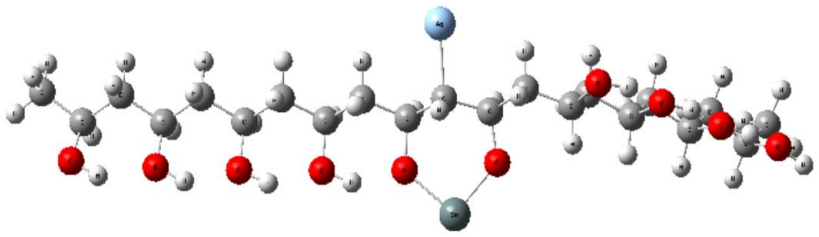
(PVA-TiO_2-Ag) nanocomposites	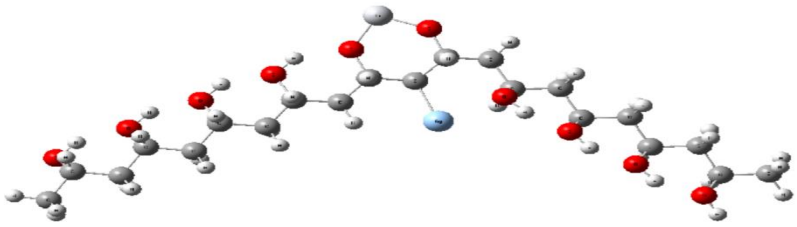

Figure 4.3. The relax structures of the pure polymer (PVA) and its nancomposite.

The results show that adding nanoparticles to polymer and it is nanocomposite has direct effect on bond length and angle between atoms. To be more specific, as well as result show that all bond length and angle between atoms are an agreement with experimental calculation [139-141].

We can conclude that the bond (O-H) is the shortest bond in molecules, this is due to the weak bonding between atoms. The difference in angle values (C-C-C, H-O-C, H-C-H, C-C-H, and O-Ti-O) can also be seen in the same Table, and this difference is due to the difference in atomic numbers, which affects the strength of their interaction. To be more specific, it is discovered that the geometric parameters obtained from the DFT calculations agree well with those obtained from previous studies which in the Table (4.1)

Table 4.1. B3LYP/ SDD-DFT calculations of bond length in angstroms (Å) and bond angle in degree of pure PVA and its nanocomposites.

linear	The optimization parameters	Present work	The previous studies
Bond Length (Å)	**(C–C)**	**1.531-1.055**	**1.510 [142]**
	(C–O)	**1.473-1.507**	**1.478[143]**
	(O–H)	**0.978-1.003**	**0.993 [144]**
	(C–H)	**1.096-1.106**	**1.098 [145]**
	(O–Sn)	**1.012-2.060**	**-**
	(C–Ag)	**1.710-2.110**	**-**
	(O–Ti)	**1.040-1.980**	**2.299 [146]**
Bond Angle (degree)	**(C–C–C)**	**110.796-120.791**	**109.014[147]**
	(H–O–C)	**106.759-111.958**	**109.132 [148]**
	(H–C–H)	**106.772-108.963**	**-**
	(C–C–H)	**108.977-109.890**	**109.63 [149]**
	(O–C–H)	**106.270-109.269**	**109.95 [150]**
	(C–C–O)	**109.867-108.2983**	**-**
	(O–Ti–O)	**96.413-113.970**	**-**
	(C–C–Ti)	**107.722**	**-**

The scanning electron microscope is one of the most important microscopic imaging devices for studying the structural properties of samples, it is characterized by enlarging the image with a high resolution of up to (100000) times, and it gives us images of the sample surface in black and white color.

Where the SEM microscope use to find images of the samples and the effect of nanoparticles on the crystal structure of nanocomposites. Figures (4.4, 4.5) shows images of silver nanoparticle concentrations in (PVA-SnO_2) and (PVA-TiO_2) nanocomposites. Through SEM analysis found that micrograph of pure PVA as showed in Figure (4.4-A) represent a surface for pure PVA without any impurities [151].

While Figures (4.4, 4.5-B-E) show SEM images of (PVA-SnO_2-Ag) and (PVA-TiO_2-Ag) nanocomposites for the purpose of studying the morphology of the nanocomposites and the distribution of the network-like nanoparticles AgNPs distributed on the surface of the pure polymer . SEM images show that the network of pathways of AgNPs formed inside the nanocomposites (PVA-SnO_2) and nanocomposites (PVA-TiO_2) as the passage of charge carriers is allowed through the paths. It was found that these results are in agreement with the results of previous studies [152].

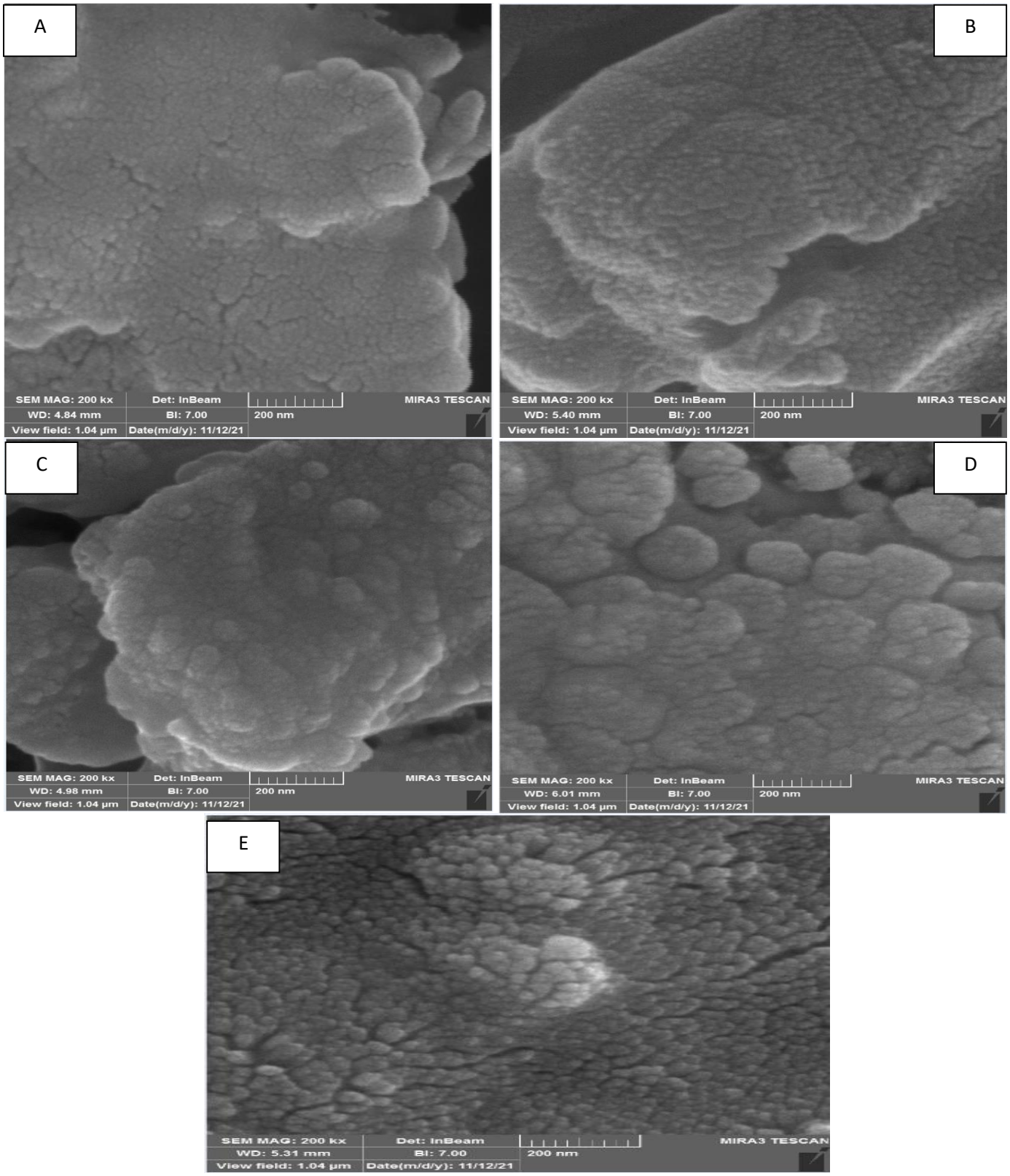

Figure 4.4. SEM images (×200 nm) of (PVA-SnO_2-Ag) nanocomposites. A- for pure PVA B- for (PVA-SnO_2-Ag) nanocomposites for 0.75 wt.% Ag NPs, C- for 1.5 wt.% Ag NPs , D- for 2.5wt.% Ag NPs, and E- for 3 wt.% Ag NPs.

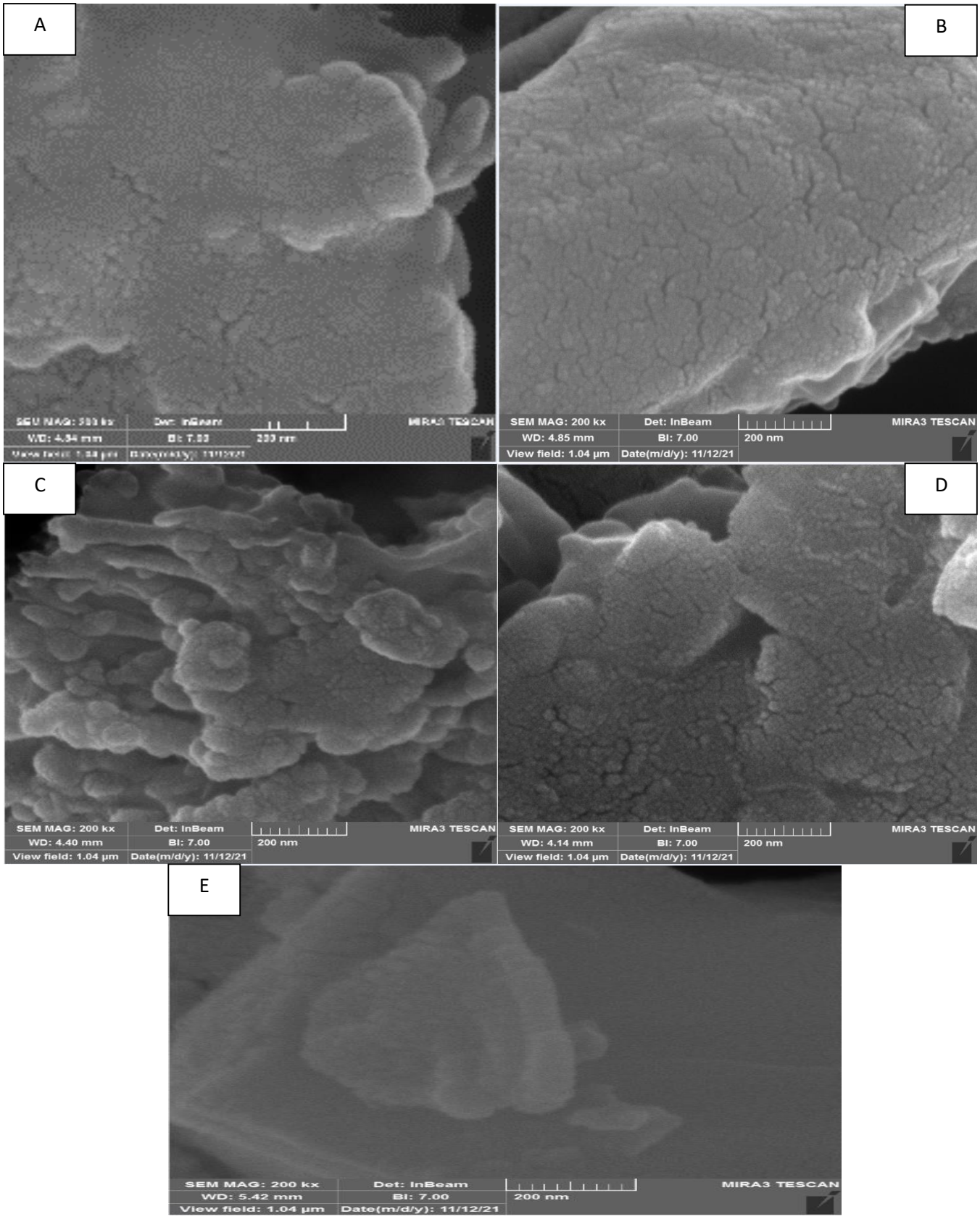

Figure 4.5. SEM images (×200 nm) of (PVA-TiO_2-Ag) nanocomposites. A- for pure PVA B- for (PVA-TiO_2-Ag) nanocomposites for 0.75 wt.% Ag NPs, C- for 1.5 wt.% Ag NPs , D- for 2.5wt.% Ag NPs, and E- for 3 wt.% Ag NPs.

4.2.2 Fourier Transform Infrared Radiation (FT-IR) of Nanocomposites

In this part investigate the Fourier transformation infrared radiation (FT-IR) of the pure and doped nanocomposite, it is necessary to determine the free radical of systems. The active group of the prepared materials was diagnosed using infrared spectroscopy, and the Figures (4.6, 4.7) and (4.8-4.12) represent the infrared spectrum of the samples experimental and theoretical. It is noticed from the Figures (4.6, 4.7), which represent the infrared spectrum of the nanocomposite model, the wave number of the peaks (836.70, 1085) cm^{-1} represents the active group (Ti–O) and (C–C) stretching, [153,154]. The appearance of an absorption band at the wave number (1415.33, 2906) cm^{-1}, which represents the active group (C–O) bending and (C–H) stretching, respectively [154]. The band at (3265.61) cm^{-1} is attributed to the (O–H) stretching groups [155]. While in the Figures (4.8-4.12), for the nanocomposites (PVA-SnO_2-Ag), the result showed that the absorption band at (1350.03) cm^{-1} represent (–CH_2) bending, the peak at (2998.35) cm^{-1} represent (C–H) symmetric stretching vibration [156]. The strong bands at (3054.69, 3212.68 and 3429.85) cm^{-1} represents (–CH_2), (–CH_3) and (O–H) symmetric stretching, asymmetric stretching and stretching vibration, respectively [157, 158]. The peaks at (1128.96, 693 and 396.56) cm^{-1} represents (C–C), (O–Sn–O) and (Ag–C) stretching and bending, asymmetric stretching and stretching vibration, respectively [159]. While for the nanocomposites (PVA-TiO_2-Ag) it show broad bands at around (3411.26, 3150.08) cm^{-1} for the samples of nanocomposites represents (O–H) groups and (–CH_2), stretching and asymmetric stretching, respectively [160, 161]. The region at (1503.28) cm^{-1} is attributed to the (C–C) stretching and binding vibration. While the region at (899.905) cm^{-1} is attributed to the (O–Ti–O) symmetric stretching

vibration [162]. The peaks at (2997.56, 720.93) cm^{-1} represents (C–H) and (Ag–C) symmetric stretching, stretching vibration, respectively [156].

So the figures shows that when SnO_2 or TiO_2 is added to the PVA, there is no new peak or bond that is specific to SnO_2 or TiO_2. However, we only see a change in the number of PVA peaks, which remains within the specified range. The FT-IR calculations of the samples show that the addition of AgNPs causes a displacement of some bonds rather than the emergence of new peaks, which is the basic idea of nanocomposites. There was more than one approximate value for all samples with the results of the mentioned experiment when comparing the theoretical value and the experimental value.

A Pure PVA (0.5 gm PVA)	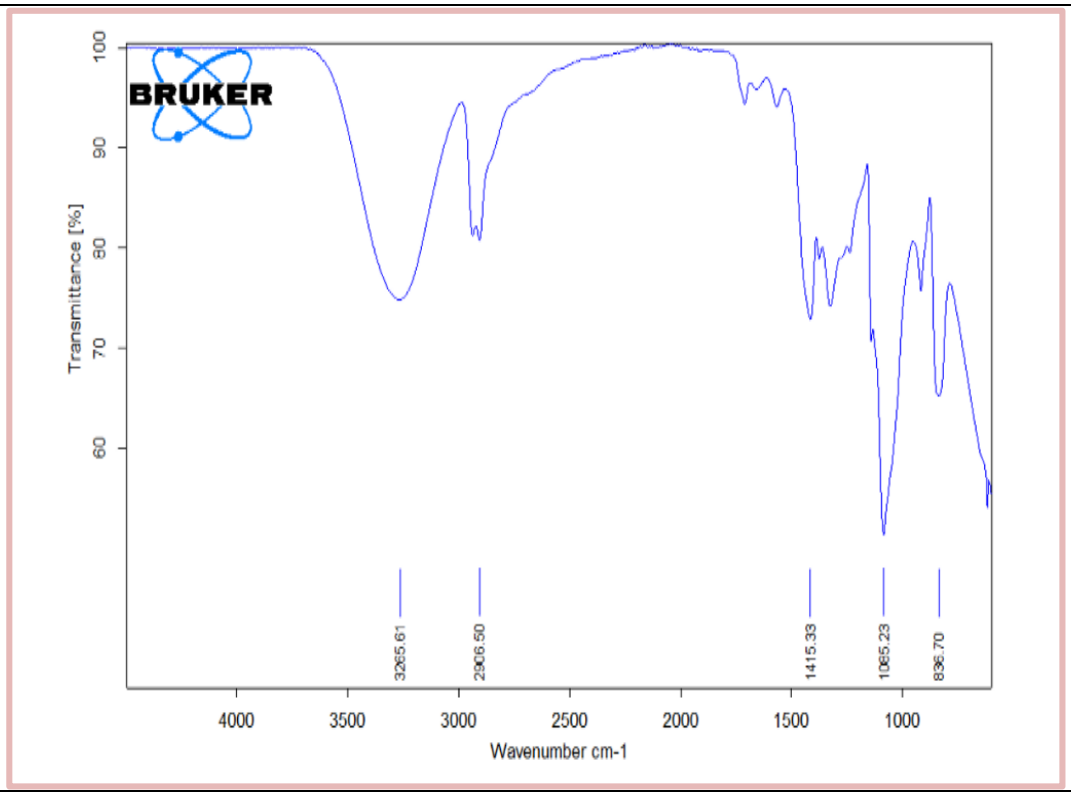

B **(PVA-SnO_2-Ag)** (0.485 gm PVA 0.0075 gm SnO_2 0.0075 gm Ag)	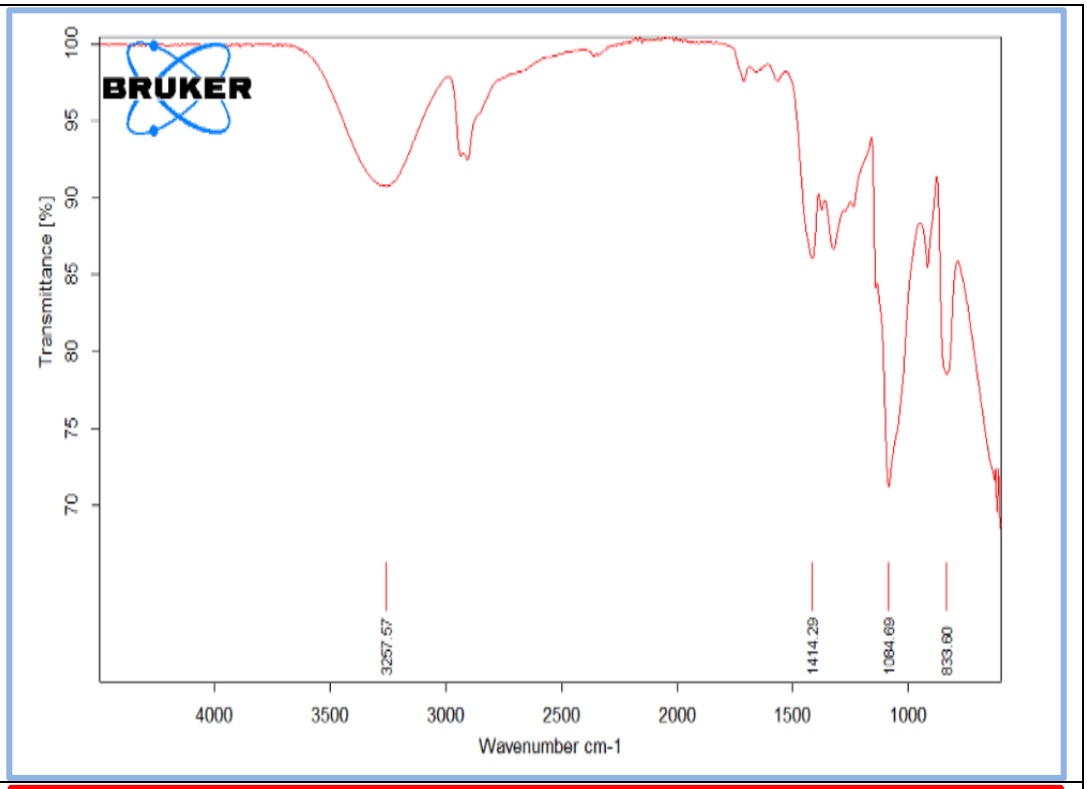
C **PVA-SnO_2-Ag)** (0.47 gm PVA 0.015 gm SnO_2 0.015 gm Ag)	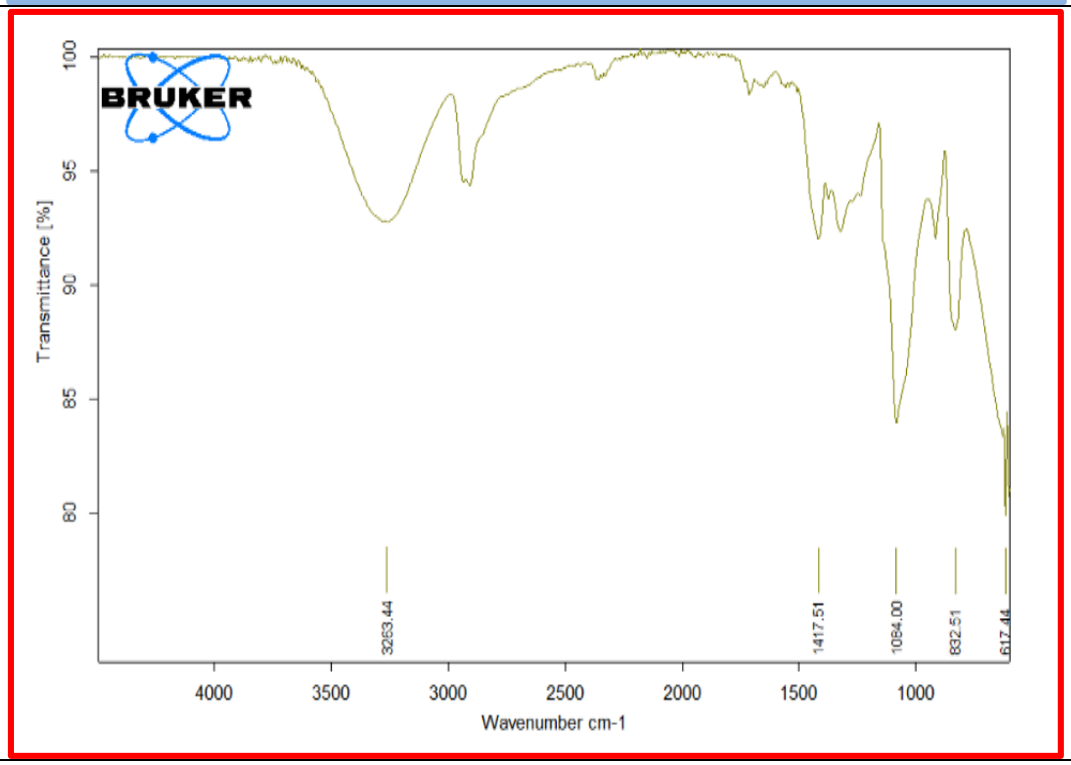

D **(PVA-SnO_2-Ag)** (0.455 gm PVA 0.0225 gm SnO_2 0.025 gm Ag)	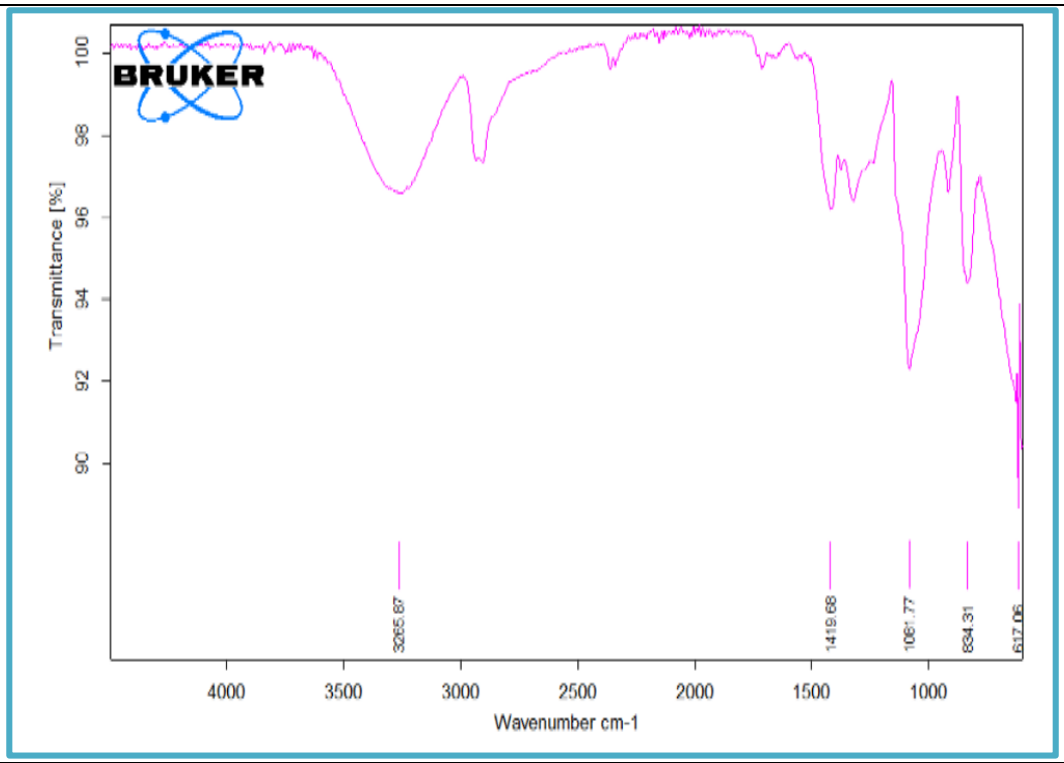
E **(PVA-SnO_2-Ag)** (0.44 gm PVA 0.03 gm SnO_2 0.03 gm Ag)	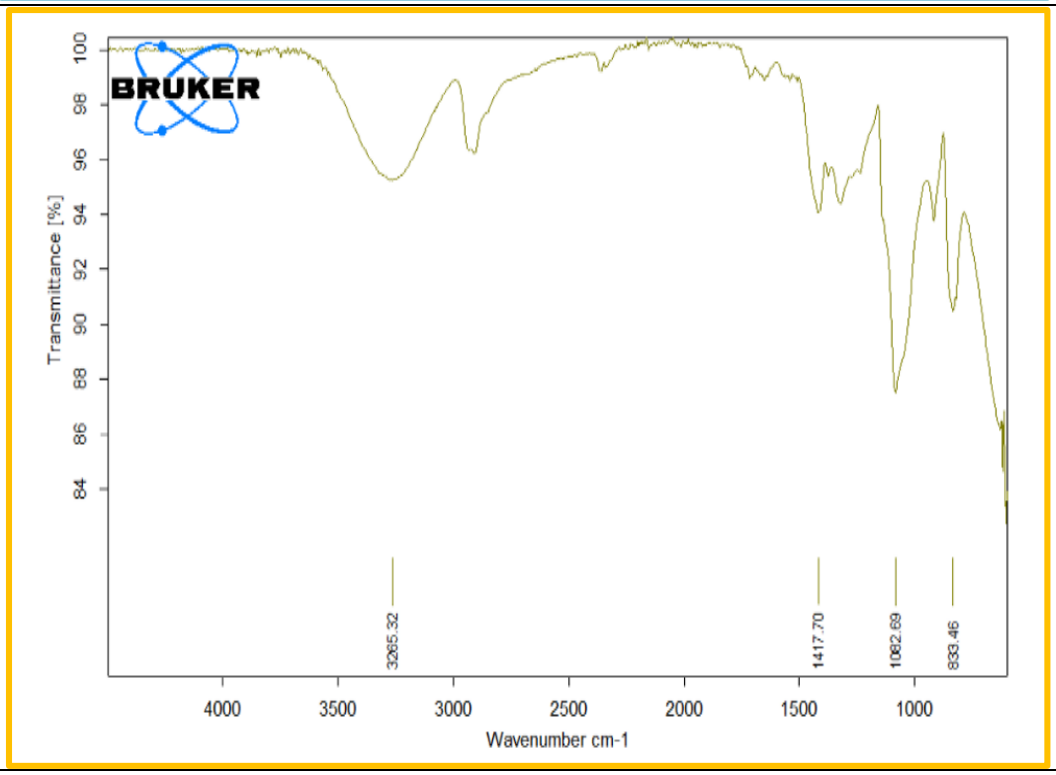

Figure 4.6. FT-IR spectra for (PVA- SnO_2-Ag) nanocomposites (experimentally).

A Pure PVA (0.5 gm PVA)	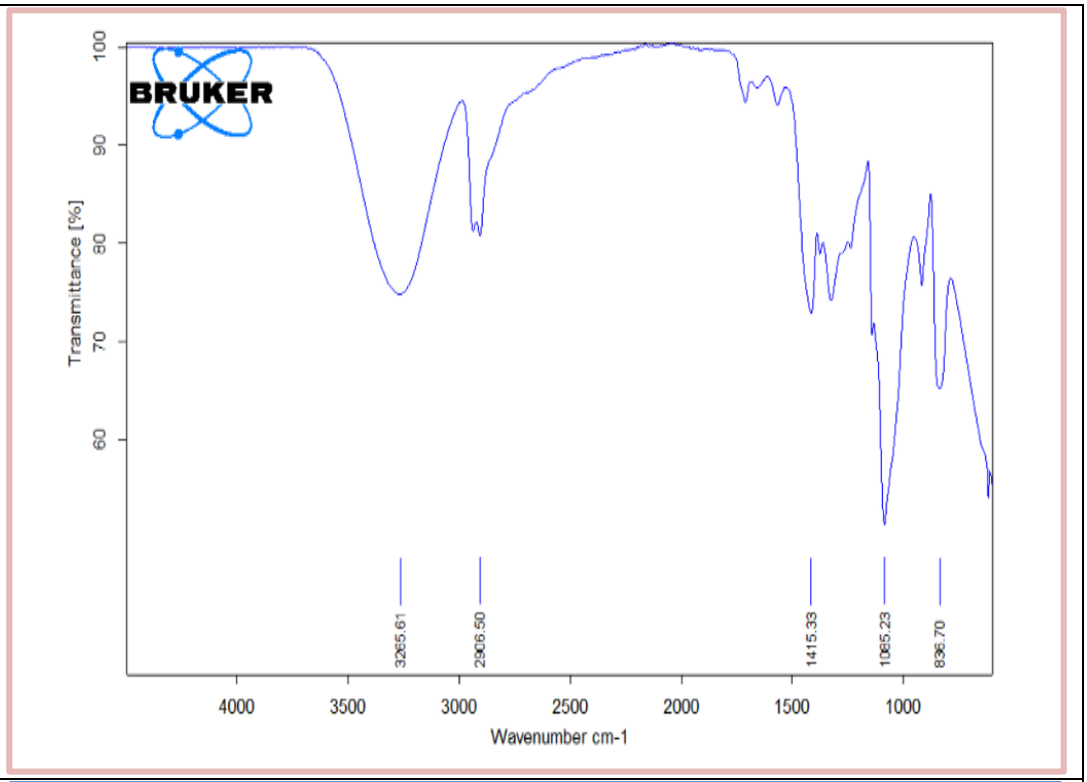
B **(PVA-TiO_2-Ag)** (0.485 gm PVA 0.0075 gm TiO_2 0.0075 gm Ag)	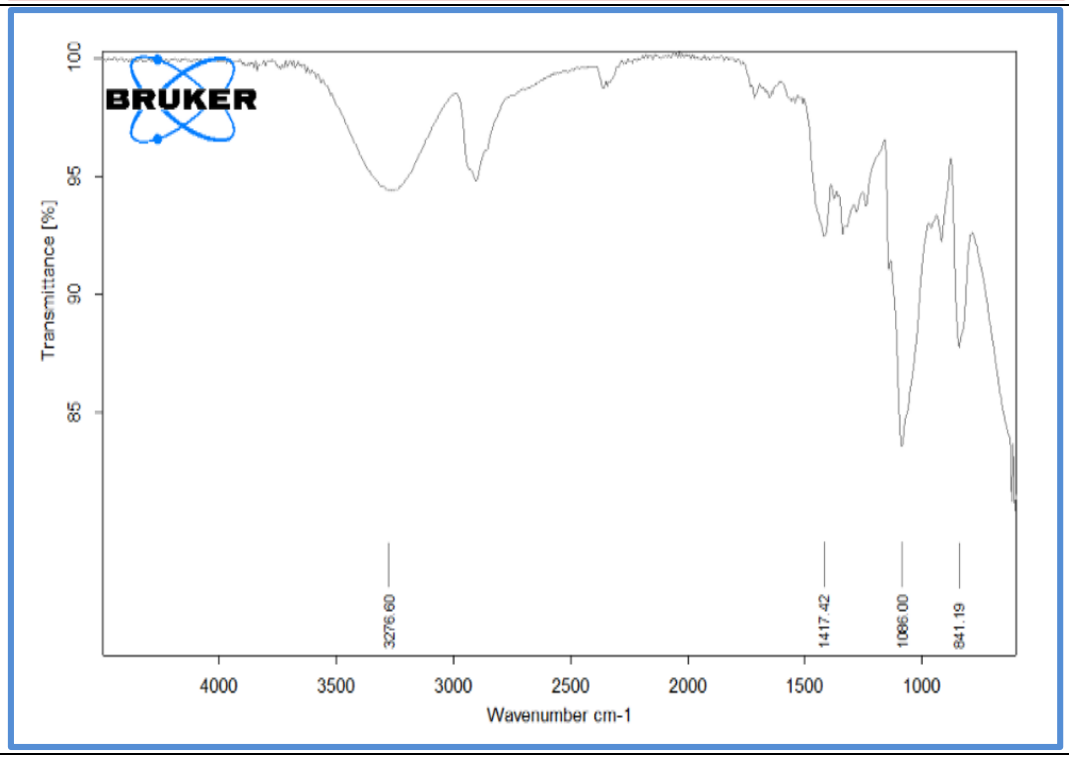

C **(PVA-TiO_2-Ag)** (0.47 gm PVA 0.015 gm TiO_2 0.015 gm Ag)	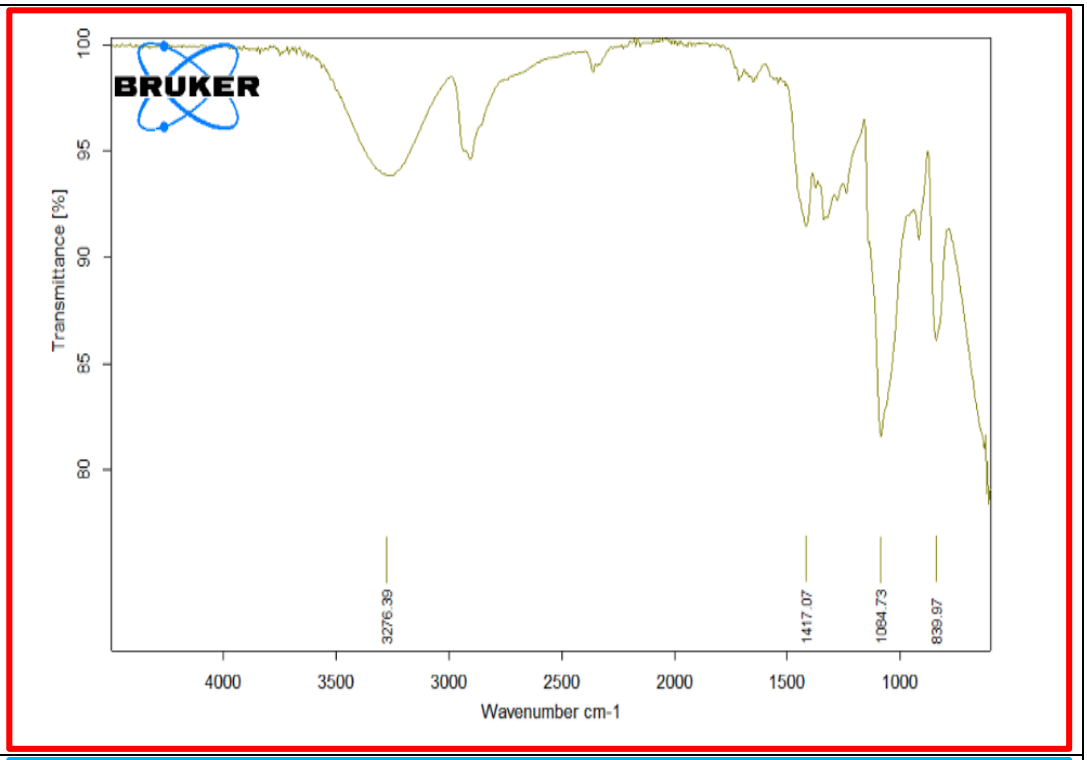
D **(PVA- TiO_2-Ag)** (0.455 gm PVA 0.0225 gm TiO_2 0.025 gm Ag)	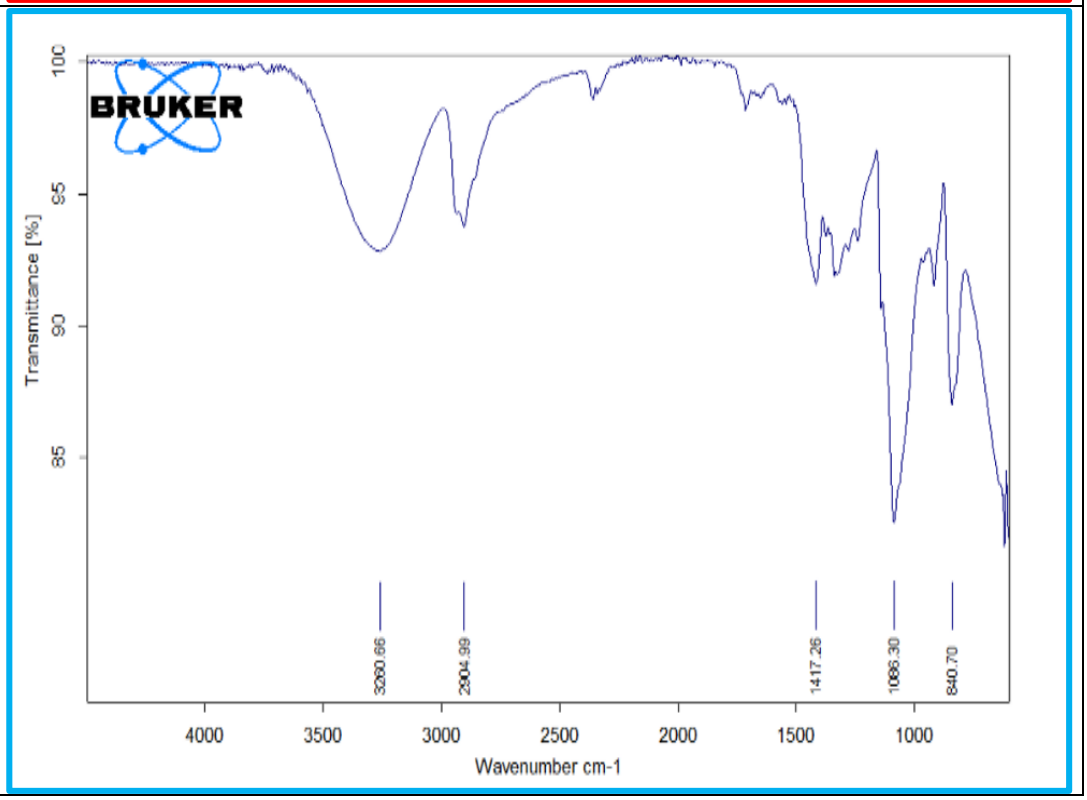

E **PVA- TiO_2-Ag)** (0.44 gm PVA 0.03 gm TiO_2 0.03 gm Ag)	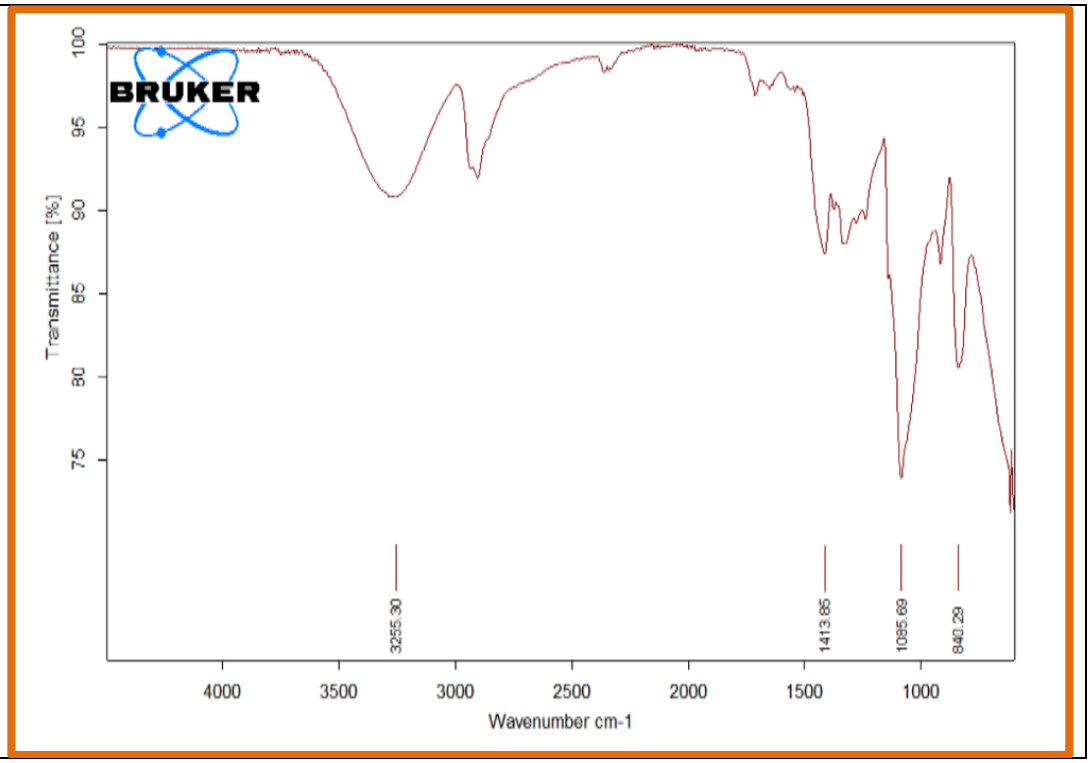

Figure 4.7. FT-IR spectra for (PVA-TiO_2-Ag) nanocomposites (experimentally).

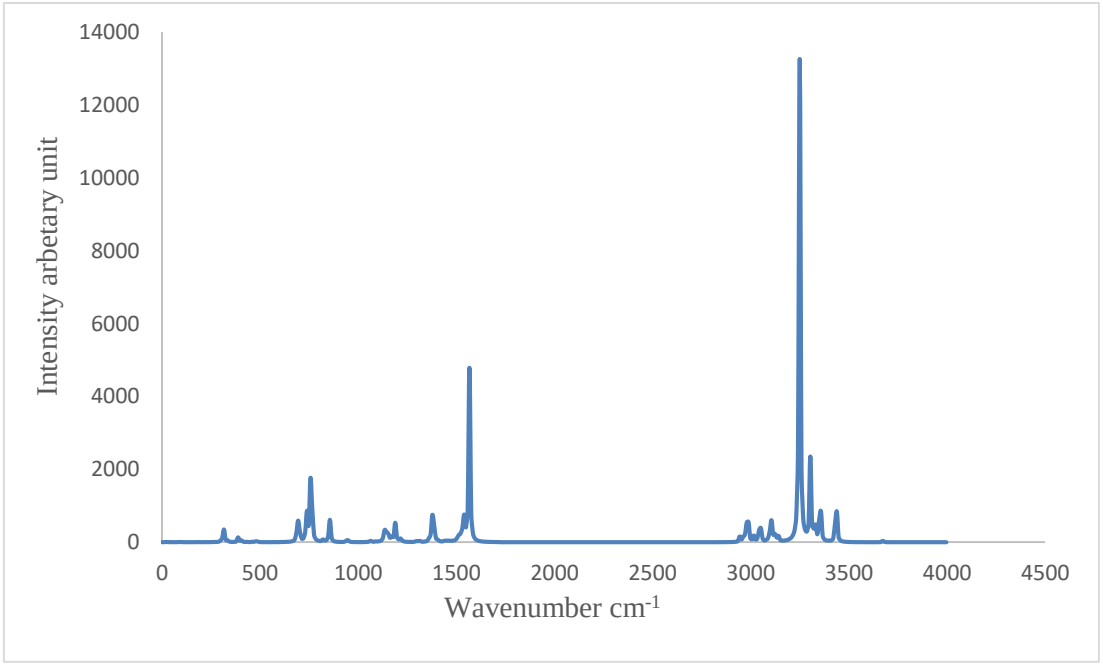

Figure 4.8. IR-spectra of pure PVA (theoretical).

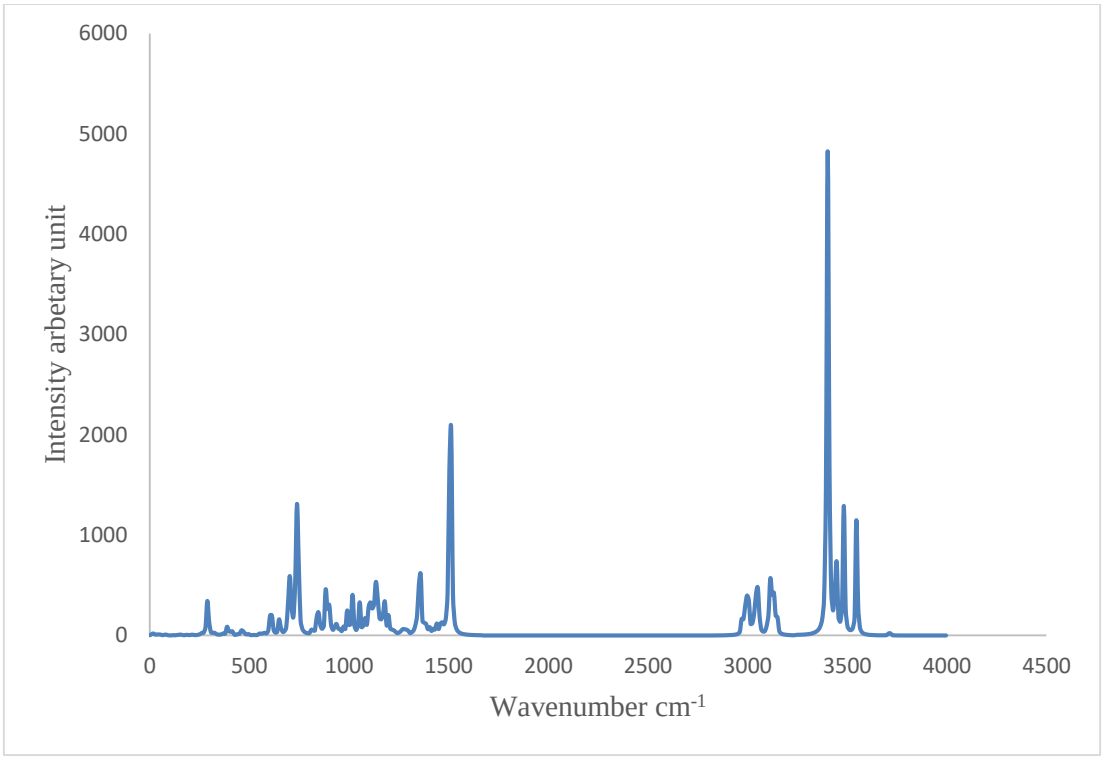

Figure 4.9. IR-spectra of (PVA-TiO_2) nancomposite (theoretical).

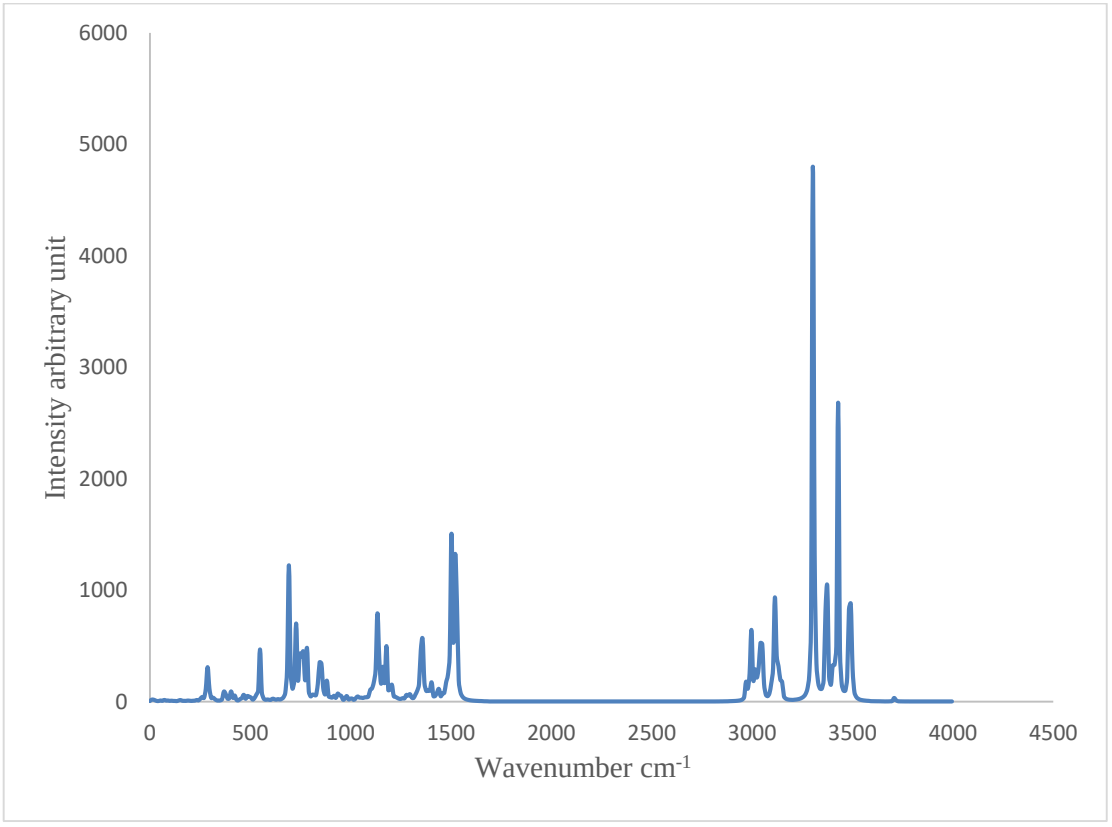

Figure 4.10. IR-spectra of (PVA-SnO_2) nancomposite (theoretical).

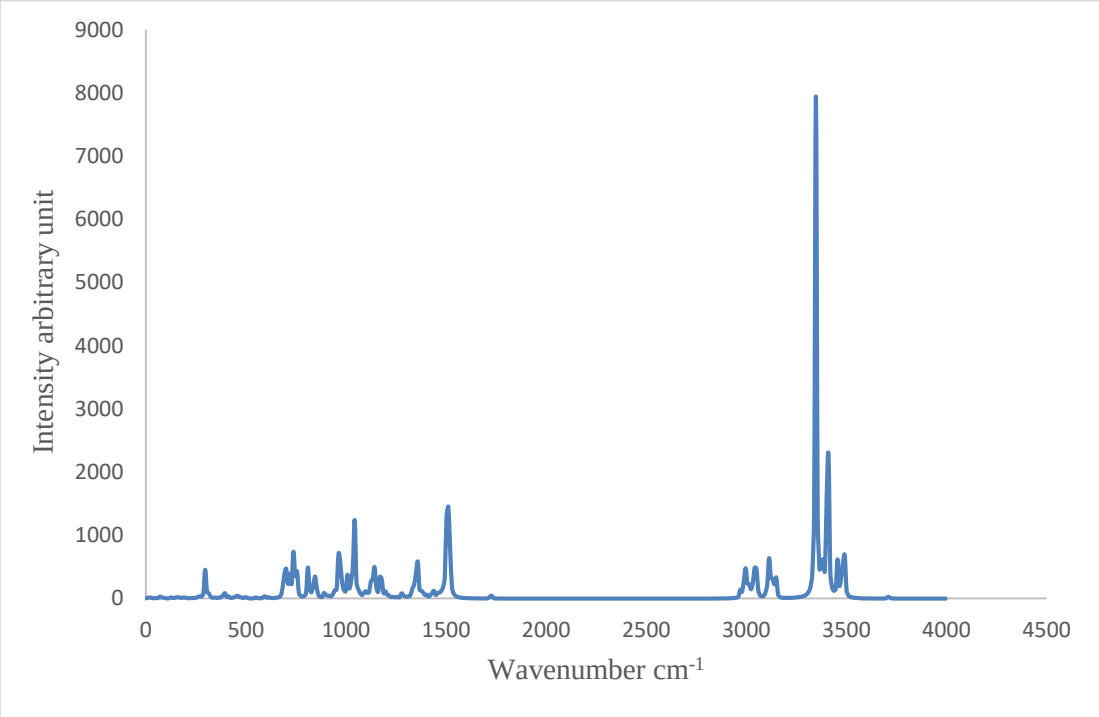

Figure 4.11. IR-spectra of (PVA-TiO_2-Ag) nancomposite (theoretical).

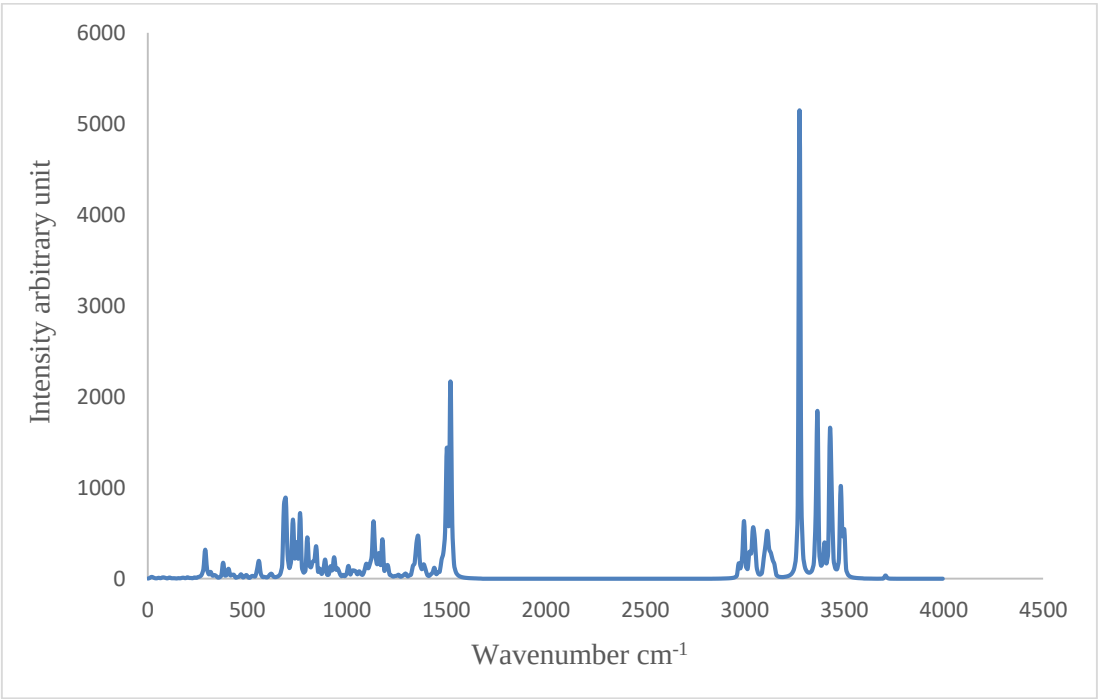

Figure 4.12. IR-spectra of (PVA-SnO_2-Ag) nancomposite (theoretical).

4.2.3 The Ultraviolet-Visible Spectra of Pure PVA and its Nanocomposites

In this section, TD-DFT method was used to simulate UV- Visible spectrum for PVA polymer and it is nanocomposite. TD-DFT calculation shows that a maximum wavelength of absorption for PVA polymer was (162.66) nm, from this result conclude that absorption occurred in the ultraviolet region for PVA polymer.

One of the important method to modify optical absorption of PVA is doping by metal- dioxide atom [163]. Metal- dioxide atom like SnO_2, TiO_2, and AgNPs will use to optical absorption. First, study the effect of SnO_2 and AgNPs metal atoms on PVA polymer. The wavelength of absorption for (PVA-SnO_2) and (PVA-SnO_2-Ag) nanocomposites are (257) nm and (404.23)nm, respectively. Result of maximum wavelength of absorption shows that spectrum pushed to blue region of electromagnetic radiation, but it is still in ultra-violet region.

In other hand, the maximum wavelength of absorption of PVA polymer was being modify. Second, adding TiO_2 and Ag metal atoms to PVA polymer, the result shows that the UV-visible spectrum of polymer compounds has two peaks of absorption, one of which is primary because it has the highest intensity and the second is considered secondary because it has the lowest intensity, and the reason behind the appearance of these two peaks is the formation of additional levels of energy within the energy bundles necessary for the transfer. For PVA-TiO_2 maximum wavelength of absorption was (338) nm and (604) nm. For PVA-TiO_2-Ag polymer composite the maximum wavelength of absorption was (352) nm and (550) nm [164]. From these result conclude that, adding TiO_2 and Ag atoms to PVA pushed spectrum to red region of electromagnetic radiation and reduce the optical band gap. Appearing two absorption peak resulting from

present secondary state inside band gap energy (optical band energy). Figures (4.13-4.17) represent UV-Visible spectrum for pure polymer and its nanocomposites.

Equation (4.1) used to determine the amount of optical energy gap value that requires an amount of energy to move into the HOMO orbit, so we can calculate how much energy each electron must have to be able to move the electron from HOMO to LUMO [165].

$$E_g^{opt} = 1240/\lambda_{max} \quad (4.1)$$

For the pure polymer PVA, the transition requires an energy of (7.623) eV, nanocomposite (PVA-SnO_2) need (4.824) eV, while the nanocomposite (PVA-SnO_2-Ag) require (3.067) eV of energy to make the transition. Where nanocomposite (PVA-TiO_2) need (3.668) eV for the first peak and the second peak require (2.052) eV. While the first peak of the (PVA-TiO_2-Ag) nanocomposite requires (3.522) eV of energy, and the second peak need (2.254) eV to get the transition.

So, in the case of pure polymer (PVA), high energy is required to explain these results because the energy bands are far apart, but when (SnO_2-Ag) is added, the energy bands become closer together. We notice a decrease in energy value, which is the reason for the increase in concentration and convergence between the energy bands, as well as for the nanocomposite (PVA-TiO_2-Ag), which requires less energy, which is due to the convergence. Energy bundles are used to increase the concentration of the additive in pure polymer.

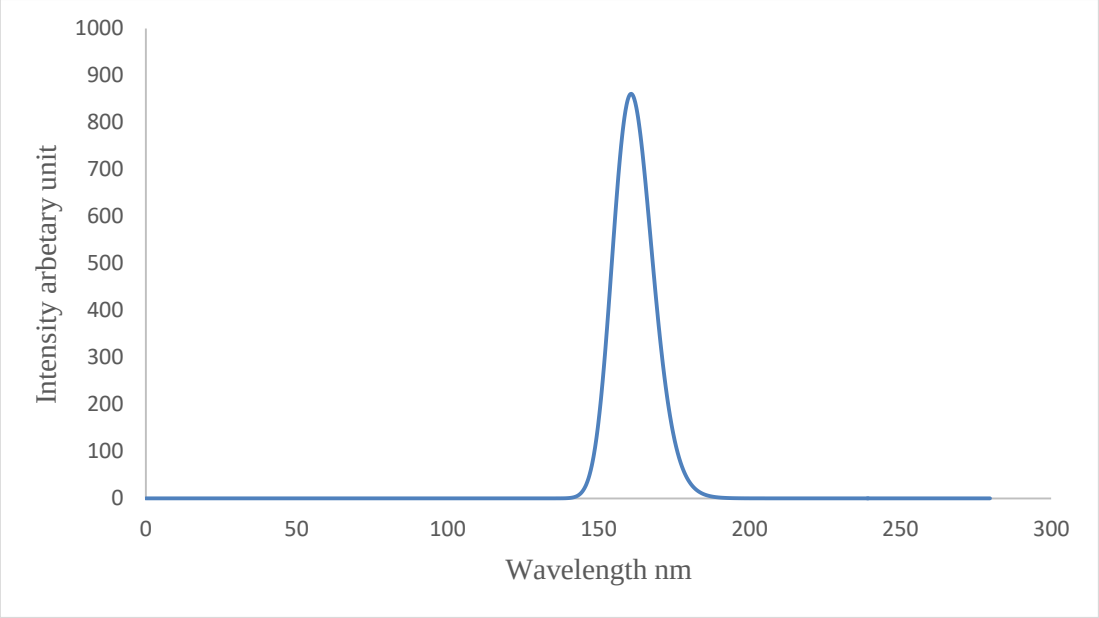

Figure 4.13. Ultraviolet-Visible spectrum for pure (PVA).

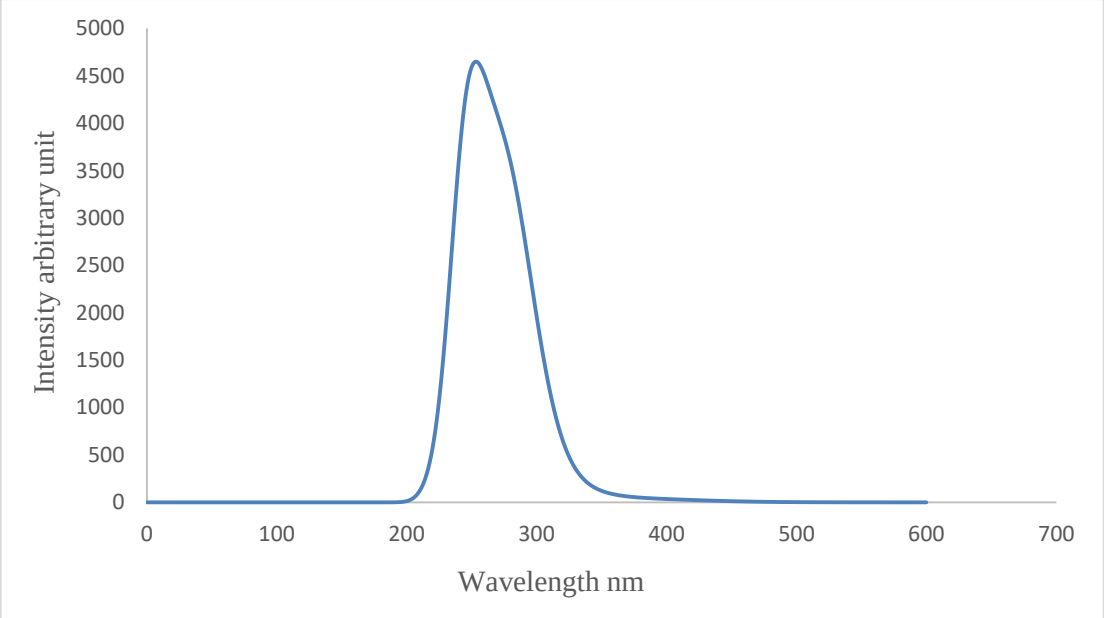

Figure 4.14. Ultraviolet-Visible spectrum for (PVA-SnO_2).

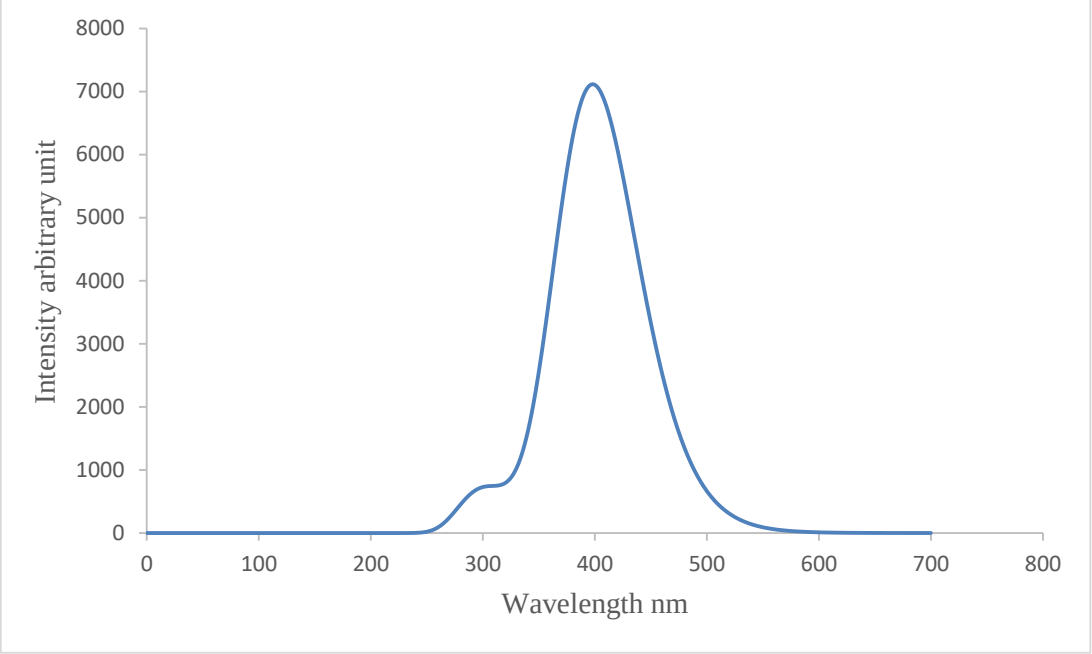

Figure 4.15. Ultraviolet-Visible spectrum for (PVA-SnO_2-Ag) nanocomposites.

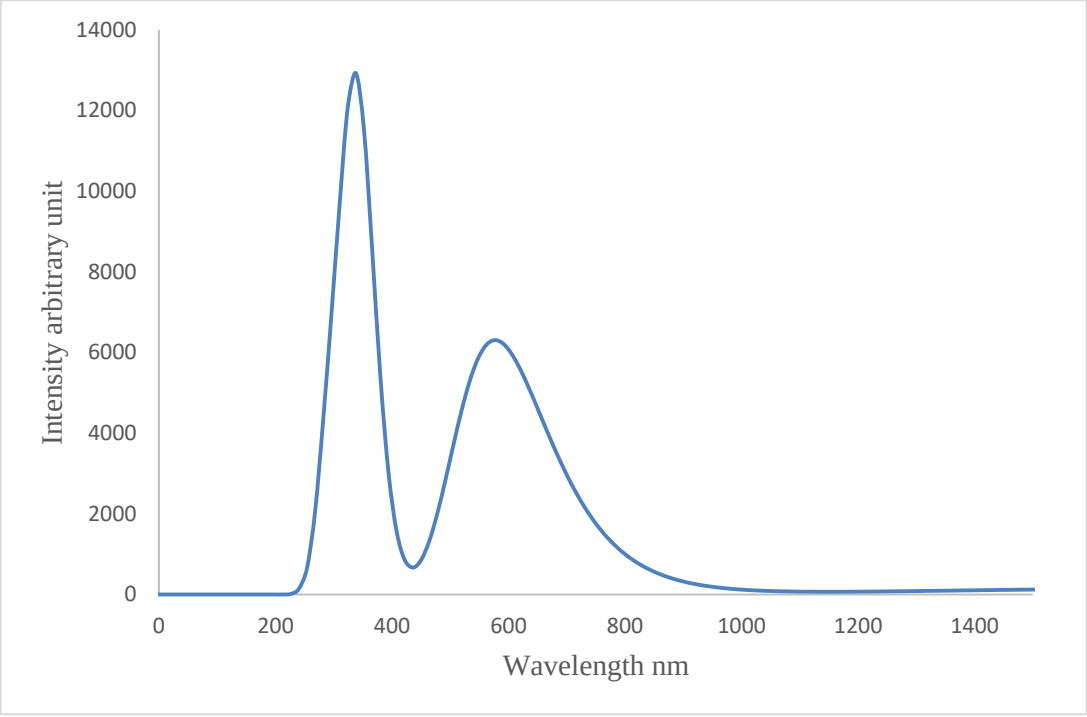

Figure 4.16. Ultraviolet-Visible spectrum for (PVA-TiO_2) nanocomposites.

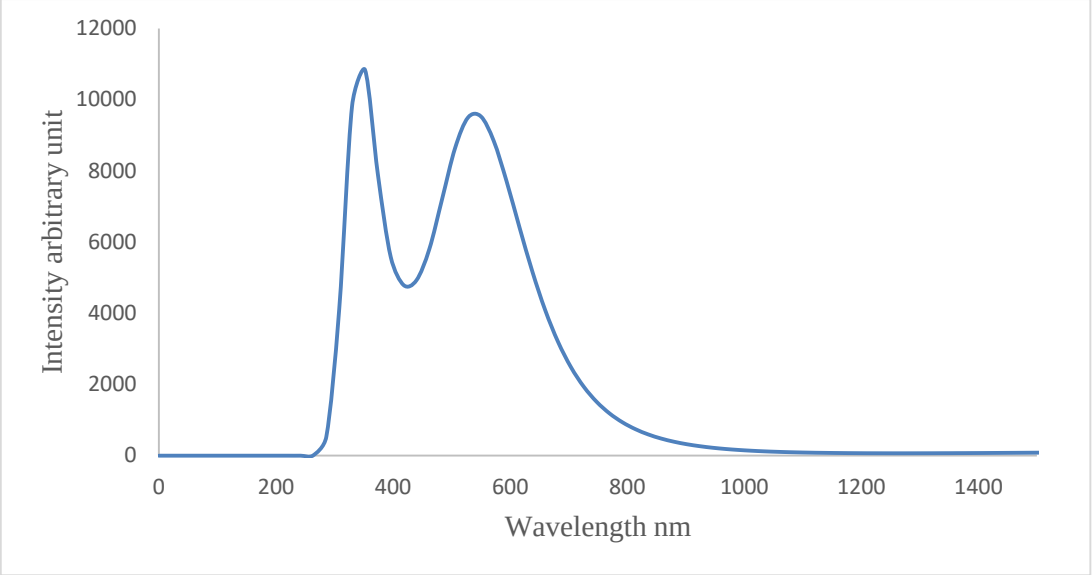

Figure 4.17. Ultraviolet-Visible spectrum for (PVA-TiO_2-Ag) nanocomposites.

4.3 The Electronic Properties of Pure PVA and its Nanocomposites

The electronic properties of pure PVA and it's nanocomposites are computed using DFT at the SDD level. The total energy $E_{(T)}$ in (a.u.), electronic state energies HOMO and LUMO (eV) and Energy gap E_g (eV) Ionization Energy I_E (eV), Electron Affinity E_A (eV), Chemical Hardness η (eV), Chemical Softness S in $(eV)^{-1}$, and electrophilic index in ω (eV) .

4.3.1 Total Energy (E_T) and Viral Ratio (-V/T)

Table (4.2) shows the total energy in (a.u.) and Viral (-V/T) ratios of pure polymer (PVA) and its nanocomposites, where total energy is defined as the total energy of the ground state, which is approximately the sum of the ground state energy of all atoms in each structure.

While the ratio (-V/T) represents potential energy to kinetic energy. We notice that the total energy value began to decrease when we added silver nanoparticles AgNPs to (PVA-TiO_2) and (PVA-SnO_2), indicating that all of the samples prepared from nanocomposites have a relaxation, so the

calculated value of the total energy depends on the number of electrons in the structures, where the energy value is inversely proportional to the increase in concentrations added to the pure polymer, as shown in the Table (4.2). When we look at the values of (-V/T), we notice that they are all equal, indicating that they all fall into the same range [166,167].

Table 4.2. The total energy (E_T) and Viral ratio (-V/T) for the pure PVA and its nanocomposites.

No. of Nanocomposites	Assignment	E_T (a.u.)	-V/T
1	PVA	-1578.477	2.003
2	PVA-SnO_2	-1578.69	2.002
3	PVA-TiO_2	-1634.95	2.021
4	PVA-SnO_2-Ag	-1727.36	2.062
5	PVA-TiO_2-Ag	-1782.37	2.080

4.3.2 Electronic States and Energy Gap

Energy band gap found by Equation (2-13). The band gap refers to energy difference between the highest occupied molecular orbital and lowest unoccupied molecular orbital. The energy gap value of the pure polymer (PVA) without any nanomaterial is (6.1015) eV, as shown in Table (4.3), which is considered an insulating material due to the very high value of the energy gap [168]. In term of adding metal atoms to polymer the energy gap was decreased, in other hand conductivity of polymer composite was enhance. Results show that energy gap was decreased rapidly when adding metal atoms and it varied from (6.101 to 1.336) eV. As well as high number of valance electron was passing through band energy and this clear in PVA-TiO_2-Ag nanocomposite.

When tin nanoparticles added to the base material (PVA), we notice a significant decrease in the energy gap value (E_g) from (6.101 to 3.81) eV, which is due to the material changing from an insulating state to a semi-conductive state due to the high electronic affinity and ionization between the PVA polymer and the additive SnO_2. When silver nanoparticles AgNPs added to (PVA-SnO_2), the energy gap value decreases due to the presence of an abundance of free electrons for the AgNPs nanomaterial. When TiO_2 added to the base material PVA, we observe a decrease in the value of the energy gap from the insulating to the semiconducting state, as well as the transformation of the semiconductor material (PVA-TiO_2) into a conductive material after the addition of AgNPs to (PVA-TiO_2), becomes conductive [169].

The reason for this is nanomaterial contains an abundance of free electrons AgNPs. Based on the findings, we conclude that the nanocomposite (PVA-TiO_2-Ag) outperforms the nanocomposite in terms of conductivity (PVA-SnO_2-Ag). A small energy gap means small excitation energies to the manifold of excited states. Therefore, soft molecules with small energy gaps. Their electron density change more easily than a hard molecule, and due to that, soft molecules will be more reactive than hard molecules [170].

Table 4.3. The electronic states and energy gap for the pure PVA and its nanocomposites.

No. of Nanocomposites	Materials	E_g(eV)	Electronic states	
			E_{HOMO}(eV)	E_{LUMO}(eV)
1	PVA	6.101	-5.417	0.683
2	PVA-SnO_2	3.816	-4.600	-0.784
3	PVA-TiO_2	2.381	-3.386	-1.005
4	PVA-SnO_2-Ag	3.283	-5.877	-2.594
5	PVA- TiO_2-Ag	1.336	-5.087	-3.751

The E_{HOMO} (is the molecular orbital of highest energy that is occupied by electrons) and E_{LUMO} (is the molecular orbital of lowest energy that is not occupied by electrons) are important in determine such properties as molecular reactivity and the ability of a molecule to absorb light [171]. HOMO and LUMO orbitals are concentrated at the ends of the base material, as shown in Figure (4.18), which represents the base material before adding SnO_2, TiO_2 and AgNPs to the polymer (PVA). When SnO_2 are added to the base polymer, the distribution of molecular orbitals is parallel and centered on the edges of the PVA system in the case of HOMO [172]. In the case of LUMO, we notice a concentration of charges in the center around the tin and silver nanoparticles as shown in Figure (4.19). When TiO_2 is added, the charges are concentrated on the TiO_2 and Ag atoms in the (PVA-TiO_2-Ag) nanocomposite as shown in Figure (4.20). We discovered that adding metal atoms to polymers improves their electrical properties, as evidenced by a decrease in the energy gap value, when these nanoparticles are added.

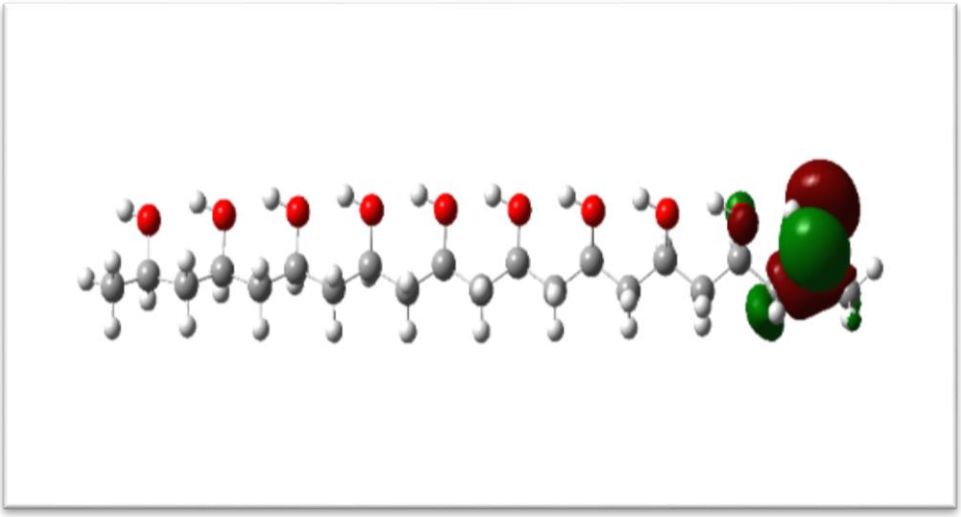

a

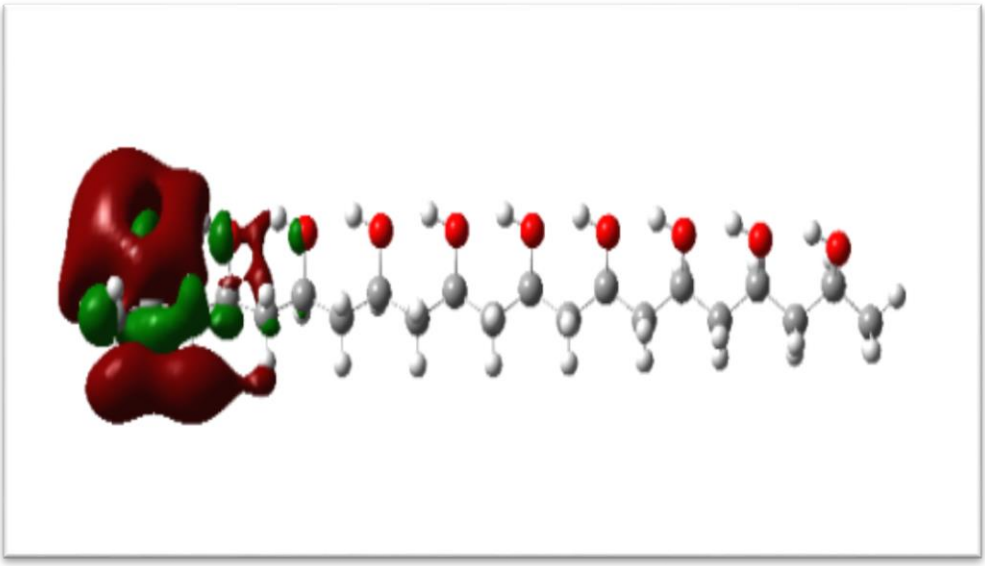

b

Figure 4.18. The distribution of HOMO (a) and LUMO (b) for (PVA).

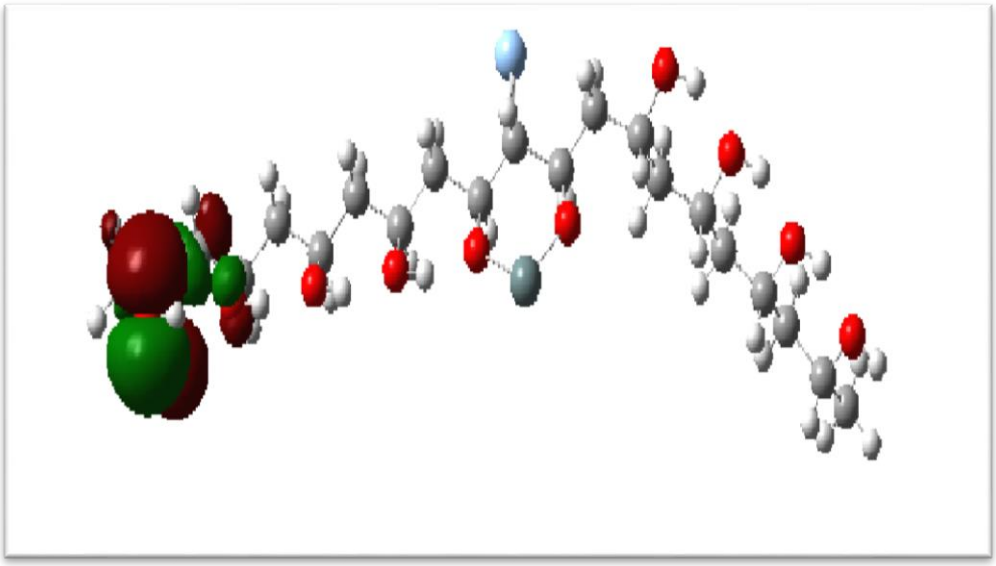

a

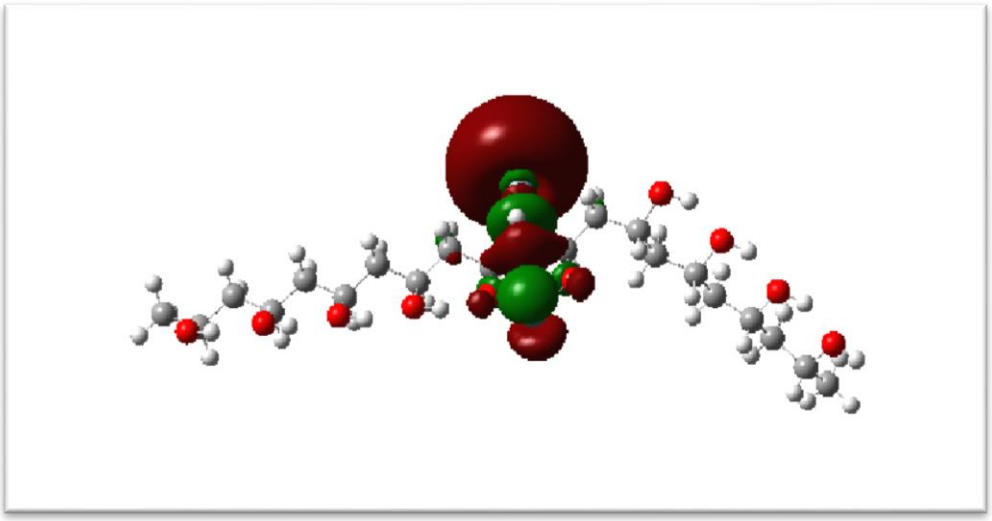

b

Figure 4.19. The distribution of HOMO (a) and LUMO (b) for (PVA-SnO_2-Ag).

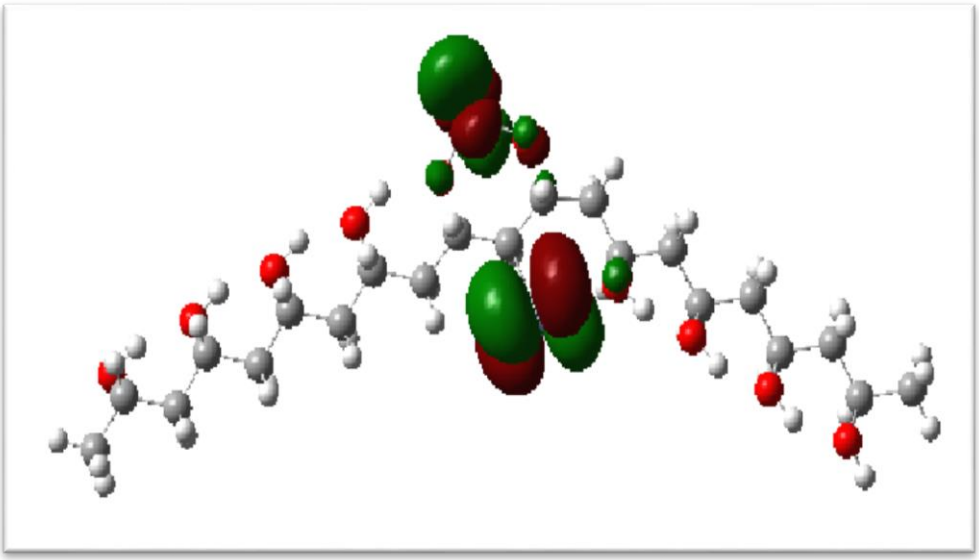

a

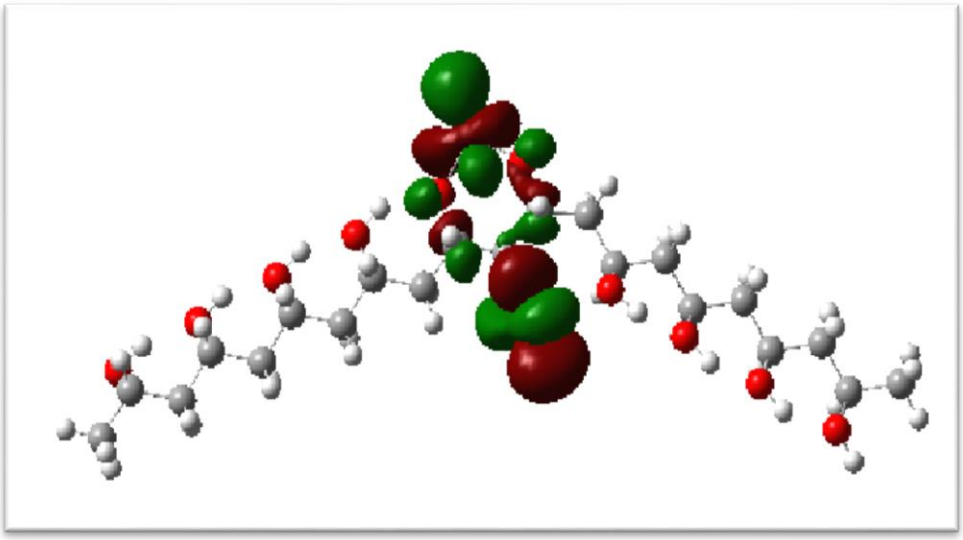

Figure 4.20. The distribution of HOMO (a) and LUMO (b) for (PVA-TiO_2-Ag).

4.3.3 Ionization Energy (I_E) and Electron Affinity (E_A)

These properties are critical in determining the ability to distinguish or escape electrons between doping systems. The results of ionization energy I_E and electron affinity E_A are shown in Table (4.4). Clearly table shows that the pure polymer PVA has the highest ionization energy value when compared with the other compounds. The ionization energy of the nanocomposites (PVA-TiO_2) is lower than that of other nanocomposites. This suggests that the nanocomposites (PVA-TiO_2) have a greater ability to donate an electron to form a cation than the others. In comparison to other nanocomposites, (PVA-TiO_2-Ag) nanocomposites have the highest E_A value because they have a high electron acceptability to become anion. The electron affinity of the pure polymer PVA is negative because it is an insulator and stable and does not interact with the environment, and when TiO_2 was added, the affinity increased, but when silver nanoparticles AgNPs were added, the affinity increased more, meaning that it became more free to interact with the environment, and this is due to the presence of abundance of electrons in AgNPs.

When SnO_2 was added to the PVA, the electronic affinity value increased, but at a slower rate than when TiO_2 added, indicating that TiO_2 interfered with PVA more than SnO_2. In general, the addition of AgNPs to (PVA-SnO_2) and (PVA-TiO_2) increased the electronic affinity, which was due to the abundance of electrons in AgNPs [173].

Table 4.4. The ionization energy (I_E) and electron affinity (E_A) in eV for the pure PVA and its nanocomposites.

No. of Nanocomposites	Materials	I_E (eV)	E_A (eV)
1	PVA	5.417	-0.683
2	PVA-SnO_2	4.600	0.784
3	PVA-SnO_2-Ag	5.877	2.594
4	PVA-TiO_2	3.386	1.005
5	PVA-TiO_2-Ag	5.087	3.751

4.3.4 Electrophilic (ω) and Electronegativity (χ)

The values of the electrophilic index and electronegativity were calculated, as shown in Table (4.5) .where the increase in the values of (ω) for nanocomposite (PVA-TiO_2-Ag) was observed when compared to the value of the pure polymer PVA, and this indicates that the nanocomposite (PVA-TiO_2-Ag) is more chemically reactive. This indicates that the presence of AgNPs gives the ability to accept an electron from the surrounding species [174].

In the same table, we note that the lowest value of electronegativity (χ) was (2.1960) (eV) for the nanocomposite (PVA-TiO_2), but the nanocomposite (PVA-SnO_2-Ag) and (PVA-TiO_2-Ag) had a value of (4.2363) (eV) and (4.4198) (eV), respectively. This means that these high electronegative nanocomposites have a high ability to donate or accept an electron to and from the surrounding species [175].

Table 4.5. The Electrophilic Index (ω) and Electronegativity (χ) in eV for the pure PVA and its nanocomposites.

No. of Nanocomposites	Materials	ω (eV)	χ (eV)
1	PVA	0.9114	2.3672
2	PVA-SnO_2	1.8992	2.6926
3	PVA-SnO_2-Ag	5.4706	4.2363
4	PVA-TiO_2	2.0151	2.1960
5	PVA-TiO_2-Ag	14.5569	4 .4198

4.3.5 Chemical Hardness (η) and Chemical Softness (S)

Pure PVA has a high chemical Hardness, while all nanocomposites have a low chemical Hardness, according to Table (4.6). The low hardness easily indicates low transition an electron in molecule from the valence to the conduction band. When compared to pure PVA, all nanocomposites have the highest softness value, indicating that these molecules require little excitation energy to transfer electrons [176].

Table 4.6. Chemical Hardness (η) and Chemical Softness (S) for the pure PVA and its nanocomposites.

No. of Structure	Materials	η (eV)	S $(eV)^{-1}$
1	PVA	3.050	0.163
2	PVA-SnO_2	1.908	0.262
3	PVA-SnO_2-Ag	1.641	0.304
4	PVA-TiO_2	1.190	0.419
5	PVA-TiO_2-Ag	0.668	0.748

4.4 The Optical Properties of (PVA-SnO_2-Ag) and (PVA-TiO_2-Ag) Nanocomposites

Absorption, transmittance, absorption coefficient, energy band gap, extinction coefficient, reflection index, dielectric constants, and optical conductivity are some of the optical properties studied for (PVA-SnO_2-Ag) and (PVA-TiO_2-Ag) nanocomposites.

4.4.1 The Absorption and Transmittance of (PVA-SnO_2-Ag) and (PVA-TiO_2-Ag) Nanocomposites

The absorbance of the PVA and nanocomposites (PVA-SnO_2-Ag) and (PVA-TiO_2-Ag) are calculate with the wavelength of the incident light. Figure (4.21) explains the comparison between pure PVA polymer and nanocomposites (PVA-SnO_2-Ag) and (PVA-TiO_2-Ag) for absorbance values, where it was found that the PVA spectrum falls within the UV range, while the addition of nanoparticles to the pure polymer caused a spectral shift towards the UV-Vis region.

The absorbance of the nanocomposites (PVA-SnO_2-Ag) and (PVA-TiO_2-Ag) with the wavelength of the incident light experimentally as shown in Figures (4.22, 4.23) and theoretically as in Figure (4.24), which explained the absorption relationship of (PVA-SnO_2-Ag) and (PVA-TiO_2-Ag) nanocomposites with the wavelength of the experimental incident light in addition to the absorption relationship with the concentrations of silver nanoparticles. Where we see an increase in the absorbance in the UV region of the nanocomposites samples with an increase in the concentration of AgNPs and gradually as the concentrations (0.75, 1.5, 2.5 and 3) wt% of AgNPs added to each of (PVA-SnO_2) and (PVA-TiO_2), this is due to electron excitation from the valence band to the conduction band at these energies. Because of the high energy of the photon that interacts with atoms, the samples have a high absorbance in the ultraviolet region, which

causes electrons to be excited and move from a low level of energy to a higher level of energy. In addition to the clear convergence in the figure with the practically calculated absorbance values. Previous studies and results are in a agreement, where changes in absorbed and transmitted radiation can determine the types of possible electronic transitions. The band transition or excitation is indicated by the basic absorption of the absorption spectra [177]. Because the energies are low, they are not enough for the interaction of the atoms, in which the wavelength increases, and as a result, the absorbance decreases [178], which increases the permeability of all nanocomposites. As shown in Figures (4.25, 4.26) with the wavelength of the incident light, as well as due to an increase the concentration of AgNPs (0.75, 1.5, 2.5 and 3) wt% , and theoretically as in Figure (4.27), which gives the transmittance of (PVA-SnO_2-Ag) and (PVA-TiO_2-Ag) the transmittance will decrease, due to the agglomeration of nanoparticles and the increase in the number of charge carriers. The two nanocomposites (PVA-SnO_2-Ag) and (PVA-TiO_2-Ag) showed absorption and transmittance values, in addition to the congruence between the theoretical and experimental curves in the figures (4.22, 4.27).

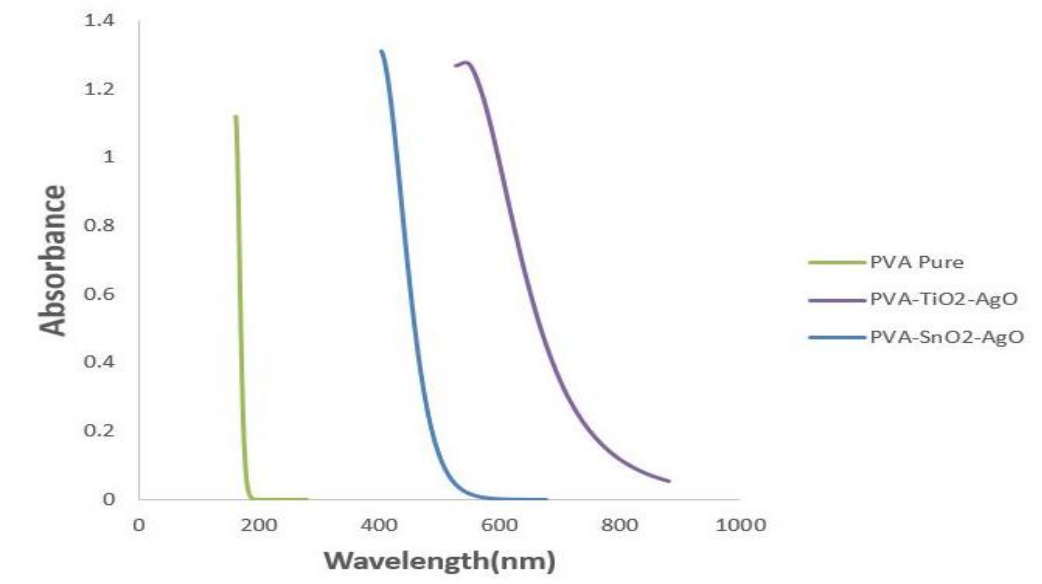

Figure 4.21. Calculation for the absorbance of PVA and its nanocomposites (theoretical).

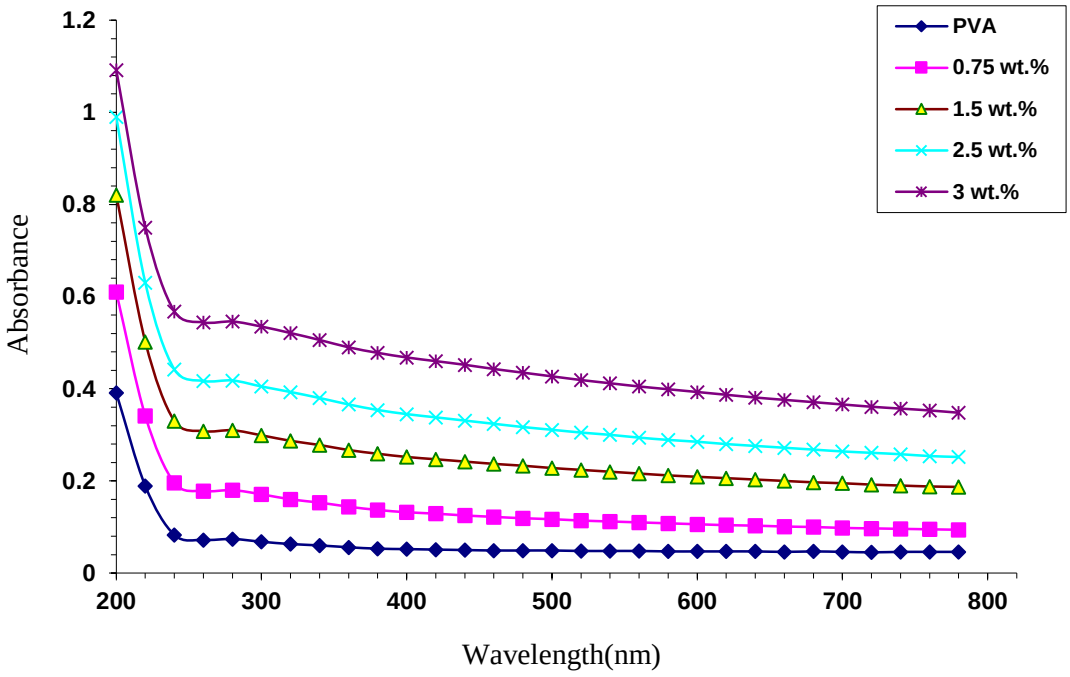

Figure 4.22. Absorption as a function of wavelength for PVA and (PVA-SnO_2-Ag) nanocomposites (experimental).

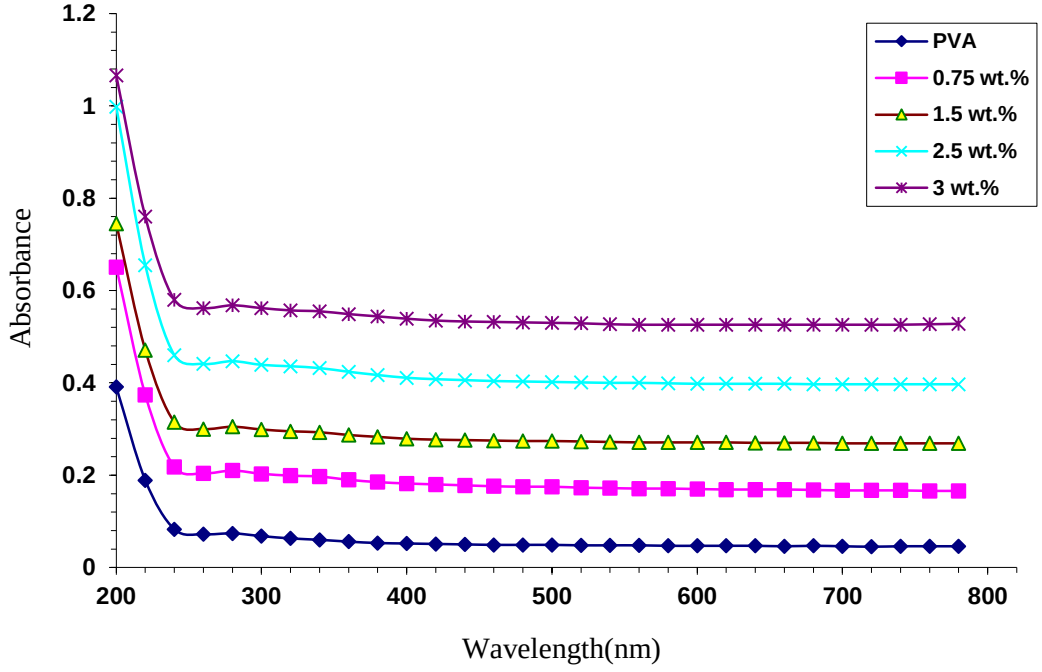

Figure 4.23. Absorption as a function of wavelength for PVA and (PVA-TiO_2-Ag) nanocomposites (experimental).

The pure polymer (PVA)	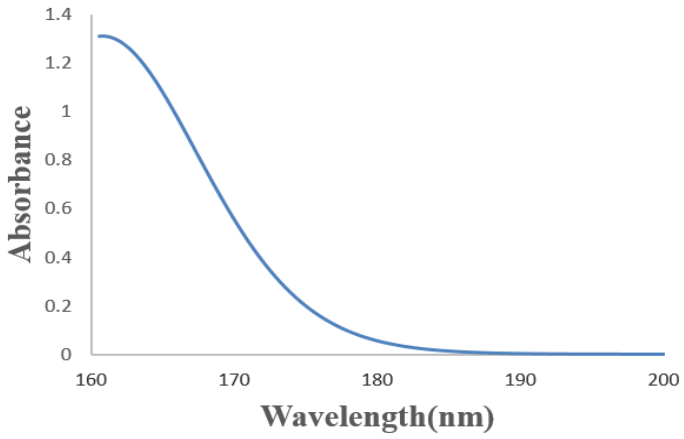
(PVA-SnO_2-Ag) nanocomposite	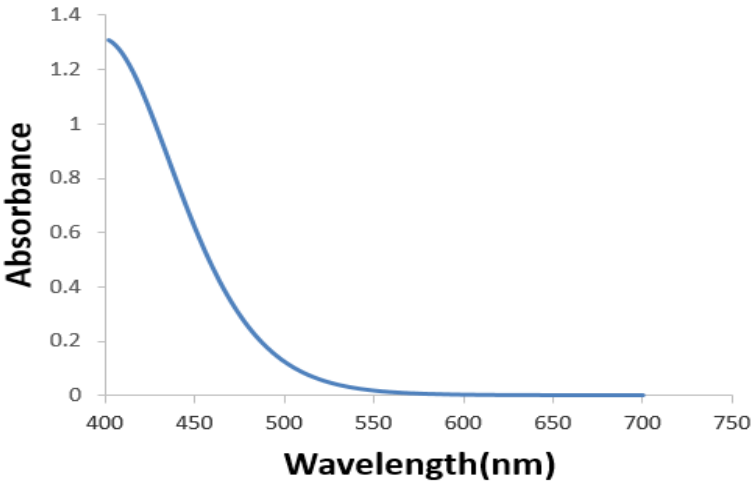
(PVA- TiO_2-Ag) nanocomposite	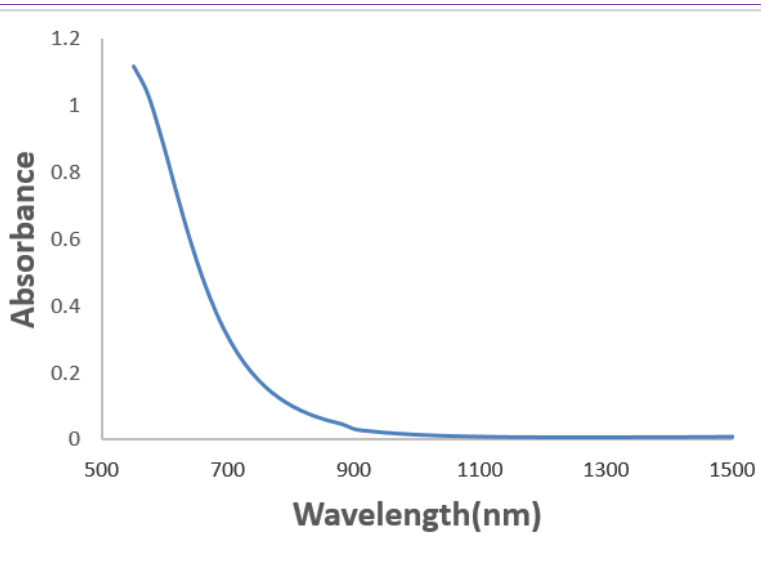

Figure 4.24. Absorption as a function of wavelength for PVA its nanocomposites (theoretical).

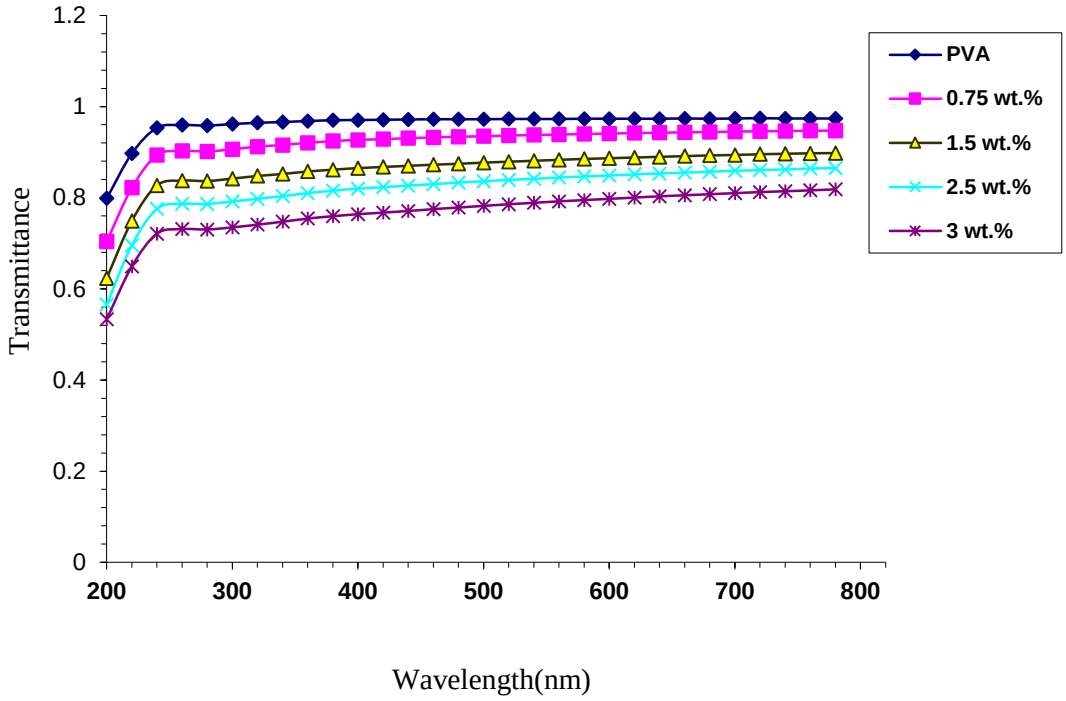

Figure 4.25. Transmittance as a function of wavelength for PVA and (PVA-SnO_2-Ag) nanocomposites (experimental).

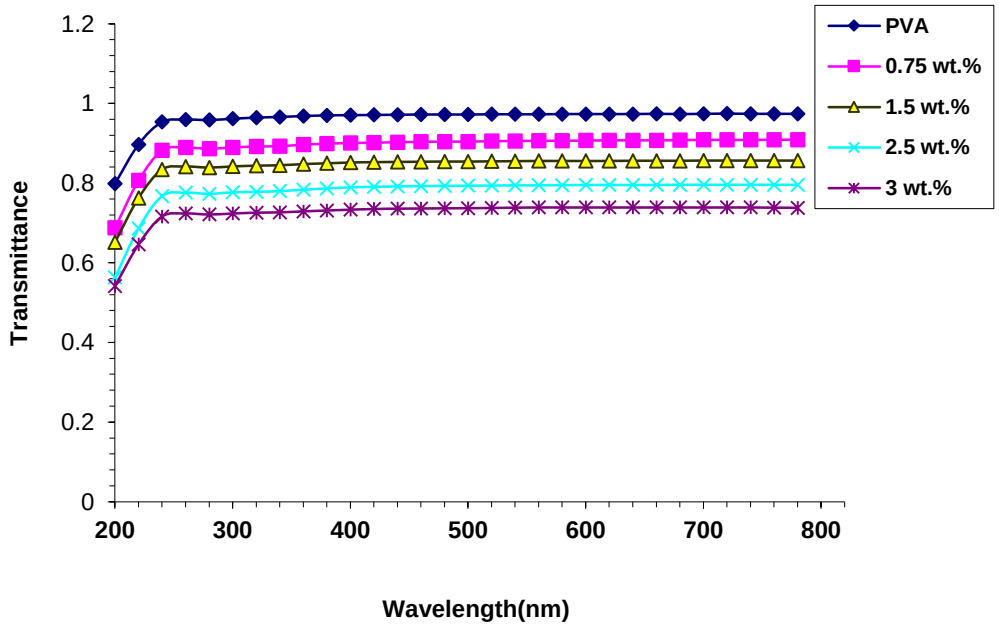

Figure 4.26. Transmittance as a function of wavelength for PVA and (PVA-TiO_2-Ag) nanocomposites (experimental).

The pure polymer (PVA)	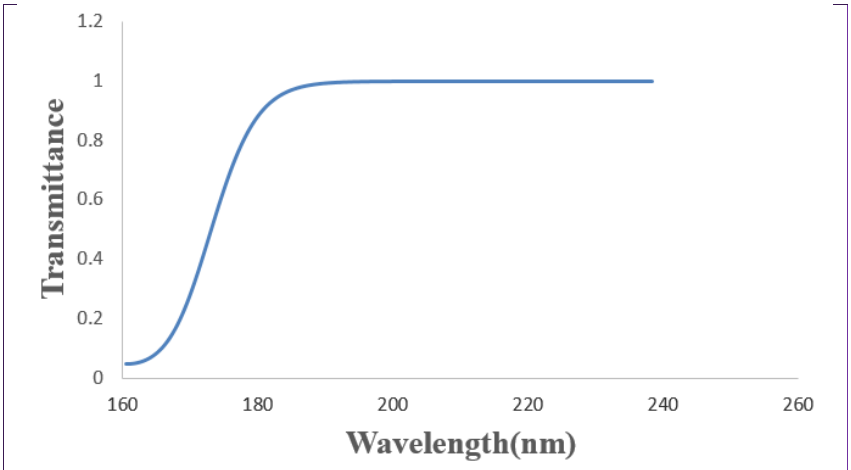
(PVA-SnO_2-Ag) nanocomposite	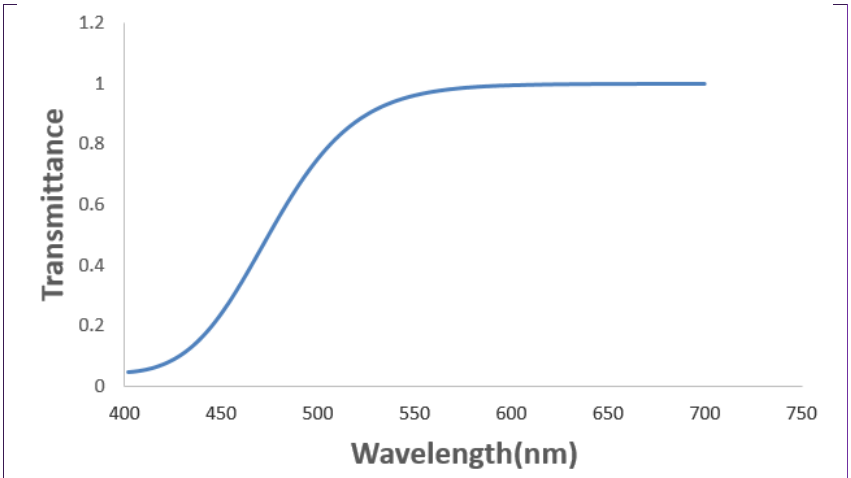
(PVA- TiO_2-Ag) nanocomposite	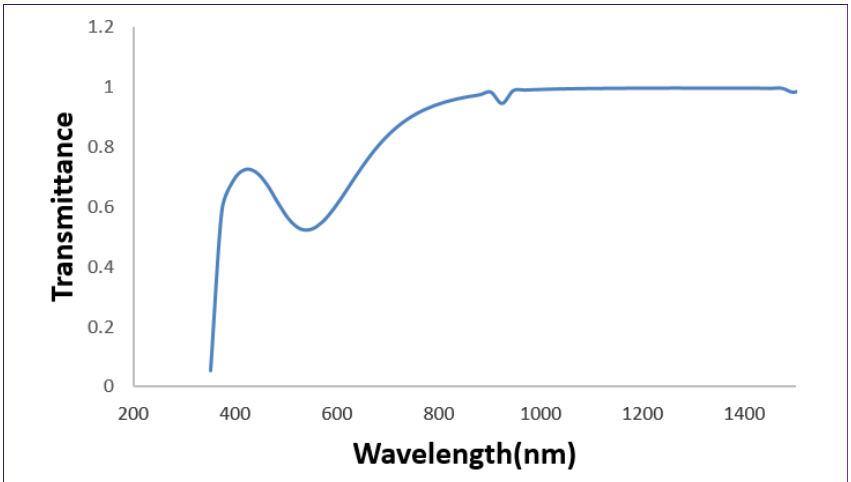

Figure 4.27. Transmittance as a function of wavelength for PVA and its nanocomposites (theoretical).

4.4.2 The Absorption Coefficient and Energy Band Gap of (PVA-SnO_2-Ag) and (PVA-TiO_2-Ag) Nanocomposites

The absorption coefficient of the nanocomposites calculated using Equation (2.25), as shown in Figures (4.28-4.29) and (4.30) of the nanocomposites (PVA-SnO_2-Ag) and (PVA-TiO_2-Ag) as a function of photon energy of the incident light experimentally and theoretically respectively. The results demonstrate that when the energy of the incident photon is high, the value of the absorption coefficient will be at the highest value. That is, the energy of the incident photon enabled the electron to move from level to a higher level, meaning that the energy of the incident photon was greater than the amount of the energy gap. As a result, the electrons had a high ability to move to higher levels. The absorption coefficient can be considered as a way to understand the nature of electronic transmission. When the absorption coefficient of the material is high ($\geq 10^4$ cm^{-1}), the electron transfer is to be direct, but when the absorption coefficient of the material is less than (10^4 cm^{-1}), the electron transfer is to be indirect the transmission of electrons is indirect [179]. The results showed that the absorption coefficient of the (PVA-SnO_2-Ag) and (PVA-TiO_2-Ag) nanocomposites is less than (10^4 cm^{-1}) so that the transmission of electrons is indirect. The absorption coefficient of nanocomposites increases with increasing nanoparticle concentrations, and thus the absorption and absorption coefficient of (PVA-SnO_2-Ag) and (PVA-TiO_2-Ag) increase due to an increase in sub-levels between HOMO and LUMO [180]. Equation (2.26) which used to calculate the energy gap for nanocomposites experimentally. The experimentally determined energies gap of the permissible indirect transformations of (PVA-SnO_2-Ag) and (PVA-TiO_2-Ag) nanocomposites are shown in Figures (4.31, 4.32) and (4.33) experimentally and theoretically, respectively. The energy gaps for the forbidden indirect transformations, as shown in the Figures (4.34,

4.35) and (4.36) experimentally and theoretically respectively. The energy gap of the allowed and forbidden indirect transformations of nanocomposites decreases with the increase of AgNPs (0.75, 1.5, 2.5 and 3) wt%, and this performance is due to more free electrons in AgNPs as shown in Table (4.7). In this case, electron transfer occurs in two stages, including the transition from the valence band to the occupation levels in the energy gap and to the conduction band as a result of the increase AgNPs, and electronic conduction is dependent on the free electrons in the nanoparticles [181]. The presence of nanoparticles causes the energy gap to narrow, increasing the density of central states in the band gap [182].

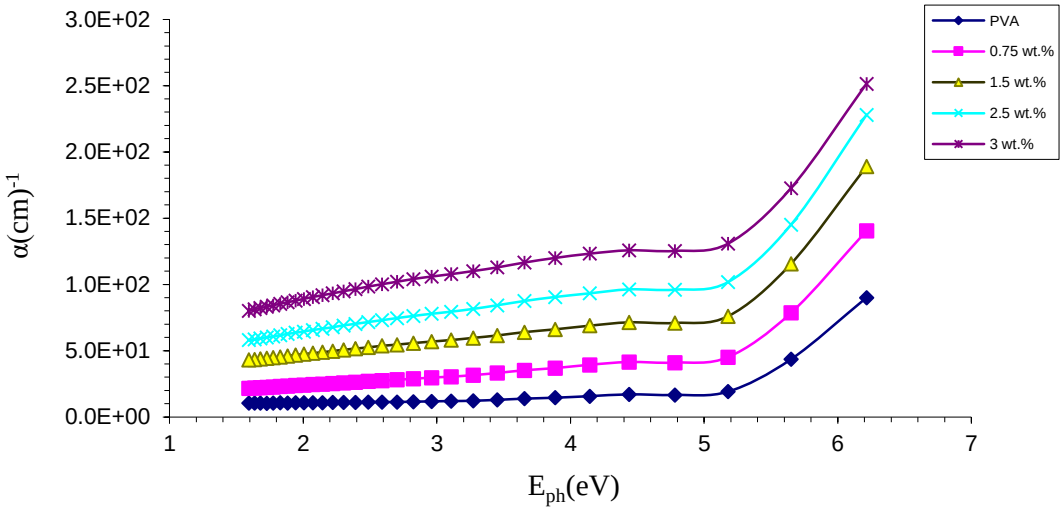

Figure 4.28. Shows absorption coefficient (α) for PVA and (PVA-SnO_2-Ag) nanocomposites with photon energy (experimental).

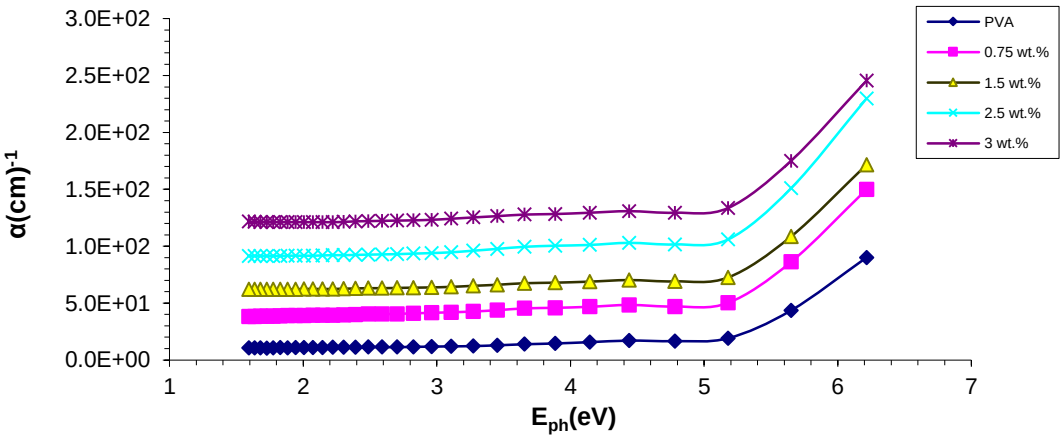

Figure 4.29. Shows absorption coefficient (α) for PVA and (PVA-TiO_2-Ag) nanocomposites with photon energy (experimental).

The pure polymer (PVA)	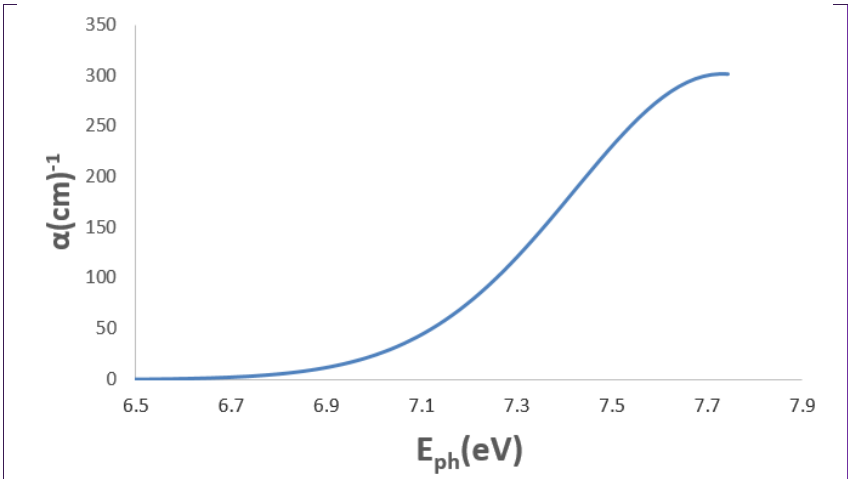
(PVA-SnO_2-Ag) nanocomposite	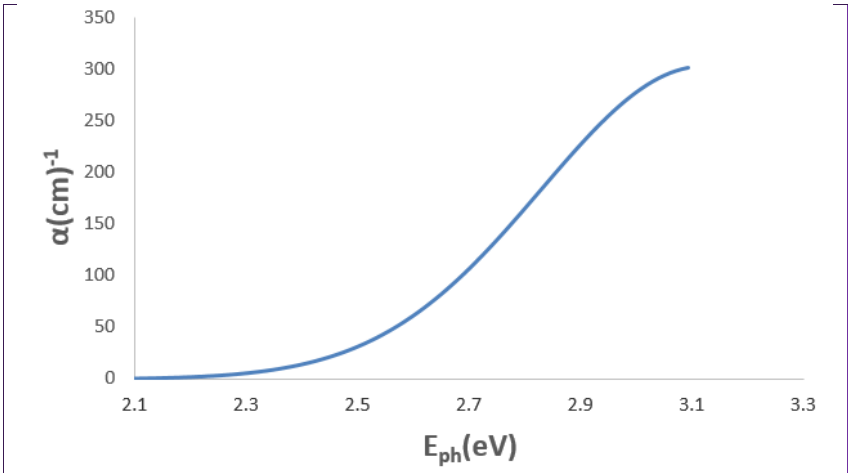
(PVA- TiO_2-Ag) nanocomposite	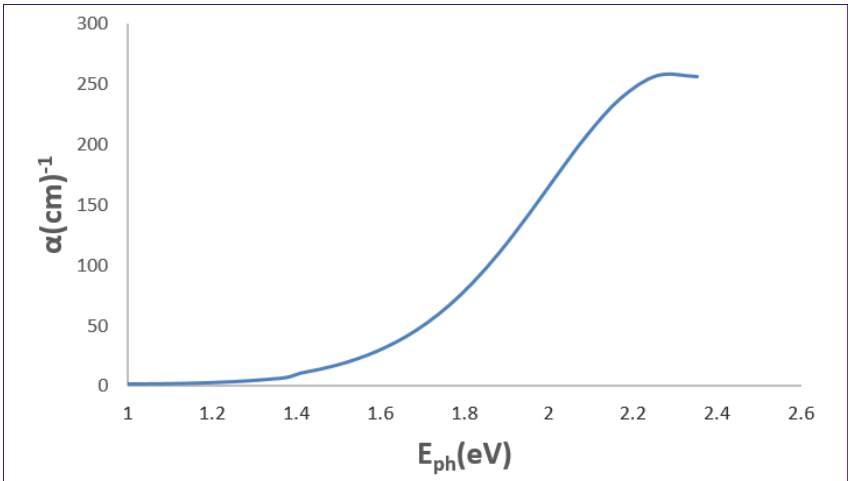

Figure 4.30. Variation of absorption coefficient (α) for PVA and its nanocomposites with photon energy (theoretical).

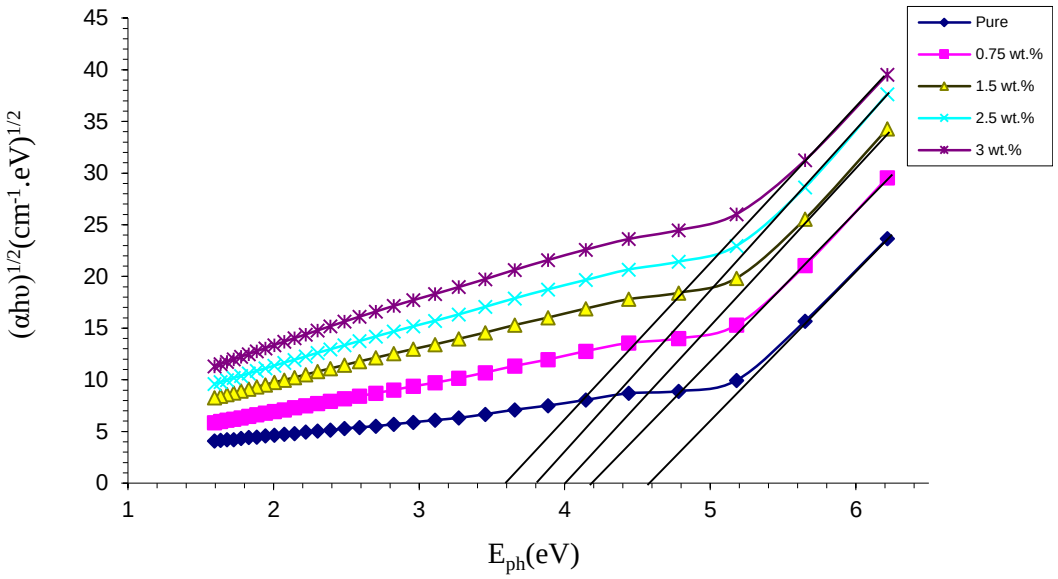

Figure 4.31. Variation of $(\alpha h\upsilon)^{1/2}$ for PVA and (PVA-SnO_2-Ag) nanocomposites with photon energy (experimental).

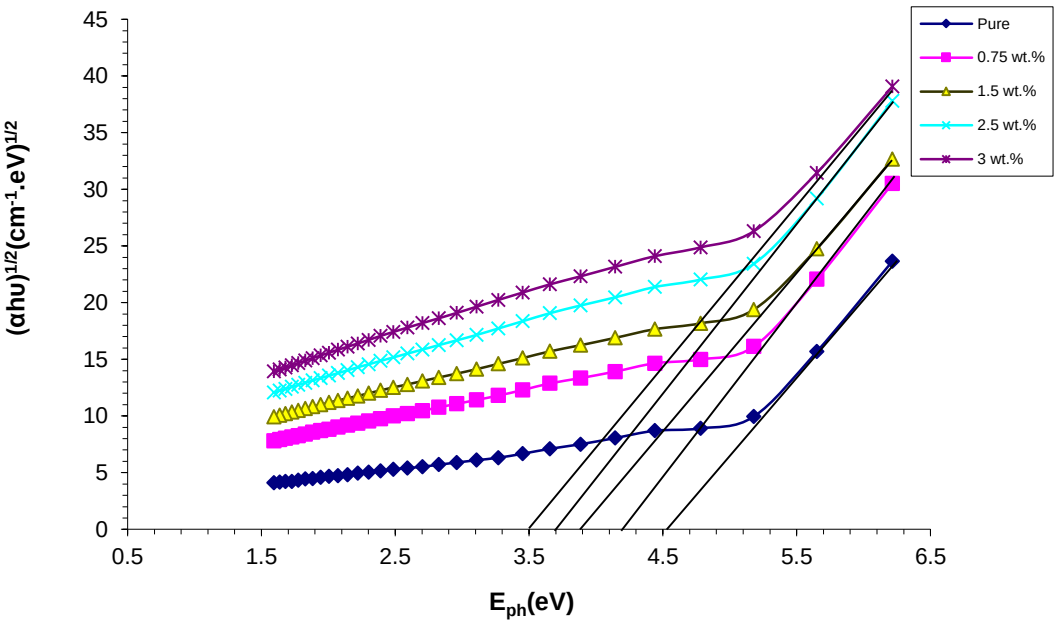

Figure 4.32. Variation of $(\alpha h\upsilon)^{1/2}$ for PVA and (PVA-TiO_2-Ag) nanocomposites with photon energy (experimental).

The pure polymer (PVA)	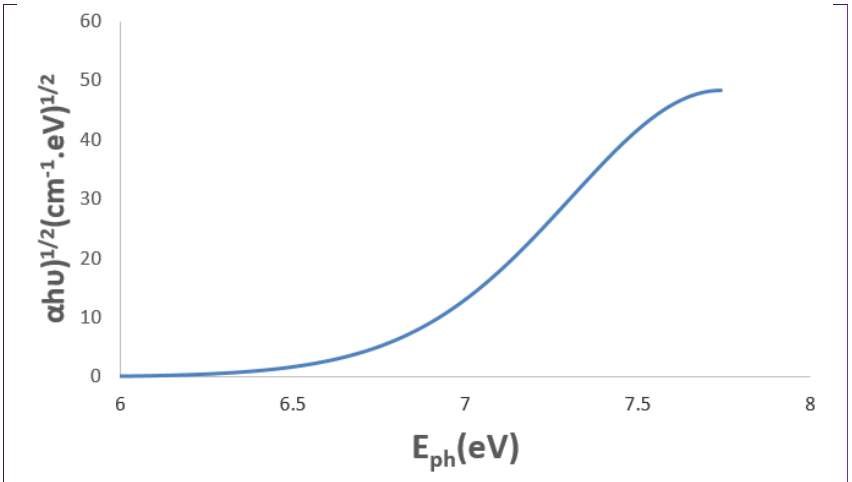
(PVA-SnO_2-Ag) nanocomposite	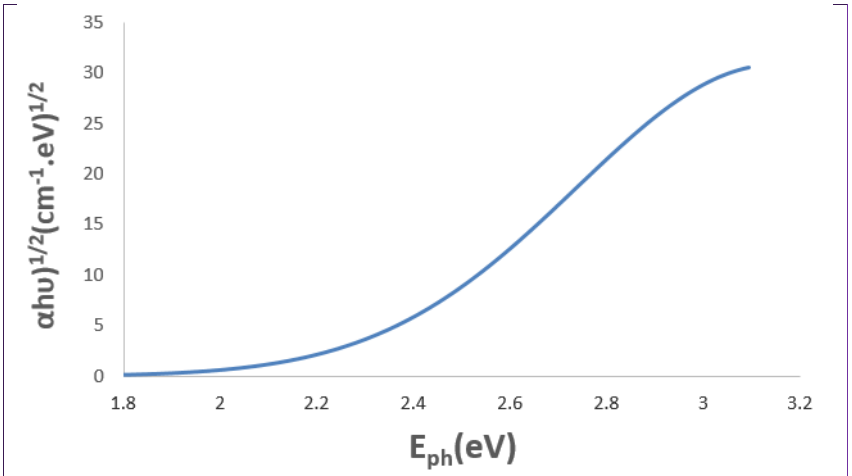
(PVA- TiO_2-Ag) nanocomposite	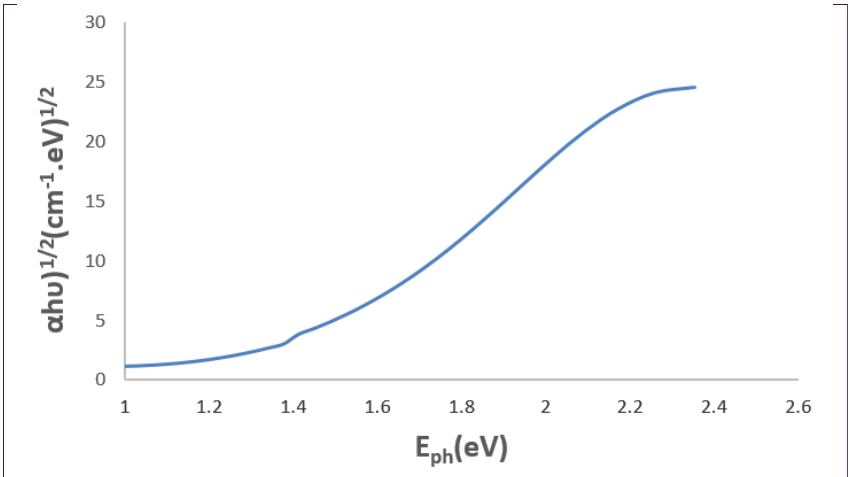

Figure 4.33. Variation of $(\alpha h\upsilon)^{1/2}$ for PVA and its nanocomposites with photon energy (theoretical).

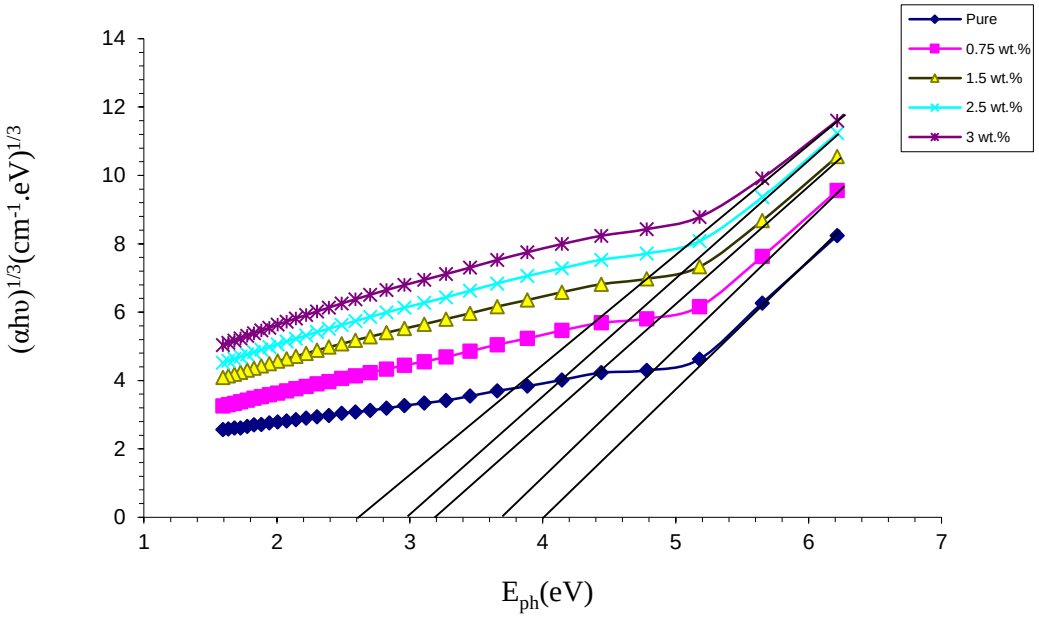

Figure 4.34. Variation of $(\alpha h\upsilon)^{1/3}$ for PVA and (PVA-SnO_2-Ag) nanocomposites with photon energy (experimental).

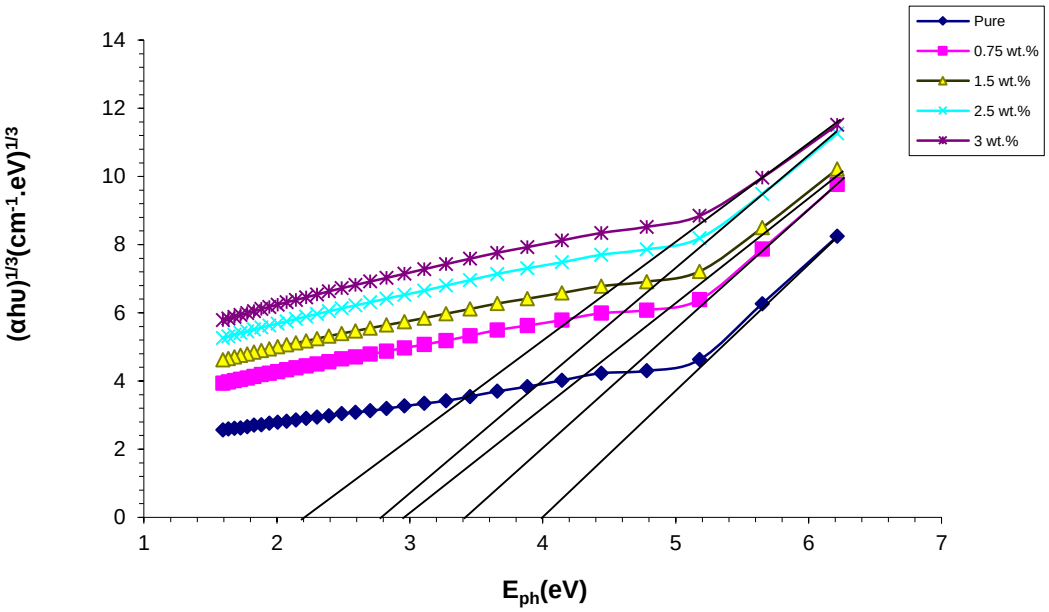

Figure 4.35. Variation of $(\alpha h\upsilon)^{1/3}$ for PVA and (PVA-TiO_2-Ag) nanocomposites with photon energy (experimental).

The pure polymer (PVA)	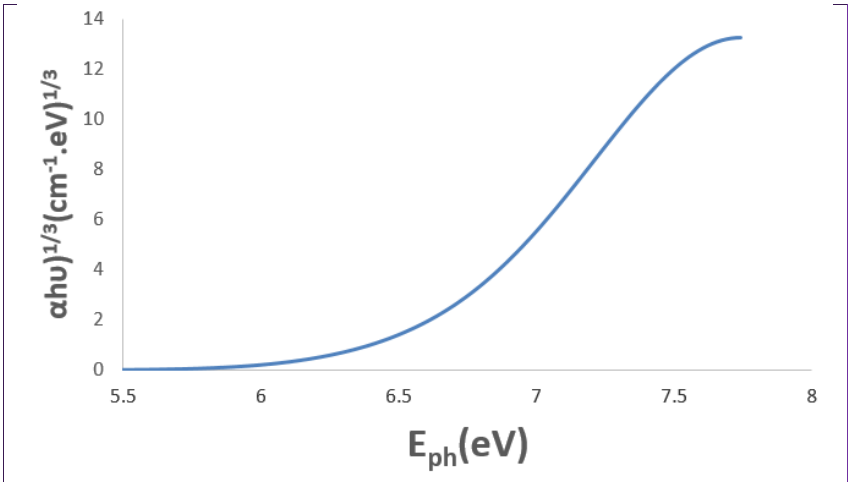
(PVA-SnO_2-Ag) nanocomposite	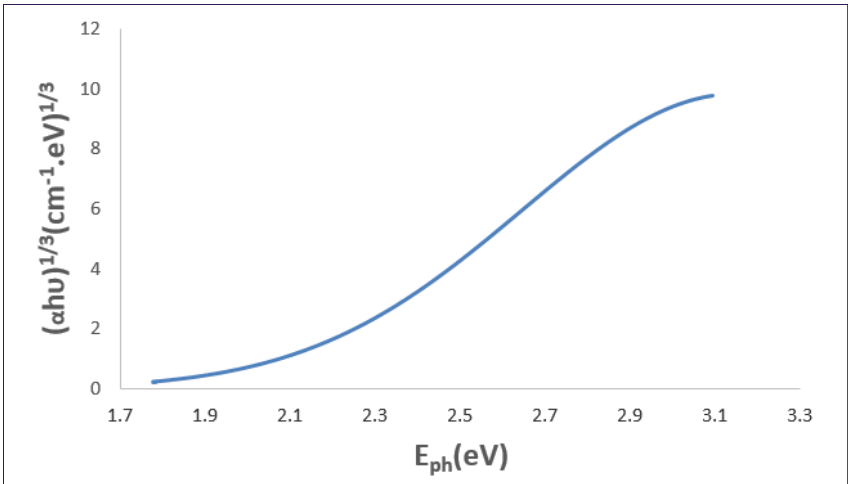
(PVA- TiO_2-Ag) nanocomposite	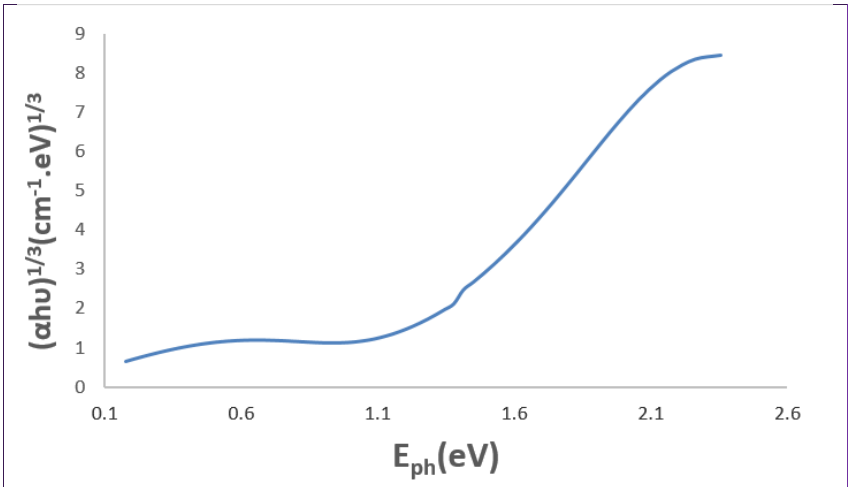

Figure 4.36. Variation of $(\alpha h\upsilon)^{1/3}$ for PVA and its nanocomposites with photon energy (theoretical).

Table 4.7. The variation of optical band gap for PVA and its nanocomposites (experimental).

Concentration (wt%)	PVA-SnO_2-Ag		PVA-TiO_2-Ag	
	Allowed indirect band gap (eV)	Forbidden indirect band gap (eV)	Allowed indirect band gap (eV)	Forbidden indirect band gap (eV)
Pure	4.6	4	4.5	4
0.75	4.2	3.7	4.2	3.4
1.5	4	3.2	3.9	3
2.5	3.8	3	3.7	2.8
3	3.6	2.6	3.5	2.4

4.4.3 The Extinction Coefficient and Refractive Index of (PVA-SnO_2-Ag) and (PVA-TiO_2-Ag) Nanocomposites

The extinction coefficient is calculated using Equation (2.30). Figures (4.37, 4.38) and (4.39) show the variation of the extinction coefficient (k) with wavelength for (PVA-SnO_2-Ag) and (PVA-TiO_2-Ag) nanocomposites experimentally and theoretically respectively. The figures show that the extinction coefficient of nanocomposites increases as the concentration increases of AgNPs (0.75, 1.5, 2.5, and 3) wt%. This type of behavior can be attributed to an increase in carrier density, which allows to an increase in the absorption coefficient with AgNPs and, as a result, an increase in the extinction coefficient with the addition of AgNPs [183]. The extinction coefficient of these nanocomposites has a high value in the UV region, which is caused by the high absorbance of all nanocomposites samples. Furthermore, the extinction coefficient of nanocomposites increases with increasing of the wavelength, implying that the extinction coefficient increases with increasing wavelength according to Equation (2.30). Through the equation (2.28), the refractive index is calculated. As

shown in Figures (4.40-4.41) while Figure (4.42) show the values of the refractive index of nanocomposites (PVA-SnO_2-Ag) and (PVA-TiO_2-Ag) as a function of wavelength experimentally and theoretically. It was found that the refractive index values increase as the concentration of AgNPs increases (0.75, 1.5, 2.5 and 3) wt. %. , while it decrease with increasing wavelength, as this behavior is attributed to the increase in the density of the nanocomposites. [184,185].

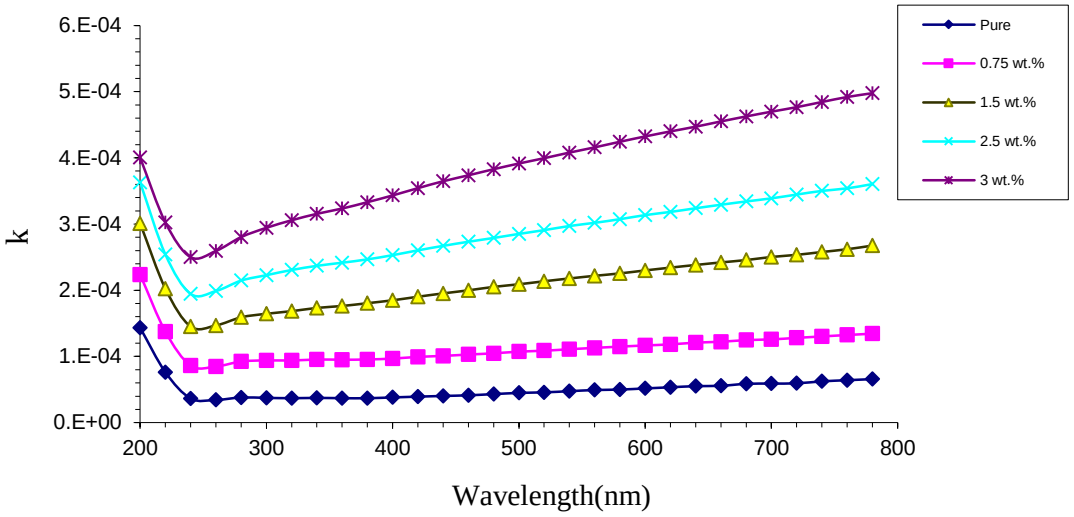

Figure 4.37. Variation of extinction coefficient for PVA and (PVA-SnO_2-Ag) nanocomposites with wavelength (experimental).

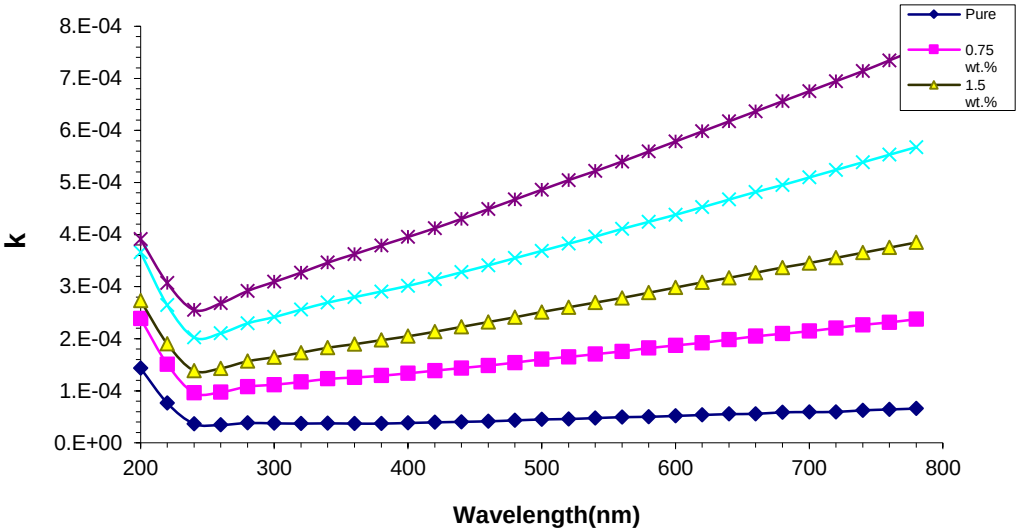

Figure 4.38. Variation of extinction coefficient for PVA and (PVA-TiO_2-Ag) nanocomposites with wavelength (experimental).

The pure polymer (PVA)	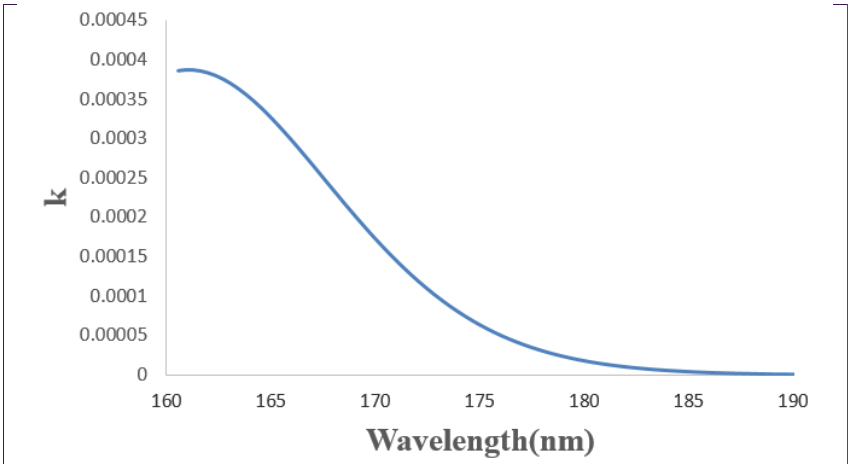
(PVA-SnO_2-Ag) nanocomposite	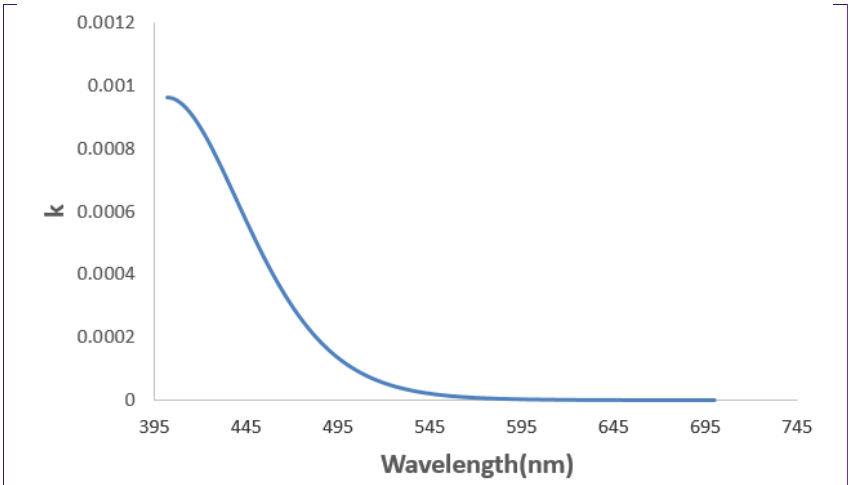
(PVA- TiO_2-Ag) nanocomposite	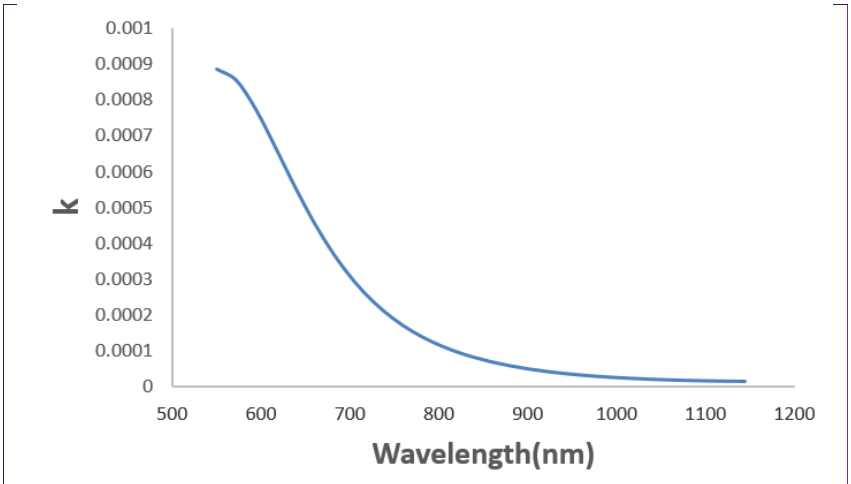

Figure 4.39. Variation of extinction coefficient for PVA and its nanocomposites with wavelength (theoretical).

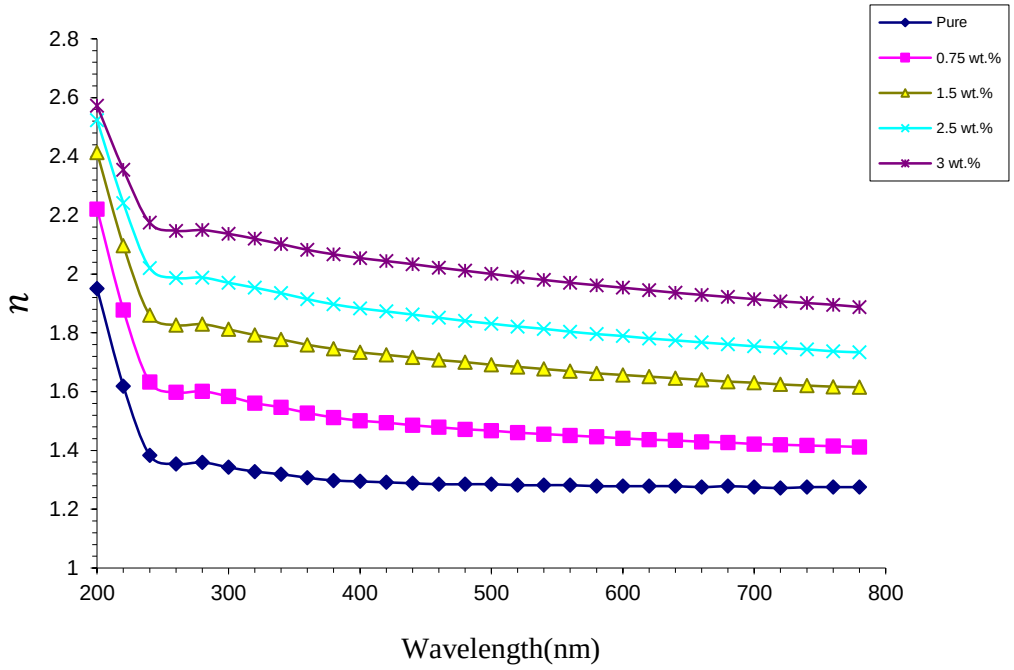

Figure 4.40. Variation of refractive index for PVA and (PVA-SnO_2-Ag) nanocomposites with wavelength (experimental).

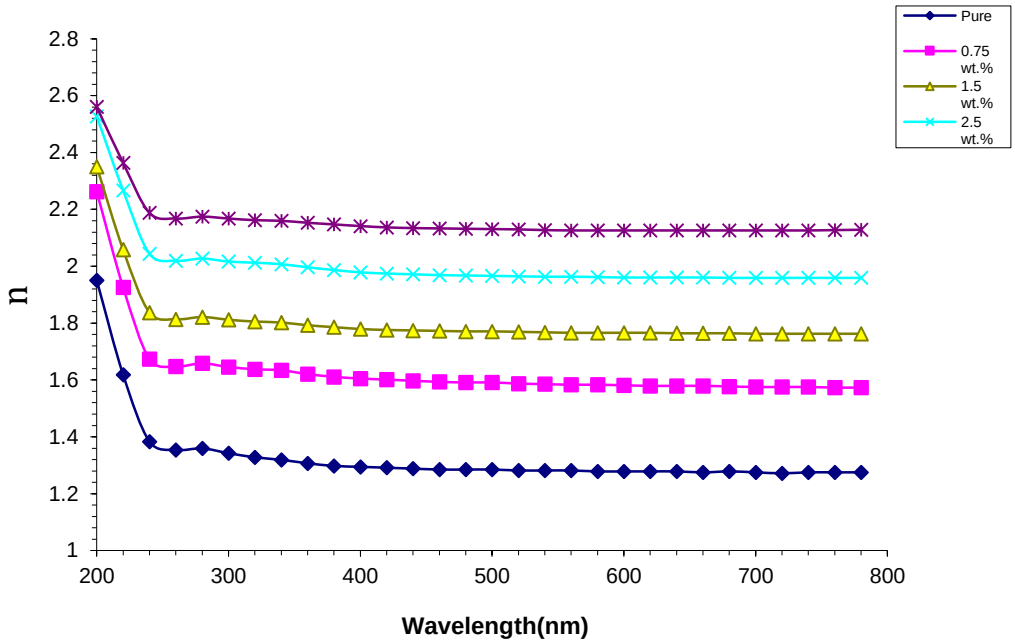

Figure 4.41. Variation of refractive index for PVA and (PVA-TiO_2-Ag) nanocomposites with wavelength (experimental).

The pure polymer (PVA)	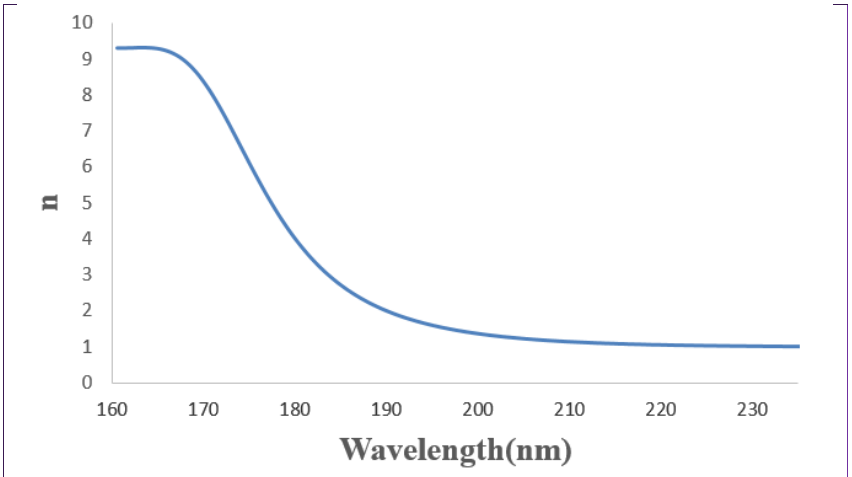
(PVA-SnO_2-Ag) nanocomposite	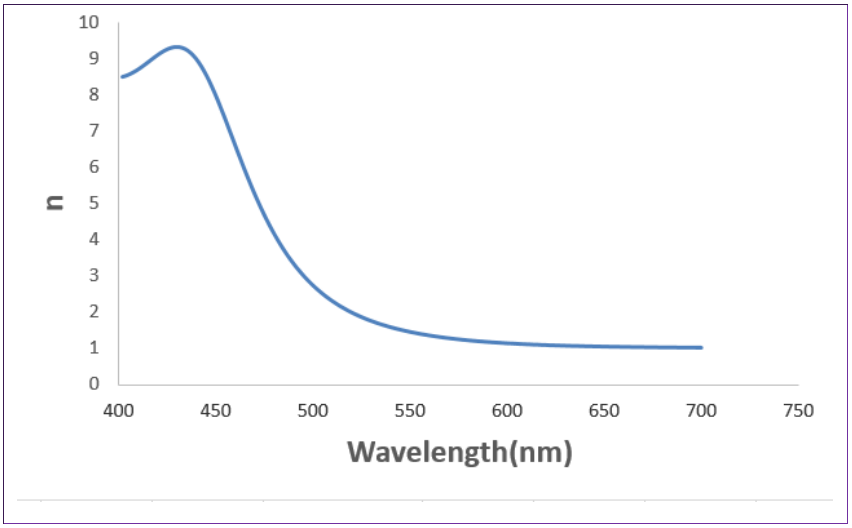
(PVA- TiO_2-Ag) nanocomposite	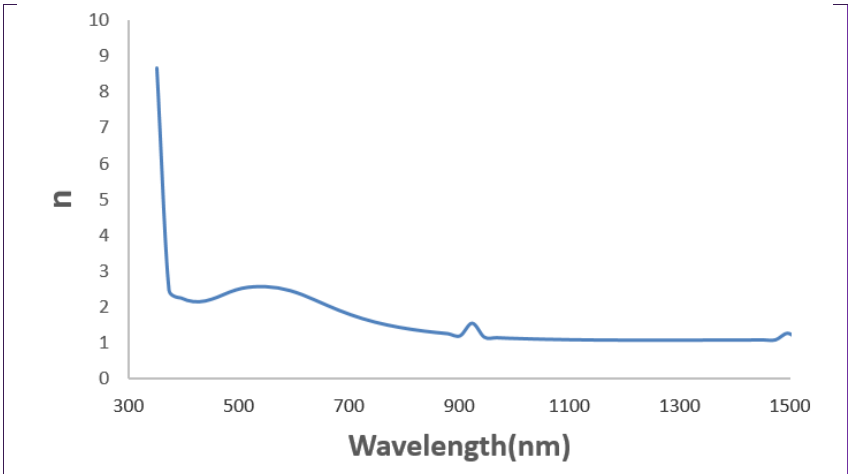

Figure 4.42. Variation of refractive index for PVA and its nanocomposites with wavelength (theoretical).

4.4.4 The Real and Imaginary Parts of Dielectric Constant

Equations (2.33) and (2.34) are used to calculate the real (ε_1) and imaginary (ε_2) dielectric constants. Figures (4.43, 4.44) and (4.45) show the real parts of the dielectric constant of (PVA-SnO_2-Ag) and (PVA-TiO_2-Ag) nanocomposites change with wavelength, experimentally and theoretically respectively. The change of the real part of the dielectric constant depends on the refractive index according to equation (2.33), while the extinction coefficient becomes smaller compared to the refractive index and because the values of the refractive index of nanocomposites (PVA-SnO_2-Ag) and (PVA-TiO_2-Ag) are larger slightly more than that of pure PVA, which was interpreted on the basis of the nature surfaces, resulting in increased values of the real part of the dielectric constant, noting that the increase in the concentrations of AgNPs led to an increase in the values of the real dielectric constant. Figures (4.46, 4.47) and (4.48) show the influence of AgNPs on the imaginary part of dielectric constant (ε_2) for (PVA-SnO_2-Ag) and (PVA-TiO_2-Ag) nanocomposites, where there is an increase in the imaginary dielectric constant of the (PVA-SnO_2-Ag) and (PVA-TiO_2-Ag) nanocomposites with the increase of AgNPs (0.75, 1.5, 2.5 and 3) wt% [186]. The imaginary part of the dielectric constant (ε_2) is affected by the extinction coefficient, particularly in the visible and near-infrared wavelength regions where the refractive index is approximately constant, whereas the extinction coefficient increases as a nanoparticles ratio in the nanocomposites increases [187].

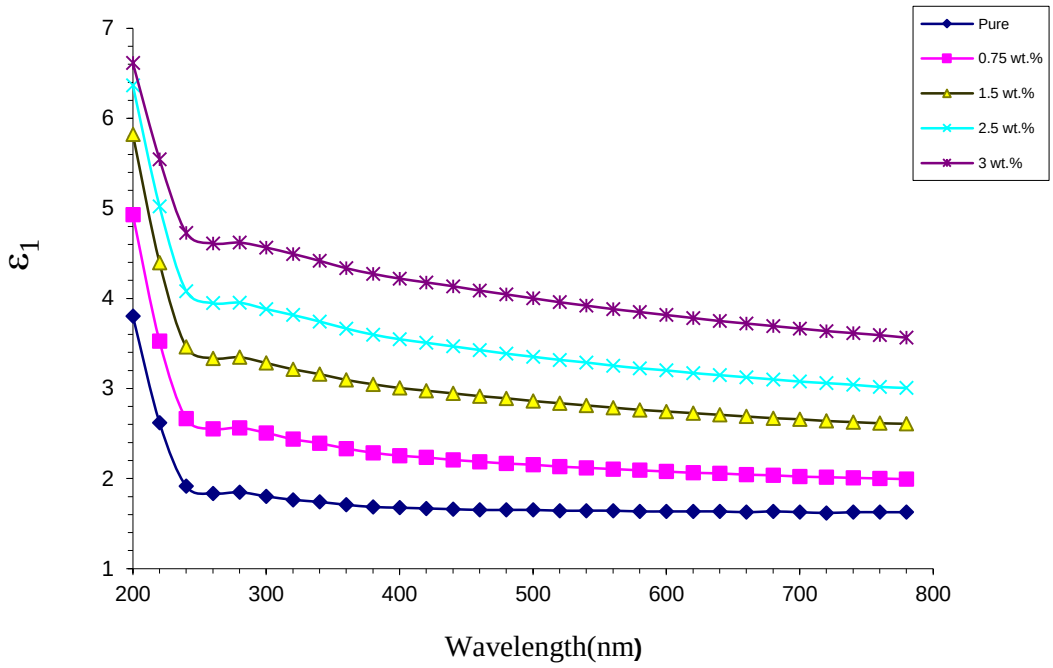

Figure 4.43. Real dielectric constant as a function of wavelength for PVA and (PVA-SnO_2-Ag) nanocomposites (experimental).

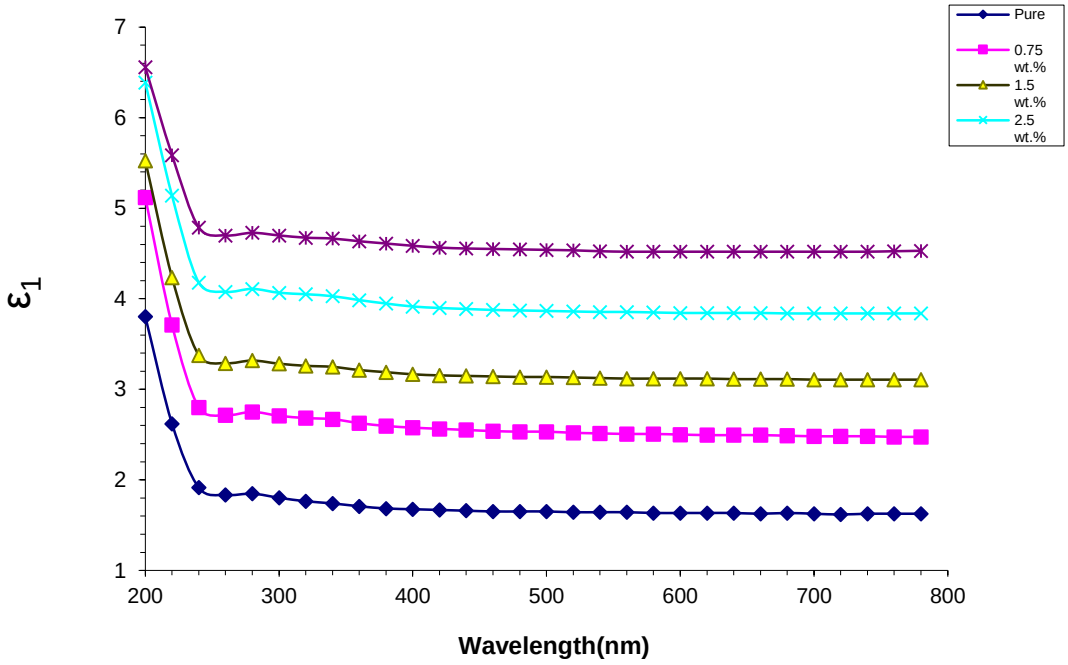

Figure 4.44. Real dielectric constant as a function of wavelength for PVA and (PVA-TiO_2-Ag) nanocomposites (experimental).

The pure polymer (PVA)	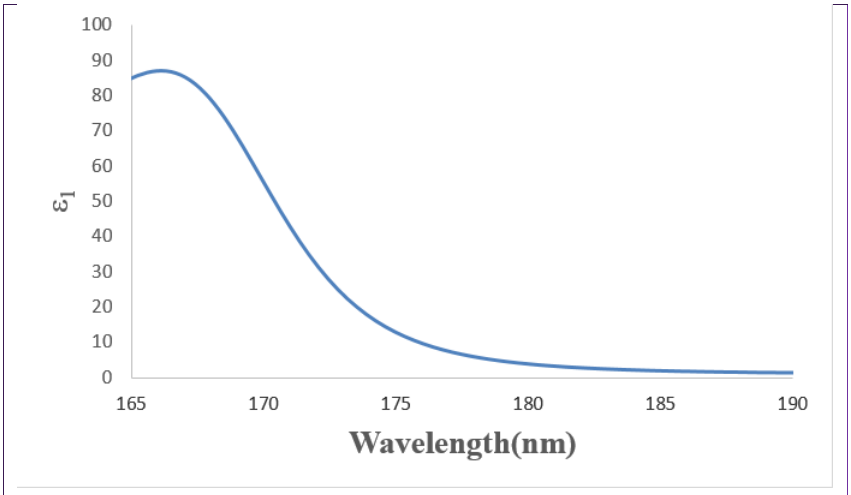
(PVA-SnO_2-Ag) nanocomposite	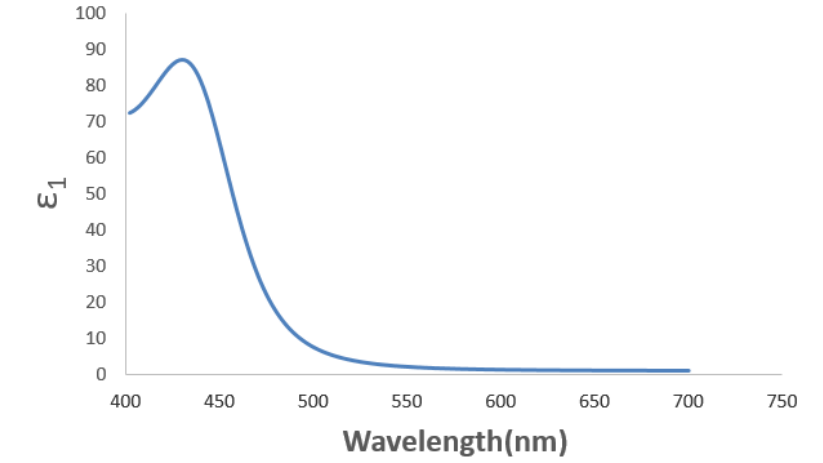
(PVA- TiO_2-Ag) nanocomposite	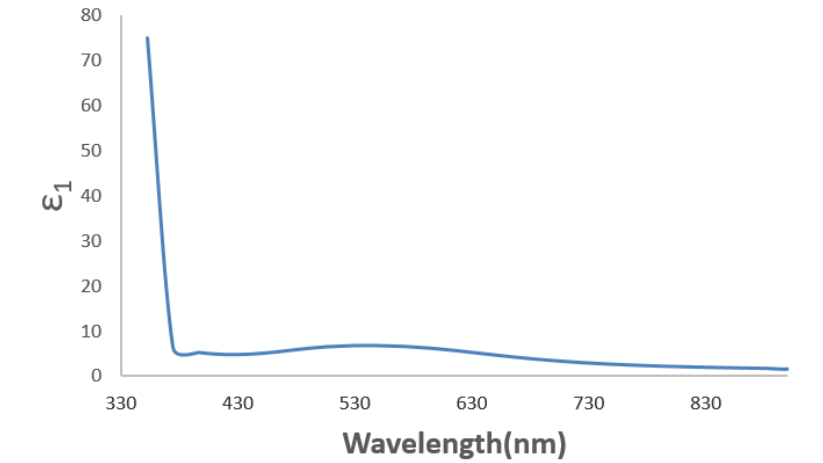

Figure 4.45. Real dielectric constant as a function of wavelength for PVA and its nanocomposites (theoretical).

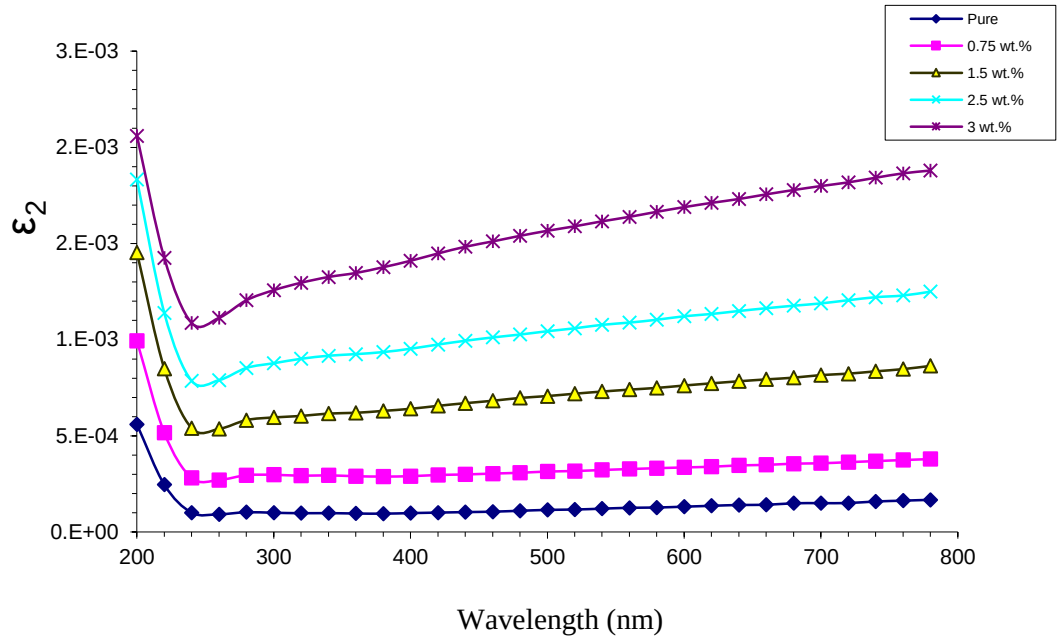

Figure 4.46. Imaginary dielectric constant as a function of wavelength for PVA and (PVA-SnO_2-Ag) nanocomposites (experimental).

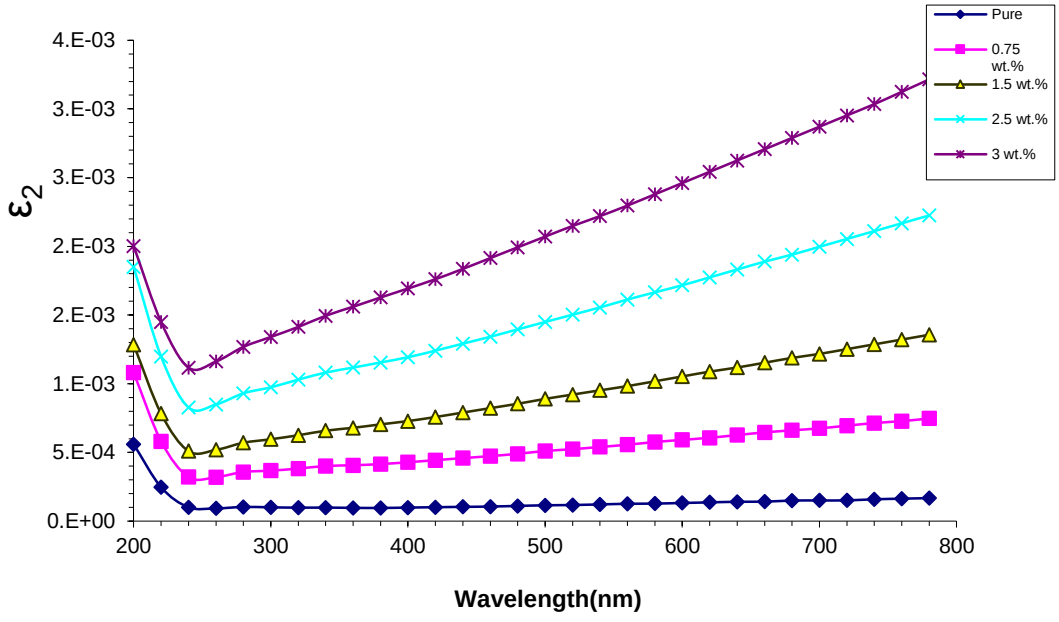

Figure 4.47. Imaginary dielectric constant as a function of wavelength for PVA and (PVA-TiO_2-Ag) nanocomposites (experimental).

The pure polymer (PVA)	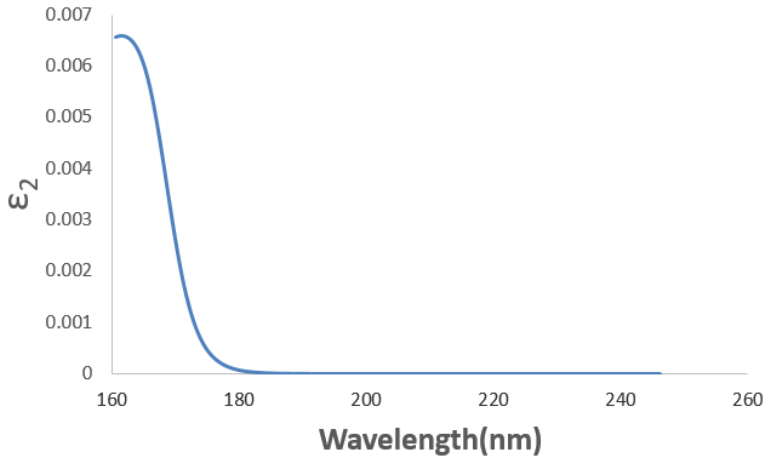
(PVA-SnO_2-Ag) nanocomposite	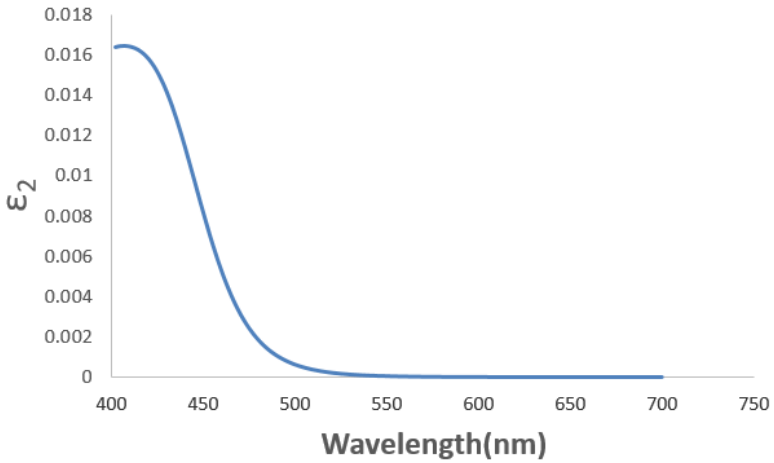
(PVA- TiO_2-Ag) nanocomposite	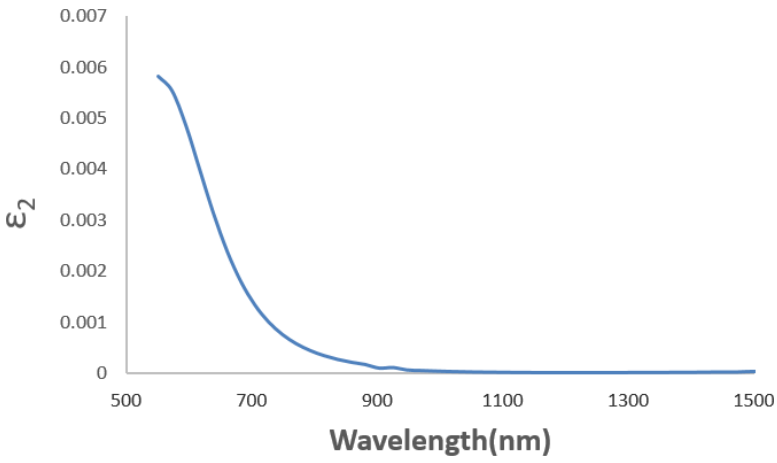

Figure 4.48. Imaginary dielectric constant as a function of wavelength for PVA and its nanocomposites (theoretical).

4.4.5 The Optical Conductivity of (PVA-SnO_2-Ag) and (PVA-TiO_2-Ag) Nanocomposites.

Relying on Equation (2.35), the optical conductivity characteristic was calculated, as in Figures (4.49, 4.50) and (4.51) where the variation in optical conductivity as a function of the wavelength of (PVA-SnO_2-Ag) and (PVA-TiO_2-Ag) nanocomposites, which calculated experimentally and theoretically respectively. It is clear from these figures that the high value of the optical conductivity was by increasing the concentration of AgNPs (0.75, 1.5, 2.5 and 3) wt%, that the reason for this behavior is the formation of local levels in the energy gap region, and thus the intensity of these levels increases whenever the concentration of AgNPs is high and this means increasing the absorption coefficient, which in turn leads to an increase in the optical conductivity of the nanocomposites [188]. At the same time, it was found that the optical conductivity depends on the wavelength. In the figures, we note that at the ultraviolet region, in other words, at low wavelengths, an increase in the optical conductivity of the nanocomposites is observed due to the increase in energy in this region, and thus the electron is excited due to the high absorption. As for increasing wavelengths in the visible and infrared regions, the optical conductivity begins to decrease as the wavelength increases due to the decrease in the energy at this values of the wavelengths [189]. So, when calculating the optical properties of the nanocomposites, we find that the nanocomposite (PVA-SnO_2-Ag) showed higher optical properties than (PVA-TiO_2-Ag) nanocomposites, and this gives the possibility of using it in many optical applications such as solar cells, photocatalyst and sensors.

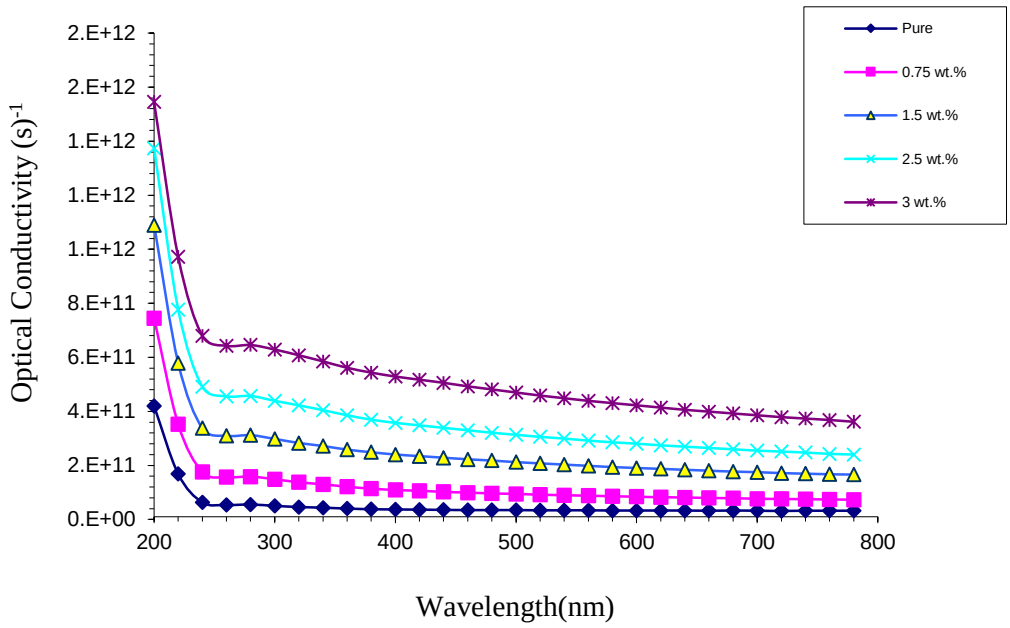

Figure 4.49. Variation of optical conductivity for PVA and (PVA-SnO_2-Ag) nanocomposites with wavelength (experimental).

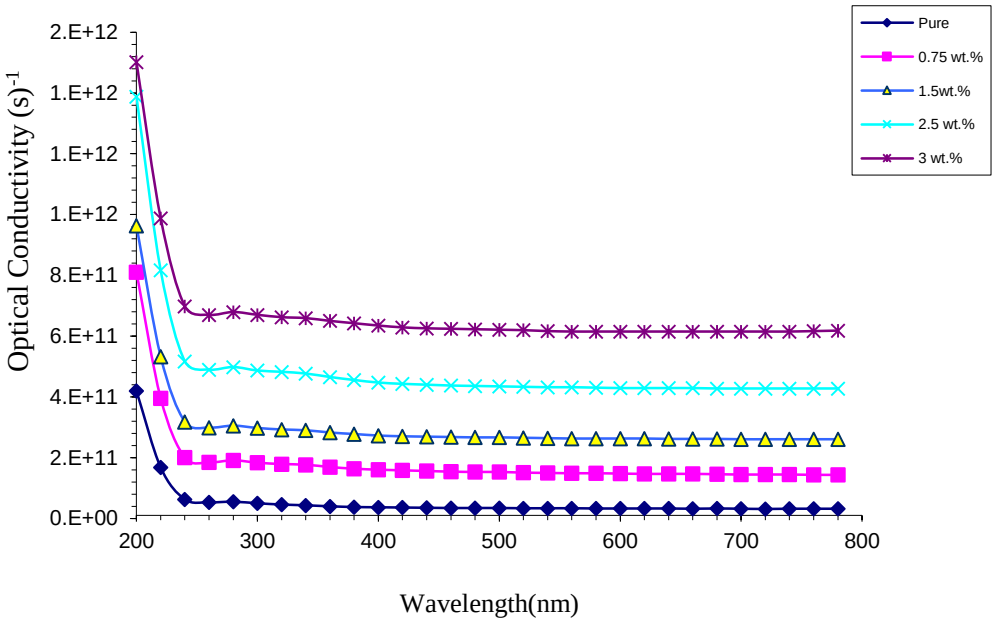

Figure 4.50. Variation of optical conductivity for PVA and (PVA-TiO_2-Ag) nanocomposites with wavelength (experimental).

The pure polymer (PVA)	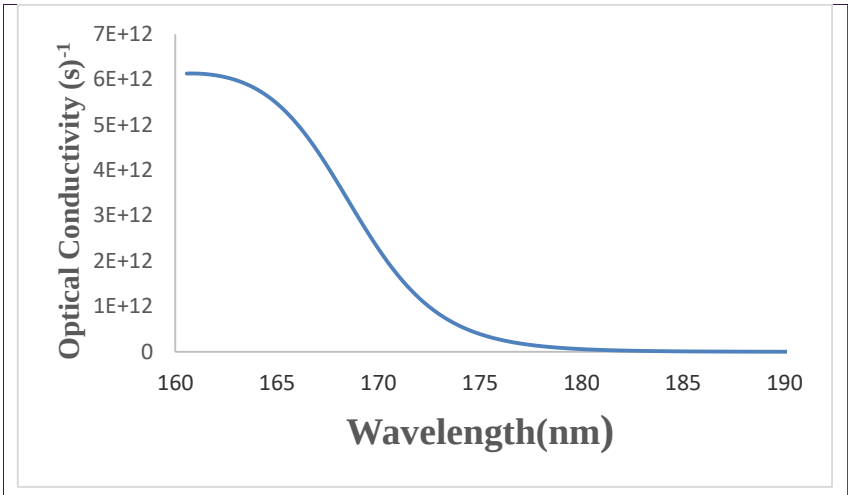
(PVA-SnO_2-Ag) nanocomposite	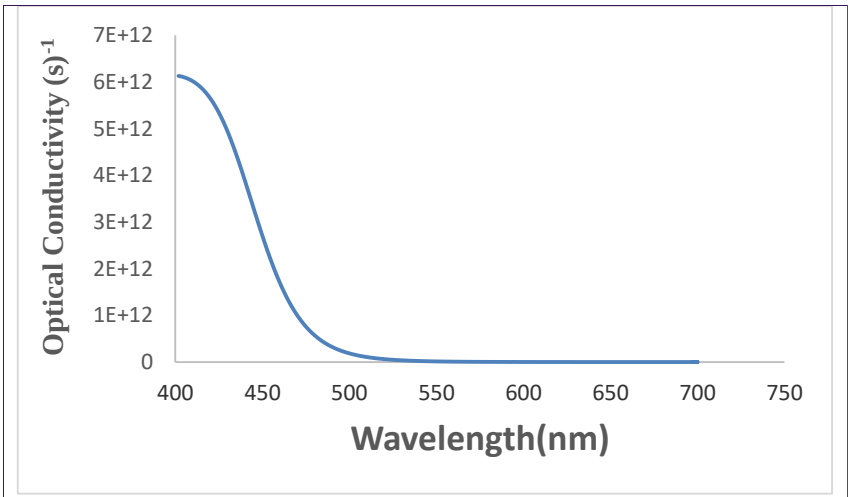
(PVA- TiO_2-Ag) nanocomposite	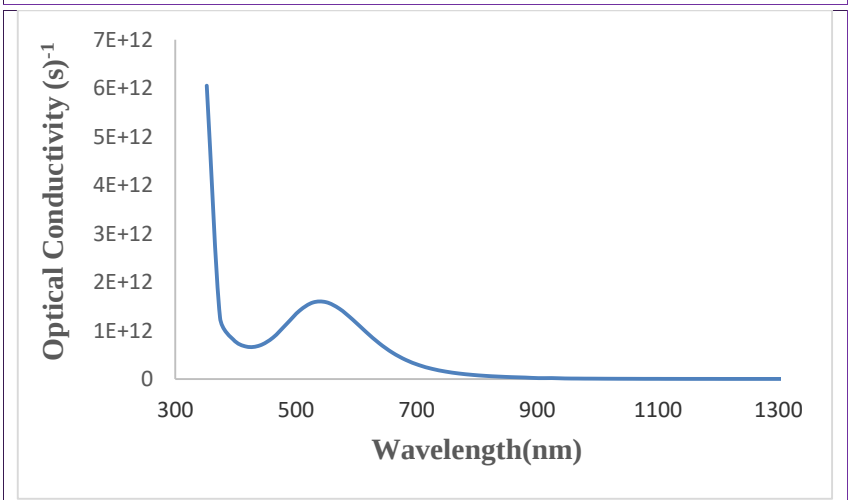

Figure 4.51. Variation of optical conductivity for PVA and its nanocomposites with wavelength (theoretical).

4.5 The Application of (PVA-SnO_2-Ag) and (PVA-TiO_2-Ag) Nanocomposites as Antibacterial Activity

The antibacterial activity of the (PVA-SnO_2-Ag) and (PVA-TiO_2-Ag) nanocomposites samples tested against gram-negative Salmonella, Escherichia coli, Stenotrophomonas maltophilia and gram positive Bacillus cereus. Figure (4.52) shows the samples of nanocomposites grown among the types of bacteria used for the purpose of studying the effectiveness of these nanocomposites to inhibit bacteria.

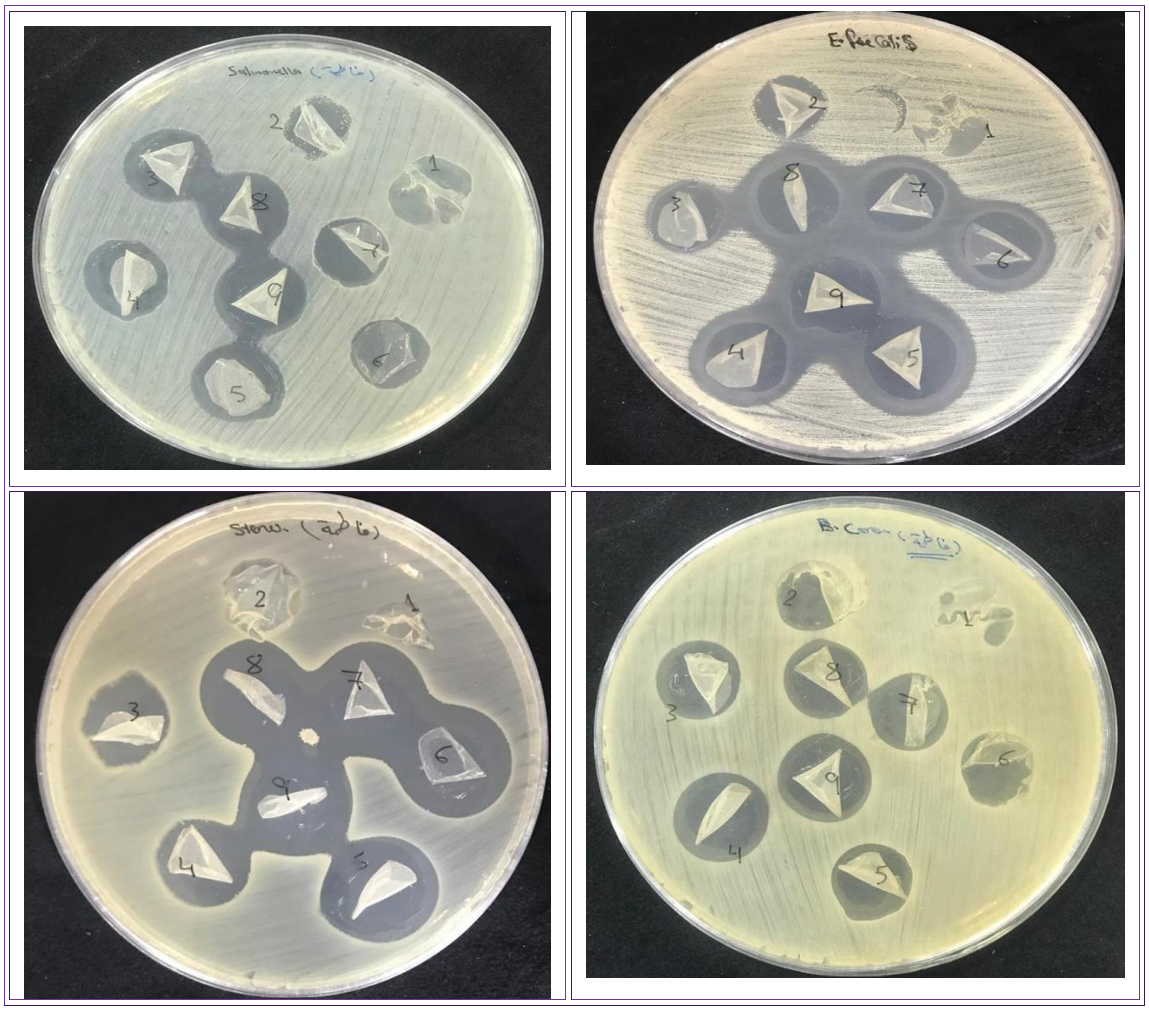

Figure 4.52. Antibacterial activity of (PVA-SnO_2-Ag) and (PVA-TiO_2-Ag) against the bacteria (Salmonella, Escherichia coli, Stenotrophomonas maltophilia and Bacillus cereus)

The data obtained are represented in the Tables (4.8, 4.9),which shows the inhibition diameters in millimeters. The reason for the bactericidal activity of the (PVA-SnO_2-Ag) and (PVA-TiO_2-Ag) nanocomposites is due to the Silver nanoparticles which interact with bacterial membrane proteins, intracellular proteins, phosphate residues in DNA, and to interfere with cell division, leading to bacterial cell death [191]. Figures (4.53, 4.56) shows the comparison between the nanocomposites (PVA-SnO_2-Ag) and (PVA-TiO_2-Ag) in terms of their effectiveness to inhibit the types of bacteria used. From Figure (4.53) we find that the inhibition diameters ranged between (21-28) mm for both nanocomposites, but the nanocomposite (PVA-TiO_2-Ag) showed a higher ability than the nanocomposites (PVA-SnO_2-Ag) in inhibiting Salmonella type bacteria, where the highest percentage of inhibition diameter was (28) mm at a concentration of (3) Wt. % of AgNPs, and this indicates that the inhibition area increases with the increase of AgNPs concentrations.

Figure (4.54) shows that the nanocomposites (PVA-SnO_2-Ag) gave higher values of inhibition diameters for Escherichia coli bacteria, where the ratio ranged between (30-31) mm at AgNPs concentrations (0.75, 1.5, 2.5, and 3) Wt. % compared to the nanocomposites (PVA-TiO_2-Ag). As for Figure (4.55), the nanocomposites (PVA-SnO_2-Ag) showed a high effectiveness for inhibiting Stenotrophomonas maltophilia bacteria, with a percentage ranging between (30-32) mm, while the activity of the nanocomposites (PVA-TiO_2-Ag) was lower and ranged between (25-32) mm at concentrations of AgNPs (0.75, 1.5, 2.5, and 3) Wt.%.

As for Figure (4.56), we find that the percentage of inhibition diameters for Bacillus cereus are somewhat close and ranged between (20-26) mm for both compounds, but the nanocomposites (PVA-TiO_2-Ag) showed a slightly higher percentage than the nanocomposites (PVA-SnO_2-Ag). From

this we conclude that the concentration of AgNPs has an effect on the inhibition zone for all types of bacteria. For example, we find in Figures (4.57-4.64) a difference in the percentages of resistance of bacteria types at concentrations AgNPs (0.75, 1.5, 2.5, and 3) Wt.%, For example, at the concentration of (0.75) Wt.%, we find that the bacteria Salmonella and Bacillus cereus showed a higher resistance to the nanocomposites (PVA-SnO_2-Ag) compared to bacteria Escherichia coli and Stenotrophomonas maltophilia as shown in Figure (4.57), when we increase the concentration of AgNPs to (1.5) Wt.%, we notice a decrease in the resistance of Salmonella and Bacillus cereus than it was at the concentration of (0.75) Wt.%. In Figure (4.59), and so for the rest of the concentrations, we find that the higher the concentration, the lower the resistance of bacteria and the higher the activity of the nanocomposites (PVA-SnO_2-Ag) in inhibiting, as in Figures (4.61, 4.63). While the nanocomposites (PVA-TiO_2-Ag), the concentration has an effect on the resistance of bacteria and we find it clear in Figure (4.58) at the concentration of (0.75) Wt. % of AgNPs, where the resistance of bacteria was Escherichia coli and the Bacillus cereus higher than resistance Salmonella and Stenotrophomonas maltophilia, while at a concentration of (1.5) Wt. % of AgNPs, and as in Figure (4.60), we find that the resistance of both Salmonella and Stenotrophomonas maltophilia started decreasing due to increased concentration of AgNPs, and also for the rest of the forms (4.62, 4.64). From this we conclude that the weakness of bacterial resistance is because of the increased concentrations of AgNPs, which interact with the cell wall of bacteria and cause death or weakness of the cell. So, in general from the above results, we find that the nanocomposites (PVA-SnO_2-Ag) gave a higher activity than the nanocomposites (PVA-TiO_2-Ag) in inhibiting bacteria.

Table 4.8. The effect of the pure PVA and PVA-SnO_2-Ag nanocomposite as antibacterial activity.

Type of nanocomposite	Concentration of AgNPs Wt.%	Salmonella	Escherichia coli	Stenotrophomonas maltophilia	Bacillus cereus
PVA	0	0	0	0	0
PVA-SnO_2-Ag	0.75	21	30	30	21
	1.5	23	30	32	22
	2.5	24	31	32	23
	3	25	31	32	25

Table 4.9. The effect of the pure PVA and PVA-TiO_2-Ag nanocomposite as antibacterial activity.

Type of nanocomposite	Concentration of AgNPs Wt.%	Salmonella	Escherichia coli	Stenotrophomonas maltophilia	Bacillus cereus
PVA	0	0	0	0	0
PVA-TiO_2-Ag	0.75	21	20	25	20
	1.5	26	23	26	23
	2.5	27	27	28	24
	3	28	31	32	26

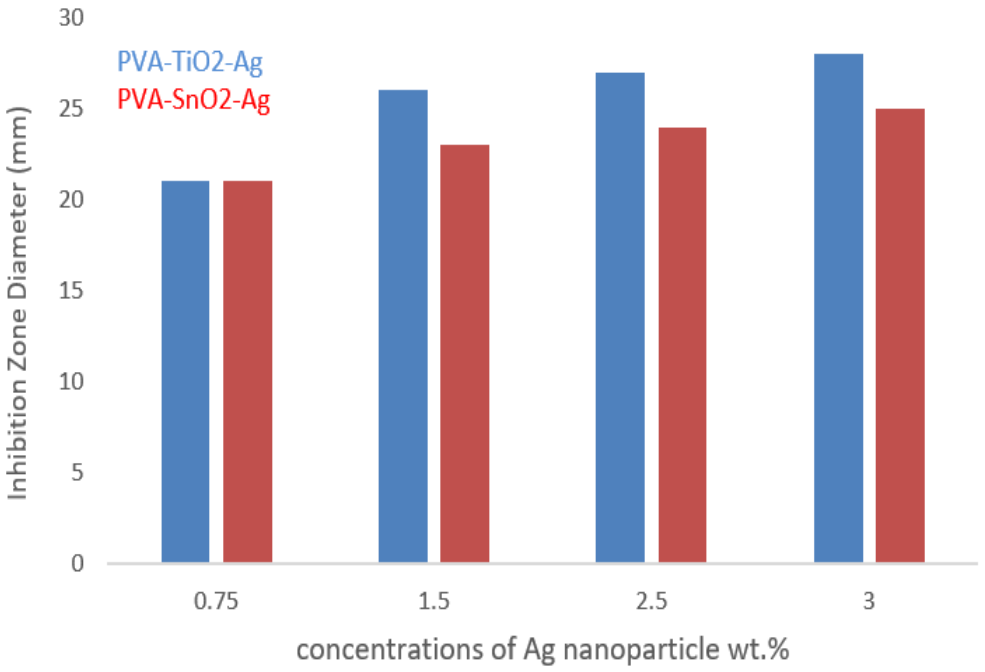

Figure 4.53. Antibacterial application of (PVA-SnO_2-Ag) and (PVA-TiO_2-Ag) as a function of $AgNP_S$ concentrations against Salmonella.

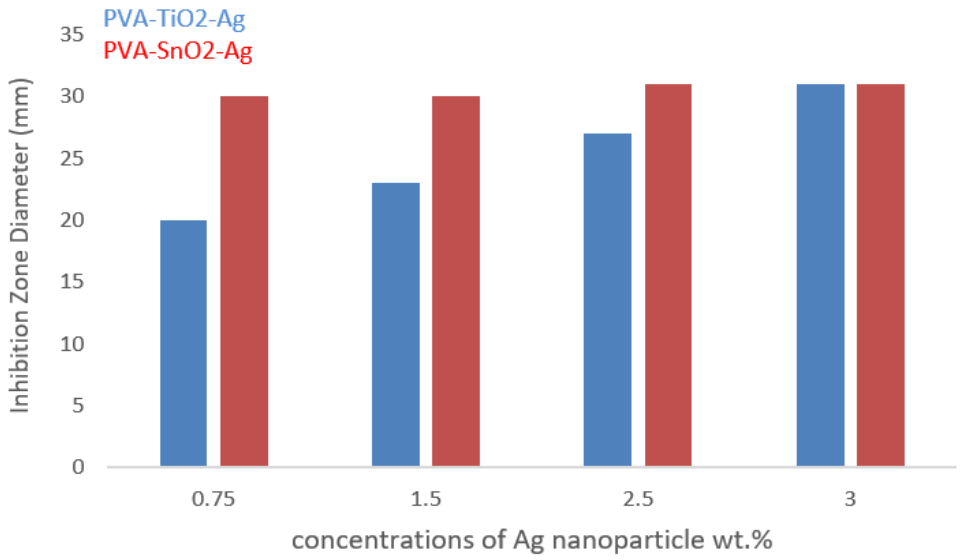

Figure 4.54. Antibacterial application of (PVA-SnO_2-Ag) and (PVA-TiO_2-Ag) as a function of $AgNP_S$ concentrations against Escherichia coli.

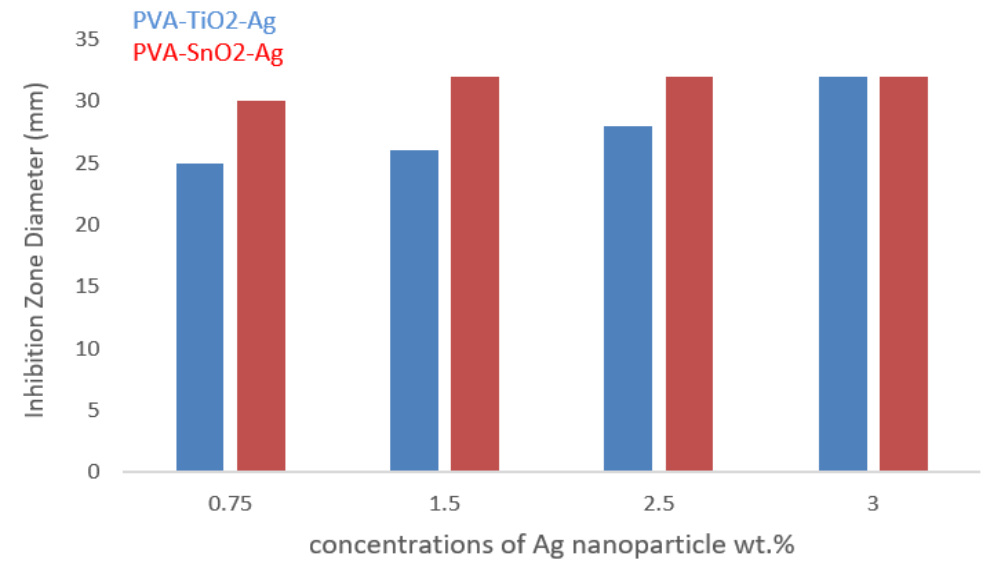

Figure 4.55. Antibacterial application of (PVA-SnO_2-Ag) and (PVA-TiO_2-Ag) as a function of $AgNP_S$ concentrations against Stenotrophomonas maltophilia.

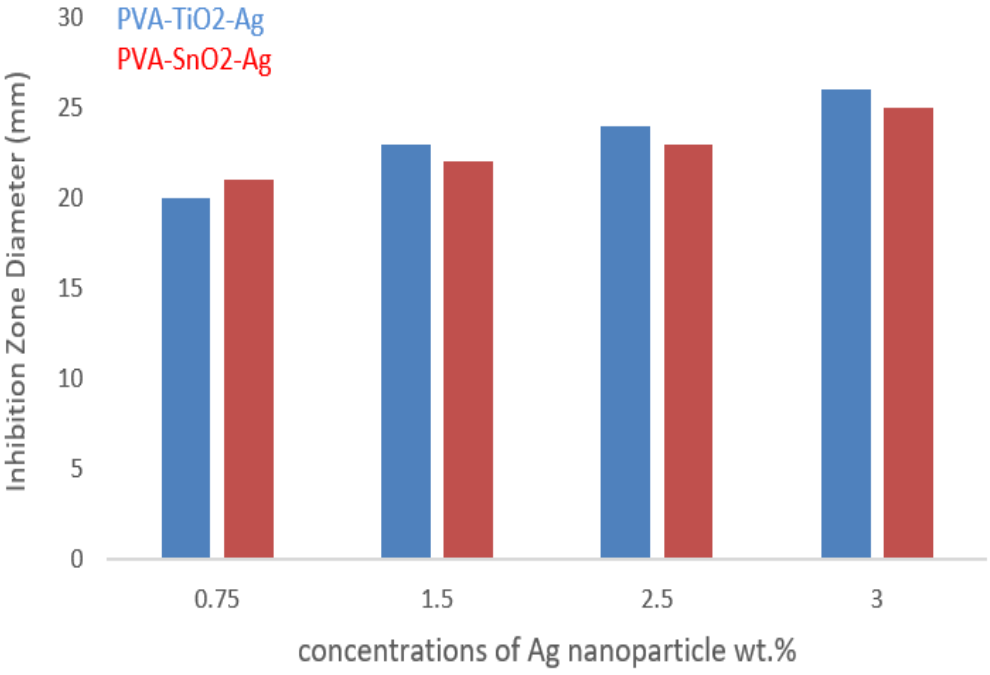

Figure 4.56. Antibacterial application of (PVA-SnO_2-Ag) and (PVA-TiO_2-Ag) as a function of $AgNP_S$ concentrations against Bacillus cereus.

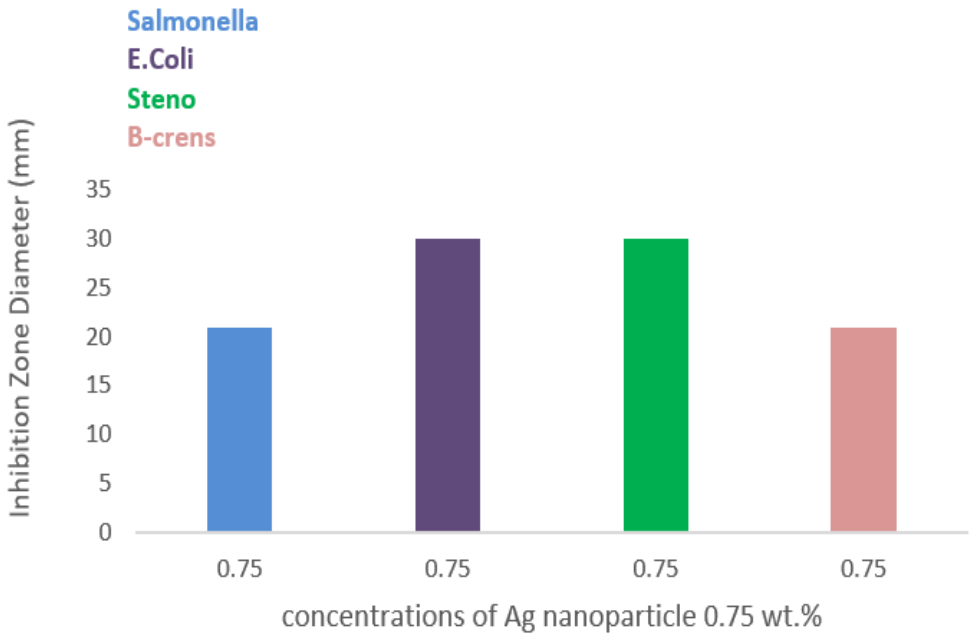

Figure 4.57. Effect of AgNPs concentration (0.75 wt. %) on the bacteria in the nanocomposite (PVA-SnO_2-Ag).

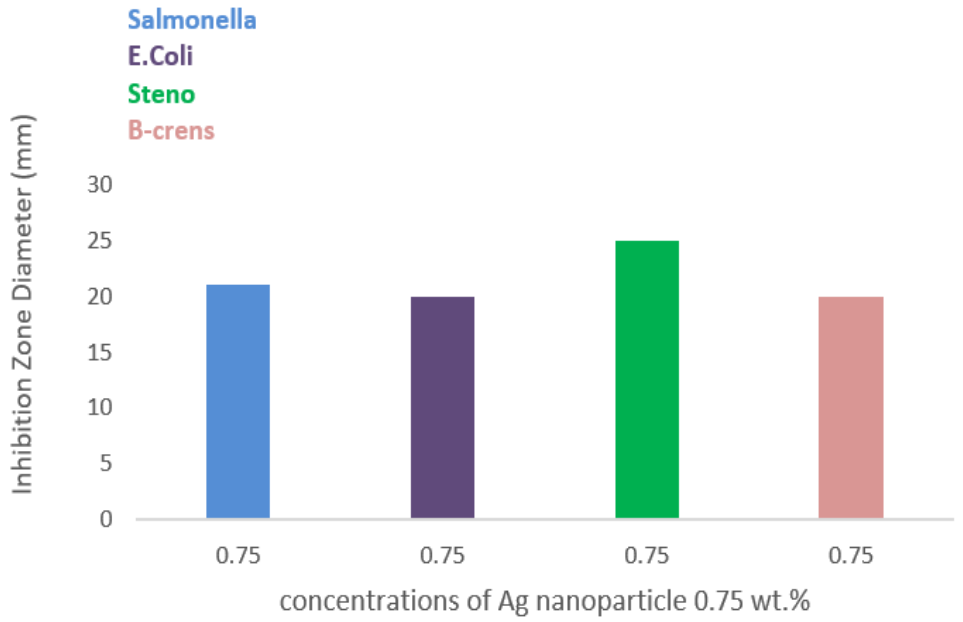

Figure 4.58. Effect of AgNPs concentration (0.75 wt. %) on the bacteria in the nanocomposite (PVA-TiO_2-Ag).

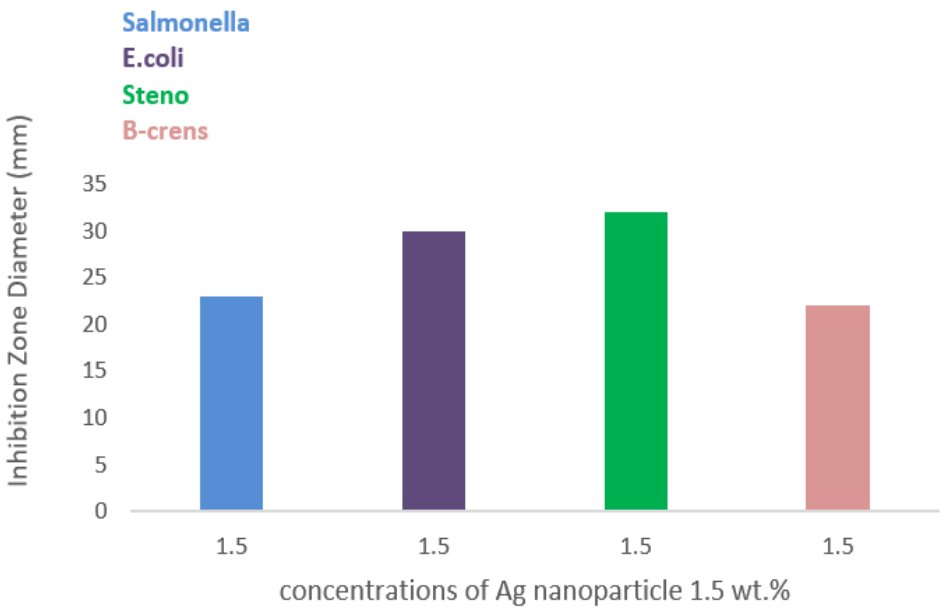

Figure 4.59. Effect of AgNPs concentration (1.5 wt. %) on the bacteria in the nanocomposite (PVA-SnO_2-Ag).

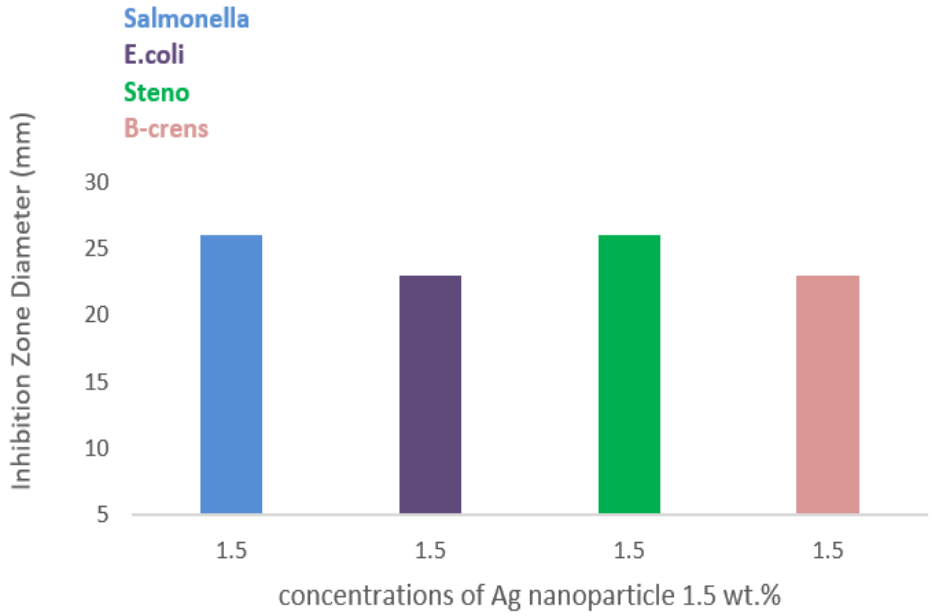

Figure 4.60. Effect of AgNPs concentration (1.5 wt. %) on the bacteria in the nanocomposite (PVA-TiO_2-Ag).

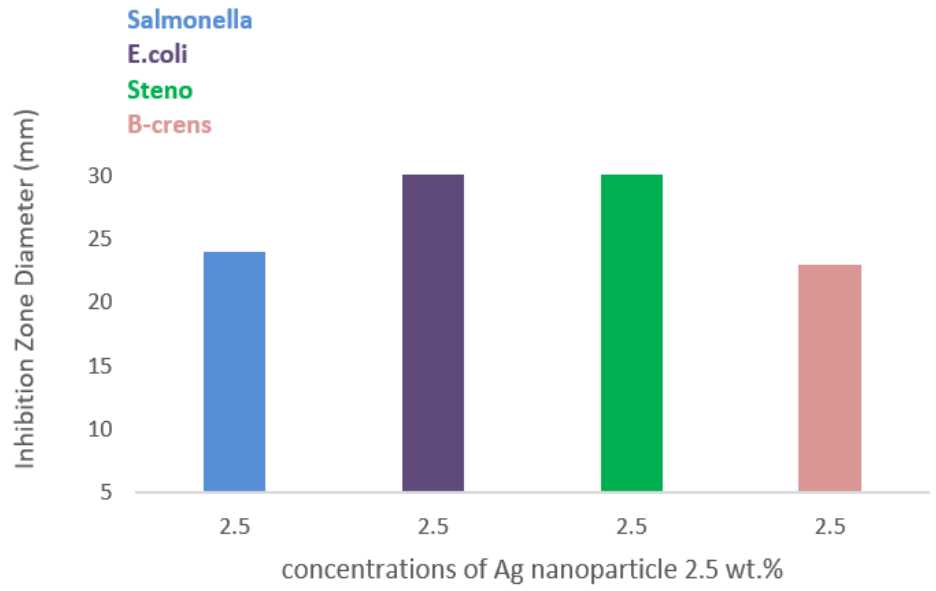

Figure 4.61. Effect of AgNPs concentration (2.5 wt. %) on the bacteria in the nanocomposite (PVA-SnO_2-Ag).

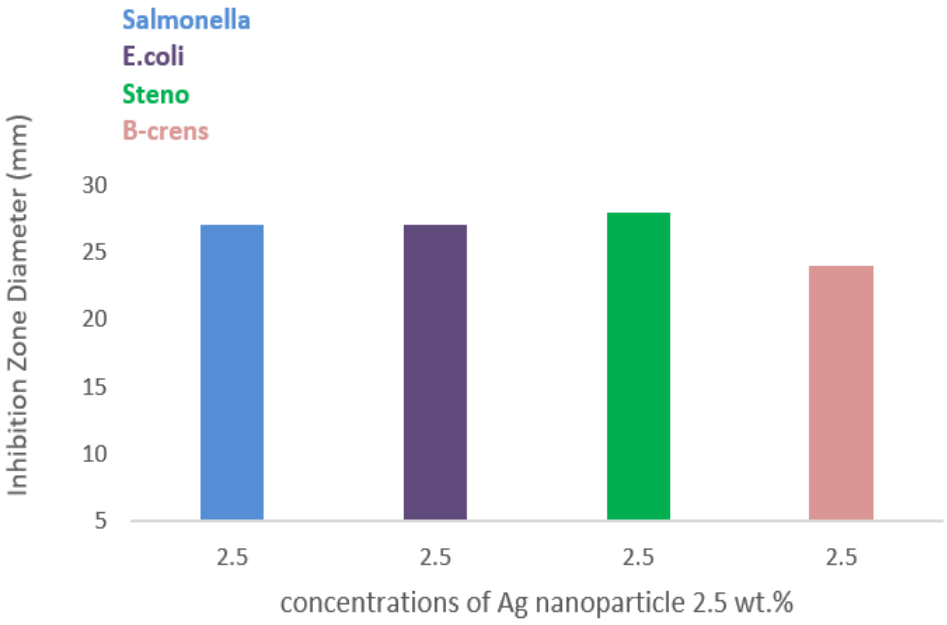

Figure 4.62. Effect of AgNPs concentration (2.5 wt. %) on the bacteria in the nanocomposite (PVA-TiO_2-Ag).

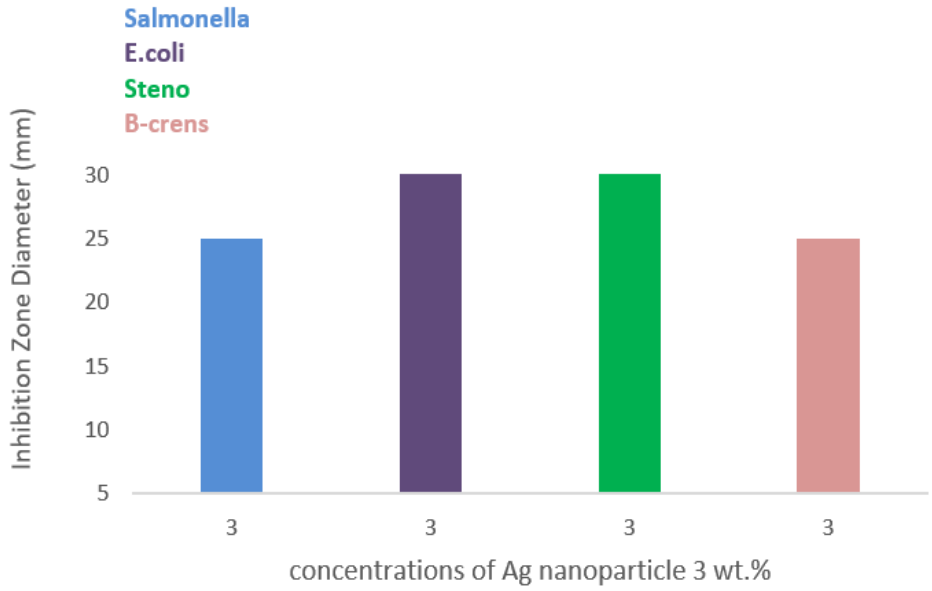

Figure 4.63. Effect of AgNPs concentration (3 wt. %) on the bacteria in the nanocomposite (PVA-SnO_2-Ag).

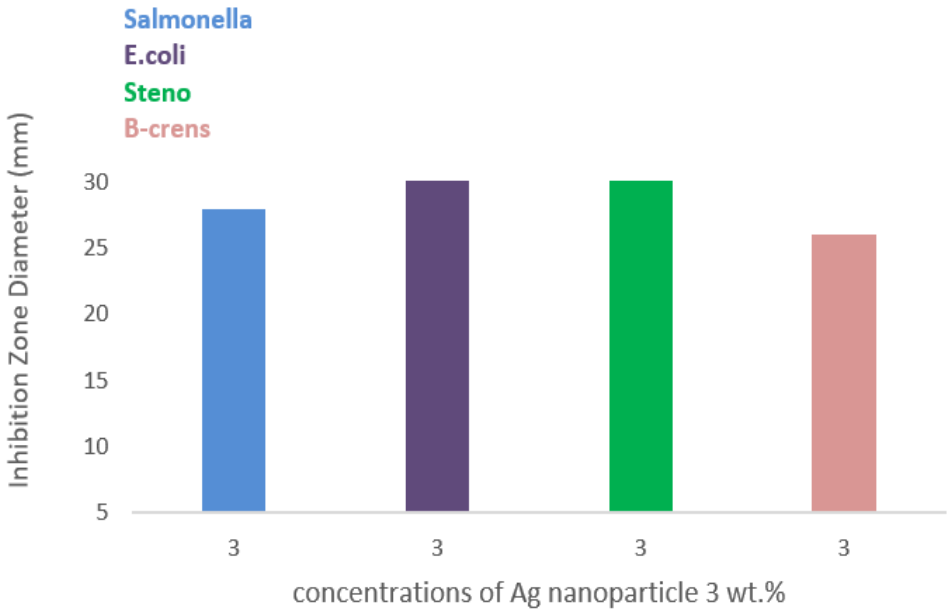

Figure 4.64. Effect of AgNPs concentration (3wt. %) on the bacteria in the nanocomposite (PVA-TiO_2-Ag).

5.1 Conclusions

In this thesis, there are many conclusions that can be summarized in the following points:

1. The functional hybrid B3LYP, based on the Gaussin program, proved that it is valid in determining the relaxation and calculating the geometric parameters of pure PVA by the base set 6-31G the results obtained are in good agreement with previous studies.

   For the others nanocomposites, were used the base set SDD, there is no reference data, so our current study supplies a new data in this field.
2. The FT-IR calculations theoretical and experimental of the samples show that when SnO_2 or TiO_2 is added to the PVA, there is no new peak or bond that is specific to SnO_2 or TiO_2. However, the change in the number of PVA peaks, which remains within the specified range As well as adding AgNPs causes a displacement of some bonds rather than the emergence of new peaks, which is the basic idea of nanocomposites.
3. For UV- Visible calculations, good results were obtained and as a result, it was concluded that the higher the concentration, the higher the absorption of the UV spectrum. So the (PVA-TiO_2-Ag) and (PVA- SnO_2-Ag) nanocomposites have high absorbance in the UV-region and extends towards the Visible area.
4. Calculating the total energy value started to decrease more when adding (AgNPs) to (PVA-SnO_2) and (PVA-TiO_2), which indicates that all nanocomposites have a good relaxation, and therefore the calculated value of energy depends on the number of electrons in the structures, where the energy value is inversely proportional to the increase in concentrations added to the pure polymer.
5. In general, the addition of AgNPs to PVA-SnO_2 and PVA-TiO_2 increased the electronic affinity, which was due to the abundance of

electrons in AgNPs. As for the softness and hardness, it was found that all nanocomposites have the highest value of softness, which indicates that these molecules require little excitation energy to transfer electrons. While the hardness value is low and the reason for this is due to the transition of the electron in the molecule from the valence to the conduction band.

6. The effect of doping with AgNPs leads to reducing the energy gap and increasing the absorption coefficient. That is, it affected negatively the energy gap values, which makes this effect of great use in the field of optical and electrical applications.
7. Among the conclusions reached show that the nanocomposites have indirect electronic transitions. As the doping did not change the nature of electronic transitions.
8. About the optical properties where we see an increase in the absorbance in the UV region of the nanocomposites samples used with an increase in the concentration of silver nanoparticles AgNPs added to each of (PVA-SnO_2) and (PVA-TiO_2), this is due to electron excitation from the valence band to the conduction band at these energies. And also we got the highest value of the absorption coefficient which obtained at high incident photon energies.
9. The extinction coefficient, refractive index, real and imaginary dielectric constants and optical conductivity of (PVA-TiO_2) and (PVA- SnO_2) nanocomposites increase with an increase in AgNPs concentrations while the transmittance decrease with an increase of the AgNPs concentrations.
10. Application of (PVA-SnO_2-Ag) and (PVA-TiO_2-Ag) Nanocomposites for Antibacterial Activity the small sized nanoparticles exhibited big antibacterial activity caused weak bacterial resistance, due to increased

concentrations of AgNPs that interact with the cell wall of bacteria and cause cell death or weakening.

5.2 Future Works

1. Study of electrical and mechanical properties for (PVA-SnO_2-Ag) and (PVA-TiO_2-Ag) nanocomposites.

2. Study of the (PVA-SnO_2-Ag) and (PVA-TiO_2-Ag) nanocomposites for humidity and pressure sensors applications.

3. Study the effect of the temperature and pressure on the electronic properties of the (PVA-SnO_2-Ag) and (PVA-TiO_2-Ag).

References

[1] Patra, Jayanta K., and Kwang B. "Comparative study of proteasome inhibitory, synergistic antibacterial, synergistic anticandidal, and antioxidant activities of gold nanoparticles biosynthesized using fruit waste materials." *International journal of nanomedicine*, 11, 4691, (2016).

[2] Kumar, Anu, Kuldeep K., and Sarika S."Synthesis, characterization and antibacterial potential of silver nanoparticles by Morus nigra leaf extract." *Indian Journal of Pharmaceutical and Biological Research,* 1.04, 16-24, (2013).

[3] Shukla, Ashutosh K., and Siavash I. "Metallic nanoparticles: green synthesis and spectroscopic characterization." *Environmental Chemistry Letters*, 15.2, 223-231. (2017).

[4] Paul, Donald R., and Lioyd M. "Polymer nanotechnology: nanocomposites." *Polymer*, 49.1, 53187-3204, (2008).

[5] Khdr, Noor F., Bassam G. Rasheed, and Baida M. "Review on Nanomaterials Properties Produced by Laser Technique." *IOP Conference Series: Materials Science and Engineering*, 1094, 1, (2021).

[6] Jaison J., Ahmed B., Yen S., Alain D. and Michael K., "Review on nanoparticles and nanostructured materials: history, sources, toxicity and regulations." *Beilstein journal of nanotechnology*, 9.1, 1050-1074, (2018).

[7] Saleh, Tawfik A. "Nanomaterials for pharmaceuticals determination." *Bioenergetic,* 5.1, 1000226, (2016).

[8] Pradell, Climent F., Molera J., Zucchiatti A., Ynsa M., Roura P., and Crespo, D., "Metallic and nonmetallic shine in luster: An elastic ion backscattering study." *Journal of Applied Physics*, 101.10, 103518, (2007).

[9] Ealia, Anu M., and Saravanakumar P., "A review on the classification, characterisation, synthesis of nanoparticles and their application."*IOP Conference Series: Materials Science and Engineering*, 263, 3, (2017).

[10] Saleh, Tawfik A. "Detection: from electrochemistry to spectroscopy with chromatographic techniques, recent trends with nanotechnology." *Detection*, 2.04, 27, (2015).

[11] Mourdikoudis, Stefanos, Roger M., and Nguyen T., "Characterization techniques for nanoparticles: comparison and complementarity upon studying nanoparticle properties." *Nanoscale* , 10.27, 12871-12934, (2018).

[12] Alagarasi, A. "Introduction to nanomaterials in Viswanathan B. (ed.), Nanomaterials." (2009).

[13] Parameswaranpillai, Jyotishkumar, Sabu Thomas, and Yves Grohens. "Polymer blends: state of the art, new challenges, and opportunities." *Characterization of polymer blends*, 1-6, (2014).

[14] Utracki, L. A. "Introduction to polymer blends." *Polymer blends handbook*, 1, (2003).

[15] White, James L., and Sug H. "Polymer blend compounding and processing." *Encyclopedia of Polymer Blends*, 2, 1-26. (2011).

[16] Hu, Hurang, Landon O, and Ayo A., "Characterizing and modeling mechanical properties of nanocomposites-review and evaluation." *Journal of minerals and materials characterization and engineering*, 9.04, 275, (2010).

[17] Bhaiswar J., Salunkhe M., Dongre S., Kumbhare B., "Comparative study on thermal stability and optical properties of PANI/CdS and PANI/PbS nanocomposite." *IOSR Journal of Applied Physics (ICAET-2014)*, 80, 79-82, (2014).

[18] Wasan A., Mohammed A., Rahimi M., Emad Y., Bashar Mudhaffar Abdullah, Jumat Salimon, Nadia Salih, and Saiful Irwan Zubairi, "Effect of nano ZnO on the optical properties of poly (vinyl chloride) films." *International journal of polymer science* (2014).

[19] Adeosun, Samson O., "Review of green polymer nanocomposites." *Journal of Minerals and Materials Characterization and Engineering*, 11.04, 385, (2012).

[20] Divya R., Meena M, Mahadevan C., and Padma C., "Investigation on CuO dispersed PVA polymer films." *Journal of Engineering Research and Applications*, 4.5, 1-7, (2014).

[21] Nimrodh A., Umapathy S., Sophia J., Mathavan T., and Mangalaraj D., "On the optical and thermal properties of in situ/ex situ reduced Ag NP's/PVA composites and its role as a simple SPR-based protein sensor." *Applied Nanoscience*, 1.2, 87-96, (2011).

[22] Abd E., Kamal M. "Spectroscopic behavior of poly (vinyl alcohol) films with different molecular weights after UV irradiation, thermal annealing, and double treatment with UV irradiation and thermal annealing." *Journal of applied polymer science*, 88.2, 589-594, (2003).

[23] Axelevitch, Gorenstein A., and Golan G., "Investigation of optical transmission in thin metal films." *Physics Procedia* , 32, 1-13, (2012).

[24] Pan A., Zheng H., Yang Z., Liu F., Ding Z., Qian Y., "Gamma-irradiation-induced Ag/SiO_2 composite films and their optical absorption properties." *Materials research bulletin*, 38.5, 789-796, (2003).

[25] Jabbar, W., Habubi N., and Chiad S. "Optical characterization of silver doped poly (vinyl alcohol) films." *Journal of the Arkansas Academy of Science*, 64.1, 101-105, (2010).

[26] Abdelrazek, Abdelghany A., and Tarabih A. "Characterization and physical properties of silver/PVA nano-composite." *Research Journal of Pharmaceutical, Biological and Chemical Sciences*, 3.4, 448, (2012).

[27] Ranjgar, A., "Characterization and optical absorption properties of plasmonic nanostructured thin films." *Armenian Journal of Physics*, 6.4, 198-203, (2013).

[28] Mahmudin, Lufsyi, "Optical properties of silver nanoparticles for surface plasmon resonance (SPR)-based biosensor applications." *Journal of Modern Physics*, 6.08, 1071, (2015).

[29] Chou, H. L., "Interactions between silver nanoparticles and polyvinyl alcohol nanofibers." *AIP Advances*, 4.8, 087111, (2014).

[30] Kadhim, Waleed K., Maha K., and Maryam A. "Synthesis and Characteristics of (PAV-PAVC-Ti) Nanocomposites." *Iraqi Journal of Nanotechnology, synthesis and application*1, 21-26, (2020).

[31] Rashad, M. "Tuning optical properties of polyvinyl alcohol doped with different metal oxide nanoparticles." *Optical Materials*, 105, 109857, (2020).

[32] Feldman, Dorel. "Poly (vinyl alcohol) recent contributions to engineering and medicine." *Journal of composites science*, 4.4, 175, (2020).

[33] Yahia, Mohammed M., and Ahmed M., "Multifunction applications of TiO_2/poly (vinyl alcohol) nanocomposites for laser attenuation applications." *Physica B: Condensed Matter* ,556, 48-60, (2019).

[34] Arora, Rajeev, "TiO_2 and PVA Based Polyaniline Composite Materials-A Review." *Materials Today: Proceedings*, 2.4-5, 2767-2775, (2015).

[35] Sunil G., Bhajantri R., Ravindrachary V., Sheela T., Pujari P., Jagadish N., and Boja P., "Pressure sensitive dielectric properties of TiO_2 doped PVA/CN-Li nanocomposite." *Journal of Polymer Research*, 22.2, 1-14, (2015).

[36] El-Shamy, Ahmed G., Wahib M., and Kamal M. Abd El Kader. "Enhancement of the conductivity and dielectric properties of PVA/Ag nanocomposite films using γ irradiation." *Materials Chemistry and Physics,* 191, 225-229, (2017).

[37] Rashad, Shalan A., "Synthesis and optical properties of titania-PVA nanocomposites." *International Journal of Nanoparticles, 5.2*, 159-169, (2012).

[38] Ewa B., Dominik S., Patryk O. and Anna W., "Effects of titanium dioxide nanoparticles exposure on human health—a review." *Biological Trace Element Research*, 193.1, 118-129, (2020).

[39] Doyan A., Susilawati, Hakim S., Muliyadi L., Taufik M. and Nazarudin, "The Effect of Indium Doped SnO_2 Thin Films on Optical Properties Prepared by Sol-Gel Spin Coating Technique." *Journal of Physics: Conference Series*, 1397, 1, (2019).

[40] Bittaua F., Abbas A., Barth K. , Bowers J. , Walls J., "The effect of temperature on resistive ZnO layers and the performance of thin film CdTe solar cells." *Thin Solid Films, 633*, 92-96(2017).

[41] Doyan, Aris, Siti A. Fitri, and Sukainil A. "Crystal structure characterization of thin layer zinc oxide." *IOP Conference Series: Materials Science and Engineering*, 196. 1. (2017).

[42] Syamsul H. , Aris D. , Susilawati S. , Lalu M., "Synthesis Thin Films SnO_2 with Doping Indium by Sol-gel Spin coating." *Jurnal Penelitian Pendidikan IPA, 5.2*, 171-174, (2019).

[43] Ikraman, Norma, Aris D., and Susilawati S., "Penumbuhan Film SnO_2 Dengan Doping Al-Zn Menggunakan Teknik Sol-Gel Dip Coating." *Jurnal Pendidikan Fisika dan Teknologi*, 3.2, 228-231, (2017).

[44] Doyan A., Susilawati, Imawanti Y., Gunawan E., and Taufik M., "Characterization Thin Film Nano Particle of Aluminum Tin Oxide (AlTO) as Touch Screen." *Journal of Physics: Conference Series*, 1097. 1, (2018).

[45] Aris D., Susilawati Y., "Characterization Thin Film Nano Particle of Aluminum Tin Oxide (AlTO) as Touch Screen." *Journal of Physics: Conference Series*, Vol. 1097. No. 1, (2018).

[46] Xi-Feng Z., Zhi-Guo L., Wei S., Sangiliyandi G., "Silver nanoparticles: synthesis, characterization, properties, applications, and therapeutic approaches." *International journal of molecular sciences*, 17.9, 1534, (2016).

[47] Sangiliyandi G., Jung H., Jae W., and Jin-Hoi K., "Comparative assessment of the apoptotic potential of silver nanoparticles synthesized by Bacillus tequilensis and Calocybe indica in MDA-MB-231 human breast cancer cells: targeting p53 for anticancer therapy." *International journal of nanomedicine*, 10, 4203, (2015).

[48] Sangiliyand G., Kalimuthu K., Ramanathan V., "Biosynthesis, purification and characterization of silver nanoparticles using Escherichia coli." *Colloids and Surfaces B: Biointerfaces*, 74.1, 328-335, (2009).

[49] Hadi, Shaymaa, Ahmed H., and Alaa J., "Optical properties of (PVA-LiF) composites." *Australian Journal of Basic and Applied Sciences*, 5.9, 2192-2195, (2011).

[50] Abdallh, Mustafa, Osama H., and Emad Y., "Study the optical properties of poly (vinyl alcohol) doped cupper chloride." *Al-Nahrain Journal of Science*, 16.1, 17-20, (2013).

[51] Vishwa M., Narasimha R., Neela P., "Effect of TiO_2 nano-particles on optical, electrical and mechanical properties of poly (vinyl alcohol) films." *Procedia Materials Science*, 5, 847-854, (2014).

[52] Salman, Sabah A., Nabeel A., and Mohammed H., "Preparation and Study of Some Electrical Properties of PVA-Ni (NO 3) 2 Composites." *International Letters of Chemistry, Physics and Astronomy*, 40, (2015).

[53] Shehap, A. M., and Dana S. Akil. "Structural and optical properties of TiO_2 nanoparticles/PVA for different composites thin films." *International Journal of Nanoelectronics and Materials* 9.1 (2016).

[54] Al-Sulaimawi, Itab F. "Optical Properties of PVA/K_2CrO_4 Composite." *Ibn AL-Haitham Journal for Pure and Applied Science*, 28.2, 32-40, (2017).

[55] Jameel T., Khawla, and Raja A. "Structural and Optical Properties of polyvinyl alcohol doped silver (PVA: Ag) film." *Journal of Nanostructures*, 8.4, 359-365, (2018).

[56] Vijayalakshmi, Vanathi R., Ravichandran K., and Praveen K., "Investigation on the impact of different stabilizing agents on structural, optical properties of Ag@ SnO_2 core-shell nanoparticles and its biological applications." *Journal of Molecular Liquids*, 307, 112951, (2020).

[57] Hadi, Aseel, Ahmed H., and Yahya A. "Structural, optical and electrical properties of PVA/PEO/SnO_2 new nanocomposites for flexible devices." *Transactions on Electrical and Electronic Materials*, 21.3, 283-292, (2020).

[58] Zeena M., Mohammed A., Abdul Rahman N. Abed & Rasheed N. Abed "Influence of nano silicon carbide (SiC) embedded in poly (Vinyl Alcohol) (PVA) lattice on the optical properties." *Silicon*, 1-14, (2021).

[59] Silambarasan M., Ramesh P., Mohd S., "Influence of incorporation of gallium oxide nanoparticles on the structural and optical properties of polyvinyl alcohol polymer." *Journal of Inorganic and Organometallic Polymers and Materials*, 31.10, 4141-4149, (2021).

[60] Soliman, T., Zaki M., Hessien M., Sh.I.E., "The structure and optical properties of PVA-BaTiO3 nanocomposite films." *Optical Materials*, 111, 110648, (2021).

[61] Morsi, M. A., Abdelrazek E., Ramadan R., Elashmawi I., Rajeh A.,"Structural, optical, mechanical, and dielectric properties studies of carboxymethyl cellulose/polyacrylamide/lithium titanate nanocomposites films as an application in energy storage devices." *Polymer Testing*, 114,107705, (2022).

[62] Young, David C., Computational chemistry: a practical guide for applying techniques to real world problems. John Wiley & Sons, (2004).

[63] Mueller, Michael P., "*Fundamentals of quantum chemistry: molecular spectroscopy and modern electronic structure computations*". *Springer Science and Business Media*, (2007).

[64] Fitts, Donald D., "*Principles of quantum mechanics: as applied to chemistry and chemical physics*",*Cambridge University Press*, (2002).

[65] Bohm, David, and Basil J. Hiley. "*The undivided universe: An ontological interpretation of quantum theory*", *Routledge*, (2006).

[66] El-Nabulsi, Rami A. *"Spectrum of Schrödinger Hamiltonian operator with singular inverted complex and Kratzer's molecular potentials in fractional dimensions." The European Physical Journal plus*, 133. 7, 1-16, (2018).

[67] Cramer C., " *Essentials of Computational Chemistry: Theories and Models"*, 2nd ed., John Wiley and Sons Ltd., the Atrium, Southern Gate, Chichester, England, (2004).

[68] Rogers, Donald W., *"Computational Chemistry using the PC."* John Wiley and Sons, (2003).

[69] El-Nabulsi, Rami A., *"Spectrum of Schrödinger Hamiltonian operator with singular inverted complex and Kratzer's molecular potentials in fractional dimensions." The European Physical Journal Plus* 133.7, 1-16, (2018).

[70] Verma, Pragya, and Donald G., *"Status and challenges of density functional theory." Trends in Chemistry*, 2.4, 302-318, (2020).

[71] VERMA, Dakeshwar K., *"Density functional theory (DFT) as a powerful tool for designing corrosion inhibitors in aqueous phase", Advanced engineering testing*, 87-96, (2018).

[72] Ngoc K., Nam H., Viet V., Hanh K., *"Comprehensive resistive switching behavior of hybrid polyvinyl alcohol and TiO_2 nanotube nanocomposites identified by combining experimental and density functional theory studies", Journal of Materials Chemistry* C, 6.8: 1971-1979,(2018).

[73] Leach, Andrew R., And Andrew R., *"Molecular modelling: principles and applications", Pearson education*, (2001).

[74] Sholl, David, and Janice A. Steckel. *"Density functional theory: a practical introduction"*, John Wiley and Sons, (2011).

[75] Bhagwati P., Saini L., Rajesh O. Sharma and Brajesh T., *"Hybrid functional calculations of electronic and thermoelectric properties of GaS, GaSe, and GaTe monolayers", Physical Chemistry Chemical Physics*, 20.45: 28575-28582, (2018).

[76] Young, D. C. *"A Practical Guide for Applying Techniques to Real-World Problems*, ISBN 0-471-33368-9,434, (2001).

[77] Arbuznikov A., *"Hybrid exchange correlation functionals and potentials: Concept elaboration". Journal of Structural Chemistry*, 48.1: S1-S31, (2007).

[78] Daniel V., Oliveira, Joachim L., Michael F., *"BSSE-correction scheme for consistent gaussian basis sets of double-and triple-zeta valence with polarization quality for solid-state calculations." Journal of Computational Chemistry* 40.27, 2364-2376, (2019).

[79] Lehtola, Susi, Frank B., and Christian V., "An overview of self-consistent field calculations within finite basis sets." *Molecules*, 25.5, 1218, (2020).

[80] Rolfes, Julian D., Frank N., and Dimitrios A., *"All-electron scalar relativistic basis sets for the elements Rb–Xe." Journal of Computational Chemistry*, 41.20, 1842-1849, (2020).

[81] Aleksandr V., Junming H., Michelle L., Christopher J., and Donald G., *"Computational electrochemistry: prediction of liquid-phase reduction potentials." Physical Chemistry Chemical Physics*, 16.29, 15068-15106, (2014).

[82] Jensen, Frank. "Atomic orbital basis sets." *Wiley Interdisciplinary Reviews: Computational Molecular Science*, 3.3, 273-295, (2013).

[83] Caffarel, Michel. *"Evaluating two-electron-repulsion integrals over arbitrary orbitals using zero variance Monte Carlo: Application to full configuration interaction calculations with Slater-type orbitals." The Journal of Chemical Physics*, 151.6, 064101, (2019).

[84] Rogers, Donald W., "*Computational Chemistry using the PC*." John Wiley and Sons, (2003).

[85] Forster, Arno, and Lucas V., *"GW100: A Slater-Type Orbital Perspective." Journal of chemical theory and computation*, 17.8, 5080-5097, (2021).

[86] Valone, Steven M. "*Quantal Density Functional Theory II. Approximation Methods and Applications*", 11387-11388, (2010).

[87] Fitts, D. D. *Principles of quantum mechanics: as applied to chemistry and chemical physics*. Cambridge University Press, ISBN 0 511 00763 9, 361 page, (2002).

[88] Cha, Tong H., *"Scale factors of Gaussian type orbitals optimized in molecule's local environments." Chemical Physics Letters*, 765, 138285, (2021).

[89] Stefano B., David B., Alexis L., Stefano E., *"Distributed Gaussian orbitals for molecular calculations: application to simple systems" Molecular Physics*, 118.4, 1615646, (2020).

[90] Shaw, Robert A. "The completeness properties of Gaussian-type orbitals in quantum chemistry." *International Journal of Quantum Chemistry*, 120.17, e26264, (2020).

[91] Magalhaes, Alexandre L. "Gaussian-type orbitals versus Slater-type orbitals: a comparison." *Journal of Chemical Education*, 91.12, 2124-2127, (2014).

[92] Christoph W., Guennaddi P., Foudhil B., Peter S., Tillmann K., "Gaussian-Type Orbital Calculations for High Harmonic Generation in Vibrating Molecules: Benchmarks for H2+." *Journal of Chemical Theory and Computation*, 17.12, 7353-7365, (2021).

[93] Joonho L., Xintian F., Leonardo A., Jérôme F. , Evgeny E., and Martin ., "Approaching the basis set limit in Gaussian-orbital-based periodic calculations with transferability: Performance of pure density functionals for simple semiconductors." *The Journal of Chemical Physics*, 155.16, 164102, (2021).

[94] Clementi, E., André, J., and Mc C., "Theory and Applications in Computational Chemistry: The First Decade of the Second Millennium. American Institute of Physics, ISBN 978-0-7354-1057-2, 275 page, (2012).

[95] Frisch, M. J., "KN Kudin, JC Burant, JM Millam, SS Iyengar, J." (2003).

[96] Kaupp, Martin. "*Buchbesprechung: A Chemist's Guide to Density Functional Theory*. Von Wolfram Koch und Max C. Holthausen.", 989-990, (2001).

[97] Mueller, M. P. "*Fundamentals of quantum chemistry: molecular spectroscopy and modern electronic structure computations*. Springer Science Business Media, ISBN-0- 306-47566-9, 262 page, (2007).

[98] Gotwals J., Robert R., "Integrating Computational Chemistry (Molecular Modeling) into the General Chemistry Curriculum." *North Carolina School of Science and Mathematics*, 1-11, (2008).

[99] Gauld, James W. "Reviews in Computational Chemistry, Volume 20 Edited by Kenny B. Lipkowitz (North Dakota State University), Raima Larter (Indiana University-Purdue University), Thomas R. Cundari (University of North Texas), and Donald B. Boyd, Editor Emeritus (Indiana University− Purdue University). John Wiley and Sons, Inc.: Hoboken, NJ. 2004. xxvi+ 458 pp. $150.00. ISBN 0-471-44525-8.", 3233-3233, (2005).

[100] Frisch M., Trucks G., Schlegel H., Scuseria G., Robb M., Cheeseman J., "Gaussian 09, revision D. 01." (2009).

[101] Peverati R., Truhlar D., "M11 L: A local density functional that provides improved accuracy for electronic structure calculations in chemistry and physics". *The Journal of Physical Chemistry Letters*, *3*(1), 117-124, (2011).

[102] Abdulzahra, Ramla A. Abdulzahra A., and Abbood I., "Geometry Optimization and Energies of Donor-Bridge-Acceptor Molecular System: B3LYP/DFT Calculations." *Journal of Kufa-Physics*, 6.1, (2014).

[103] Hinchliffe, "A. Molecular modelling for beginners". John Wiley and Sons, ISBN 0 470 84309 8, 407, (2005).

[104] Zhao, Yan, and Donald G. Truhlar. "Design of density functionals that are broadly accurate for thermochemistry, thermochemical kinetics, and nonbonded interactions." *The Journal of Physical Chemistry a*, 109.25, 5656-5667, (2005).

[105] Abdulsattar, Mudar A. "Size effects of semiempirical large unit cell method in comparison with nanoclusters properties of diamond-structured covalent semiconductors." *Physica E: Low-dimensional Systems and Nanostructures*, 41.9, 1679-1688, (2009).

[106] Hugosson, Håkan W., *A theoretical treatise on the Electronic Structure of designer Hard Materials*. Diss. Acta Universitatis Upsaliensis, (2001).

[107] Wodrich, Matthew D., Clémence C., and Paul v., "Systematic errors in computed alkane energies using B3LYP and other popular DFT functionals." *Organic letters*, 8.17, 3631-3634, (2006).

[108] Oftadeh M., Naseh S., and Hamadanian M., "Electronic properties and dipole polarizability of thiophene and thiophenol derivatives via density functional theory." *Computational and Theoretical Chemistry*, 966.1-3, 20-25, (2011).

[109] Ademir J., Káthia M., Ricardo M., Fábio A., Cláudio N., and Albérico B., "A study of neolignan compounds with biological activity against Paracoccidioides brasiliensis by using quantum chemical and chemometric methods." *Journal of the Brazilian Chemical Society*, 14, 809-814, (2003).

[110] Shenghua L., Yang H., and Jin Y., "Lubrication chemistry viewed from DFT-based concepts and electronic structural principles." *International Journal of Molecular Sciences*, 5.1, 13-34, (2003).

[111] Basharnavaz, Hadi, Aziz H., and Seyed H.. "A first-principles study on the interaction of CO molecules with VIII transition metals-embedded graphitic carbon nitride as an excellent candidate for CO sensor." *Physics Letters A*, 383.21, 2472-2480, (2019).

[112] Barnes, Craig E. "Inorganic Chemistry (Catherine E. Housecroft and Alan G. Sharpe)." *Journal of Chemical Education*, 80.7, 747, (2003).

[113] Sadasivam K., Kumaresan R., "Theoretical investigation on the antioxidant behavior of chrysoeriol and hispidulin flavonoid compounds–A DFT study." *Computational and Theoretical Chemistry*, 963.1, 227-235, (2011).

[114] Putjuso, Thanin, and Peerasak S., "Influence of annealing on the giant dielectric properties of cuo ceramics prepared by a simple pva sol-gel." *Asia-Pacific Journal of Science and Technology*, 17.2, 203-210, (2012).

[115] Al-Mudhaffer, Mohammed F., Maged A., and Mohammed A., "Linear optical properties and energy loss function of Novolac: epoxy blend film." *Archives of Applied Science Research,* 4.4, 1731-7140, (2012).

[116] Ilican S., Caglar M., and Caglar Y., "The effect of deposition parameters on the physical properties of CdxZn1-xS films deposited by spray pyrolysis method", Journal of Optoelectronics and Advances Materials" 9, 5, 1414-1417, (2007).

[117] Abdullah, Omed G., and Saeed S., "Effect of NaI doping on same physical characteristic of (PVA) 0.9-(KHSO4) 0.1 composite films." *Chemistry and Materials Research*, 3.11, 19-24, (2013).

[118] Nathan, Abutu A., Onoja A., and Amah A., "Influence of PVA, PVP on crystal and optical properties of europium doped strontium aluminate nanoparticles." *Amer. J. Eng. Res*, 4.4, (2015).

[119] Hamad T., Yusop R., Al-Taa'y W., Abdullah B., and Yousif E., "Laser induced modification of the optical properties of nano-ZnO doped PVC films", International Journal of Polymer Science, 8-10, (2014).

[120] Begum, Anayara, Amir H., and Atowar R., "Optical and electrical properties of doped and undoped Bi_2S_3–PVA films prepared by chemical drop method." *Mater. Sci. Appl.* 2, 163-168, (2011).

[121] Sangawar V., Golchha M., "Evolution of the optical properties of polystyrene thin films filled with zinc oxide nanoparticles." *International Journal of Scientific and Engineering Research* 4.6, 2700-2705, (2013).

[122] Lalithambika K., Shanthakumari K., and Sriram S., "Optical properties of CdO thin films deposited by chemical bath method", International Journal of Chemistry Technology Research, 6, 5, 3071-3077, (2014).

[123] Omed G., Abdullah, Dana A., Saro S., and Hawzhin T., "Optical properties of PVA: CdC_{l2}. H_2O polymer electrolytes." *IOSR Journal of Applied Physics,* 4.3, 52-57, (2013).

[124] Fu S., "Research on the characterization of hydrogenated silicon thin film using constant photocurrent method", Master thesis, Department of Optics and Photonics, National Central University, China, (2009).

[125] Davis E., Mott N., "Conduction in non-crystalline system, optical absorption and photoconductivity in amorphous semiconductors", Philosophical Magazine 22, 903-922, (1970).

[126] Andriesh A., Iovu M., and Shutov S., "Chalcogenide non-crystalline semiconductors in optoelectronics." *Journal of Optoelectronics and Advanced Materials,* 4.3, 631-647, (2002).

[127] Nahida J., "Spectrophotometric analysis for the UV-irradiated (PMMA)." *International Journal of Basic and Applied Sciences*, 12.2, 58-67, (2012).

[128] Eczema F., "Growth and Optical properties of Ag" *Journal of the University of Chemical Technology and Metallurgy,* 42.2, 217-222, (2007).

[129] Tauc J., Menth A., and Wood D., "Optical and magnetic investigations of the localized states in semiconducting glasses." *Physical Review Letters,* 25.11, 749, (1970).

[130] Abdullah O., Aziz B., and Hussen S., "Optical characterization of polyvinyl alcohol -ammonium nitrate polymer electrolytes films", Journal of Chemistry and Materials Research, 3 9, 72-75, (2013).

[131] Tintu R., Saurav K., Sulakshn K., Nampoori V., , Radhakrishnan P., Sheenu T.,"$Ge_{28}Se_{60}Sb_{12}$/PVA composite films for photonic applications." *Journal of Non-Oxide Glasses*, 2.4, 167-174, (2010).

[132] Divya R., Meena M., Mahadevan C., and Padma C., "Investigation on CuO dispersed PVA polymer films." *Journal of Engineering Research and Applications,* 4.5, 1-7, (2014).

[133] Griffiths P., Haseth J., "Fourier transform infrared spectrometry", Wiley Blackwell, (2007).

[134] Stokes, Debbie J., "Principles and practice of variable pressure/environmental scanning electron microscopy" *(VP-ESEM)*. John Wiley and Sons, (2008).

[135] Gilligan, Lum G., Peter V., and Whittier S., Peter H., "Burkholderia, Stenotrophomonas, Ralstonia, Brevundimonas, Comamonas, Delftia, Pandoraea, and Acidovorax." *Manual of clinical microbiology*. ASM press, 729-748, (2003).

[136] Sulav I., Mahbubur R., Mohammad A., Arifur R., "Identification of marine sponge-associated bacteria of the Saint Martin's island of the Bay of Bengal emphasizing on the prevention of motile Aeromonas septicemia in Labeo rohita." *Aquaculture*, 545, 737156, (2021).

[137] Ahmed, Hind, Hayder M., and Ahmed H., "Analysis of structural, optical and electronic properties of polymeric nanocomposites/silicon carbide for humidity sensors." *Transactions on Electrical and Electronic Materials*, 20.3, 206-217, (2019).

[138] AL-humairi M., *Study the optical and electrical properties of (PVA-Ag) and (PVA-TiO_2) Nanocomposites*. Diss. M. Sc. Thesis, University of Babylon, College of Education for Pure Sciences, (2013).

[139] Jianyuan Y., Yingeng W., Yan H., Xiuwen W., Jing G., Jingkai Y., and Hongli Z., "Study of Structural and Electronic properties of Non-metal Elements doped SnO_2." *Beilstein Archives*, 2020.1, 68, (2020).

[140] Charles R., Katherine M., Geiser B., Stephen P., Rowley, and Paul D., "Structural and electron paramagnetic resonance studies of the square pyramidal to trigonal bipyramidal distortion of vanadyl complexes containing sterically crowded schiff base ligands." *Inorganic Chemistry*, 36.27, 6401-6408, (1997).

[141] Zhu H., Zhou P., Lia X., Liu M., "Electronic structures and optical properties of rutile TiO_2 with different point defects from DFT+ U calculations." *Physics Letters A*, 378.36, 2719-2724, (2014).

[142] Ding, Yi, and Yanli W., "Density functional theory study of the silicene-like SiX and XSi_3 (X= B, C, N, Al, and P) honeycomb lattices: the various buckled structures and versatile electronic properties." *The Journal of Physical Chemistry C*, 117.35, 18266-18278, (2013).

[143] Atkins, Peter W., and Ronald S., "Molecular quantum mechanics". *Oxford university press*, (2011).

[144] Ngoc K., Nam H., Viet V., Hanh K., Thi M., Nam T., and Vinh C., "Comprehensive resistive switching behavior of hybrid polyvinyl alcohol and TiO_2 nanotube nanocomposites identified by combining experimental and density functional theory studies." *Journal of Materials Chemistry C*, 6.8, 1971-1979, (2018).

[145] Ahmed, Hind, Hayder M., and Ahmed H., "Novel studies on spectroscopic, optical and electronic properties of (PVA-TiO_2/SiC) nanocomposites for biological and optoelectronics applications." *Advanced Science, Engineering and Medicine*, 11.6, 554-564, (2019).

[146] Arab, Ali, Fatemeh Z., and Mostafa F., "Electronic structure and reactivity of (TiO_2) n (n= 1–10) nano-clusters: Global and local hardness based DFT study." *Computational Materials Science*, 117, 90-97, (2016).

[147] Chen, Kuo H., and Norman L., "Molecular mechanics (MM4) study of saturated four-membered ring hydrocarbons." *Journal of Molecular Structure: THEOCHEM*, 581.1-3, 215-237, (2002).

[148] Gupta, Shipra M., and Manoj T., "A review of TiO_2 nanoparticles." *chinese science bulletin*, 56.16, 1639-1657, (2011).

[149] Hassan, Dalal, and Ahmed H., "Preparation and Studying the Structural and Optical Properties of (Poly-Methyl Methacrylate–Lead Oxide) Nanocomposites for Bioenvironmental Applications." *Journal of Bionanoscience*, 12.3, 346-349, (2018).

[150] Raheem A., Al-Shejyri K., Al-Bermany E., "Density functional theory calculations for methyl benzene molecules group". *British Journal of Science* 5, 2, (2012).

[151] Peng W., HualinW., Jingrong L., Pengfei W., Suwei J ., Xingjiang L., Shaotong J., "Montmorillonite@ chitosan-poly (ethylene oxide) nanofibrous membrane enhancing poly (vinyl alcohol-co-ethylene) composite film." *Carbohydrate polymers*, 181, 885-892, (2018).

[152] Guruswamy B., Ravindrachary V., Shruthi C., Mylarappa M., "Effect of SnO_2 nanoparticle doping on structural, morphological and thermal properties of PVA-PVP polymer blend." *Materials Science Forum*, 962.82- 88, (2019).

[153] Menon, Madhu, Ernst R., and Subbaswamy K., "Structural and vibrational properties of fullerenes and nanotubes in a nonorthogonal tight-binding scheme." *The Journal of chemical physics*, 104.15, 5875-5882, (1996).

[154] Ţucureanu, Vasilica, Alina M., and Andrei M., "FTIR spectroscopy for carbon family study." *Critical reviews in analytical chemistry*, 46.6, 502-520, (2016).

[155] Varun A., Akash D., Rajnish K., Rupesh K.,"Functionalization of graphene using carboxylation process." *Int. J. Sci. Emerg. Technol*, 4, 13-19, (2012).

[156] Kumar N., Vincent C., and Praveen B., "Advancement in microstructural, optical, and mechanical properties of PVA (Mowiol 10-98) doped by ZnO nanoparticles." *Physics Research International* (2014).

[157] Sakaguchi, Ronald L., and John M. Powers. *Craig's restorative dental materials-e-book*. Elsevier Health Sciences, (2012).

[158] Nagib A., Terin A., Ali M., Eseldin I., Aref T., Amel M., "Spectroscopic characterization of PEG-DNA biocomplexes by FTIR." *Journal of Applied Pharmaceutical Science*, 4.8, 006-010, (2014).

[159] Obaid, Zaman S., "*Physical Properties of PMMA/ZnO Composite Material*". Diss. Ph. D. dissertations, University Al-Narhrain, (2017).

[160] Vasilica S., Alina M., Ileana C., Cecilia P., "Preparation of titanium dioxide films by sol-gel route for gas sensors." *Advanced Topics in Optoelectronics, Microelectronics, and Nanotechnologies IV*, 7297, 127-130, *(*2009).

[161] Liebman, Joel F., and Susan K., "A Review of:"Molecular Modelling for Beginners" Alan Hinchliffe, John Wiley and Sons, 2003; xviii+ 410, pp., 117.00,cloth; 46.00, paper.", 442, 203-205, (2005).

[162] Barrios V., Mendez E., Aguilar N., Espinosa G., Davila R., FTIR - An Essential Characterization Technique for Polymeric Materials In Infrared Sprectroscopy–Materials Science, Engineering and Technology; Prof. Theophanides Theophile (Ed.), InTech: Rijeka, Croatia, (2012).

[163] Hashim, Ahmed, and Qassim H., "Structural, electrical and optical properties of (biopolymer blend/titanium carbide) nanocomposites for low cost humidity sensors." *Journal of Materials Science: Materials in Electronics*, 29.13, 11598-11604, (2018).

[164] Lin F., "*Preparation and characterization of polymer TiO_2 nanocomposites via in-situ polymerization*". MS thesis. University of Waterloo, (2006).

[165] Shabaz A., Shaheer A., Abdullah, Eun B., Hyung S., Sadia A., "Planar D-π-A configured dimethoxy vinylbenzene based small organic molecule for solution-processed bulk heterojunction organic solar cells." *Applied Sciences*, 10.17, 5743, (2020).

[166] Ahmed, Hind, Ahmed H., and Hayder A., "Analysis of structural, electrical and electronic properties of (polymer nanocomposites/silicon carbide) for antibacterial application." *Egyptian Journal of Chemistry*, 62.4, 767-776, (2019).

[167] Thomas B., Livia G., Fabrizio C., and Gianfranco P., "Electronic properties of rutile TiO_2 ultrathin films: Odd-even oscillations with the number of layers." *Physical Review B*, 70.3, 035419, (2004).

[168] Weimei S., Qifeng C., Yao X., Dong W., Chun f., "Investigation of the silicon concentration effect on Si-doped anatase TiO_2 by first-principles calculation." *Journal of Solid State Chemistry*, 184.8, 1983-1988, (2011).

[169] H.X. Z., Zhou P., Liu J., "Electronic structures and optical properties of rutile TiO_2 with different point defects from DFT+ U calculations." *Physics Letters A*, 378.36, 2719-2724, (2014).

[170] Licona R., Rivas S., "Ab initio density functional study of MgO (001) surface with topological defects." *International journal of quantum chemistry*, 104.6, 919-928, (2005).

[171] Young, David C. "A practical guide for applying techniques to real-world problems." *Computational Chemistry, New York*, 9, 390, (2001).

[172] Hehre W., Radom L., Schleyer P., and Pople, J., "Ab initio Molecular Orbital Theory", New York, John Wiley and Sons Inc, 7, 3, (1986).

[173] Arab, Ali, Fatemeh Z., and Mostafa F., "Electronic structure and reactivity of (TiO_2) n (n= 1–10) nano-clusters: Global and local hardness based DFT study." *Computational Materials Science*, 117, 90-97, (2016).

[174] Ahmed, Hind, and Ahmed H., "Geometry optimization, optical and electronic characteristics of novel PVA/PEO/SiC structure for electronics applications." *Silicon*, 13.8, 2639-2644, (2021).

[175] Siyamak S., Masoome S., Liudmila F., Evgenij D., Mahdieh D., Sadegh K., Mikhail and Marina D., "Optimization, Spectroscopic (Excited States, UV/Vis, and Polarization) Studies, FMO, ELF, LOL, QTAIM, NBO Analysis and Electronic Properties of Two New Azomethine Derivatives: A Theoretical and Experimental Investigations." *Russian Journal of Physical Chemistry A*, 94.9, 1848-1865, (2020).

[176] Hashim, Ahmed, Hayder A., and Hind A., "Analysis of optical, electronic and spectroscopic properties of (biopolymer-SiC) nanocomposites for electronics applications." *Egyptian Journal of Chemistry*, 62.9, 1659-1672, (2019).

[177] Tauc J., Radu G., and Anina V., "Optical properties and electronic structure of amorphous germanium." *physica status solidi (b)*, 15.2, 627-637, (1966).

[178] Phukan, Pallabi, and Dulen S., "Optical and structural investigation of CdSe quantum dots dispersed in PVA matrix and photovoltaic applications." *International Journal of Photoenergy* (2013).

[179] Amin, Abd-El S., "Optical, dielectric and electrical properties of PVA doped with Sn nanoparticles." *Materials Research Express*, 1.2, 025024, (2014).

[180] Sujatha L., Joy K., "Structural and optoelectronic properties of indium doped SnO_2 thin films deposited by sol gel technique." *Journal of Materials Science: Materials in Electronics*, 25.4, 1664-1672, (2014).

[181] Devi, Uma C., Sharma A., and VVR Narasimha Rao. "Electrical and optical properties of pure and silver nitrate-doped polyvinyl alcohol films." *Materials Letters*, 56.3, 167-174, (2002).

[182] Indolia, Ajay P., and Gaur M., "Optical properties of solution grown PVDF-ZnO nanocomposite thin films." *Journal of Polymer Research* 20.1,1-8, (2013).

[183] Al-Attiyah, Khalid H., Ahmed H., and Sroor F., "Fabrication of novel (carboxy methyl cellulose–polyvinylpyrrolidone–polyvinyl alcohol)/lead oxide nanoparticles: structural and optical properties for gamma rays shielding applications." *International Journal of Plastics Technology*, 23.1, 39-45, (2019).

[184] Hashim A., Hadi A., "Novel lead oxide polymer nanocomposites for nuclear radiation shielding applications." *Ukrainian Journal of Physics*, 62.11, 978-978, (2017).

[185] Nathan, Abutu A., Onoja A., and Amah A., "Influence of PVA, PVP on crystal and optical properties of europium doped strontium aluminate nanoparticles." *Amer. J. Eng. Res*, 4.4, (2015).

[186] Nimrodh A., Umapathy S., Sophia J., Mathavan T. and Mangalaraj D. "On the optical and thermal properties of in situ/ex situ reduced Ag NP's/PVA composites and its role as a simple SPR-based protein sensor." *Applied Nanoscience*, 1.2, 87-96, (2011).

[187] Abdullah, Omed G., "Influence of barium salt on optical behavior of PVA based solid polymer electrolytes." *European Scientific Journal* 10.33 (2014).

[188] Hdidar M., Chouikhi S., Fattoum A., Arous M., Kallel A."Influence of TiO_2 rutile doping on the thermal and dielectric properties of nanocomposite films based PVA." *Journal of Alloys and Compounds*, 750, 375-383, (2018).

[189] Abdullah, Omed G., Bakhtyar K., Aziz, and Dler M., "Structural and optical properties of PVA: $Na_2S_2O_3$ polymer electrolytes films." *Indian Journal of Applied Research*, 3.11, 477-480, (2013).

[190] Venkatarayappa, Manjunatha, "Refractive index and dispersive energy of $NiSO_4$ doped poly (ethylene oxide) films." *Journal of Materials Science and Engineering. A*, 1.7A, 964, (2011).

[191] Gamze T., Semran S., Ezgi E., Demet E., Necdet S., "Synthesis and characterization of silver nanoparticles integrated in polyvinyl alcohol nanofibers for bionanotechnological applications." *Turkish Journal of Biology*, 40.3, 643-651, (2016).